The effect of skin pigmentation on the imaging performance in photoacoustic breast tomography

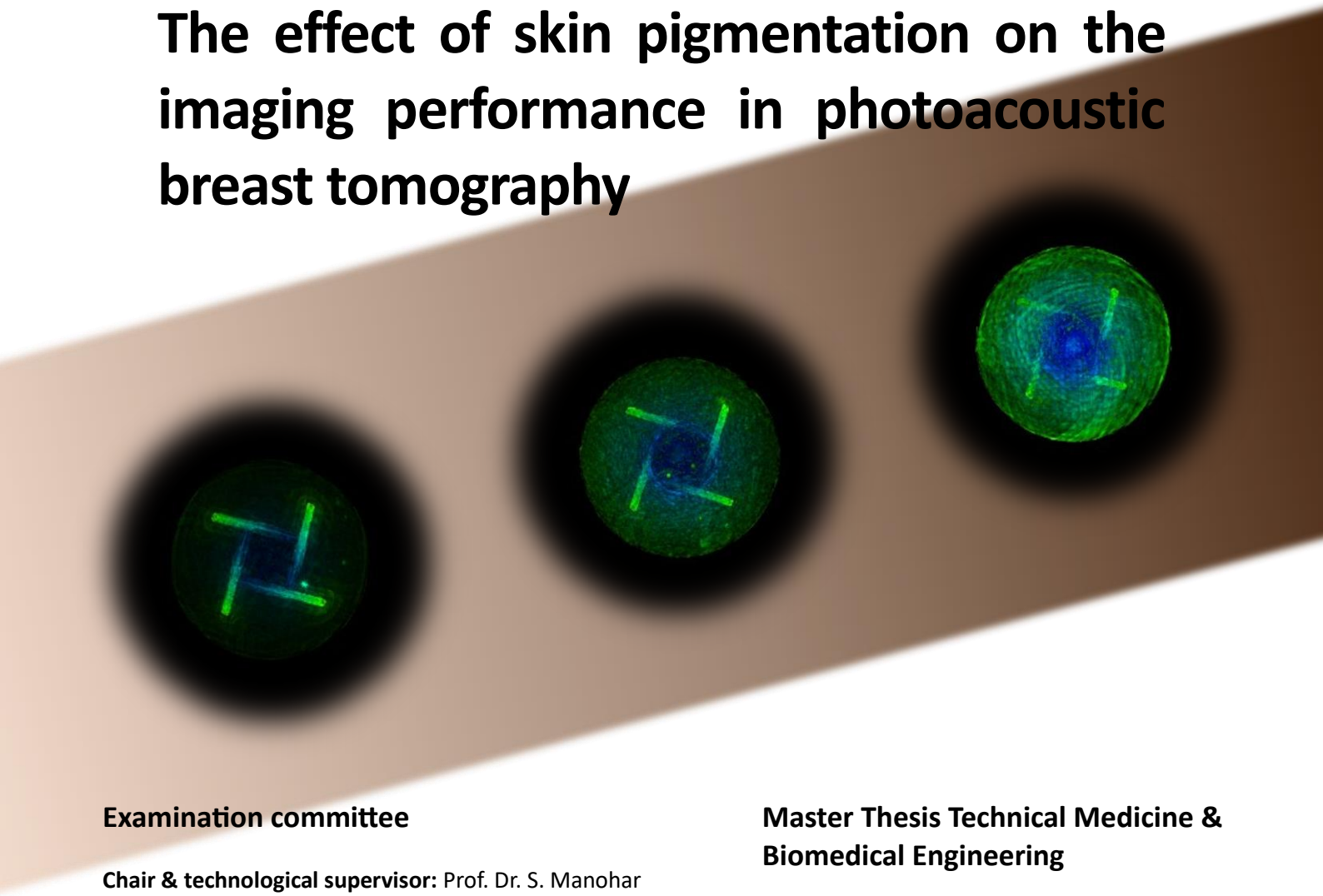

Examination committee

Chair & technological supervisor: Prof. Dr. S. Manohar
Multi-Modality Medical Imaging, Faculty of Science & Technology, University of Twente

Daily technological supervisor: R.F.G. Bulthuis MSc
Multi-Modality Medical Imaging, Faculty of Science & Technology, University of Twente

Medical supervisor: Dr. J. Veltman
Department of Radiology, Ziekenhuisgroep Twente

Professional development supervisor: E.M. Walter MSc
Faculty of Science & Technology, University of Twente

External member: Prof. Dr. Ir. N. Bosschaart
Biomedical Photonic Imaging, Faculty of Science & Technology, University of Twente

Master Thesis Technical Medicine & Biomedical Engineering

Nan S. Lubbers
Multi-Modality Medical Imaging
Faculty of Science & Technology
University of Twente

Enschede, The Netherlands

11 July 2024

MultiModality M3i Medical Imaging

UNIVERSITY OF TWENTE.

zgt Topzorg voor uw levenskwaliteit

MST Medisch Spectrum Twente

Voorwoord

Beste lezer,

Bijna anderhalve jaar geleden ben ik ter afronding van mijn dubbele master Technical Medicine en Biomedical Engineering met veel plezier begonnen aan mijn afstudeerproject in de vakgroep Multi-Modality Medical Imaging. Ik heb onderzoek gedaan naar de invloed van huidskleur op de beelden die gemaakt kunnen worden met de Twente Photoacoustic Mammoscope 3. Het werk is ondersteund vanuit het REACT-EU project “Foto-akoestische mammografie naar de kliniek met de PAM3+”. Uiteraard waren er zo zijn hoogte- en dieptepunten en zeker richting het einde begon het spannend te worden, maar dat hoort er nu eenmaal een beetje bij. Dit werk is wat mij betreft een mooie afsluiting van 7 jaar studententijd die sneller voorbijvlogen dan ik had verwacht. Ik wens jullie dan ook veel plezier met het lezen van mijn thesis.

Nan Lubbers

Dankwoord

Ik wil mijn commissie bedanken voor het lezen en beoordelen van mijn thesis. Ondanks dat het mijn thesis en afsturen is, zou ik het echter niet hebben kunnen doen zonder de steun en begeleiding van de mensen om mij heen. Zowel op de afdeling radiologie in het ZGT Hengelo en binnen de vakgroep aan de Universiteit Twente zijn er mensen die een belangrijke bijdrage hebben geleverd in mijn afstudeerperiode en die daarvoor zeker bedankt mogen worden.

Rianne Bulthuis en Srirang Manohar hebben mij, als respectievelijk dagelijks begeleider en als technologisch begeleider, veel ondersteund tijdens het afstudeeronderzoek zelf. Door hun kritische blik en goede input tijdens discussies, hebben ze mijn werk naar een hoger niveau getild. Ook hebben ze hebben me geleerd om niet alleen te kijken naar de meest logische oplossing, maar ook nieuwe en “gekke” oplossingen uit te proberen.

Op het gebied van de professionele ontwikkeling, wil ik Elyse bedanken die me niet alleen tijdens deze afstudeerperiode heeft begeleid, maar ook het jaar ervoor tijdens de vier TG-schappen. Ik moet toch wel bekennen dat ik behoor onder de groep studenten wiens eerste reactie bij het moeten reflecteren een diepe zucht is. Toch kan ik niet ontkennen dat het reflecteren zelf en de gesprekken die we hebben gehad me de afgelopen jaren veel hebben geholpen om me te ontwikkelen in de persoon die ik nu ben. Uiteraard hebben mijn intervisiegroepsgenoten met hun input en gerichte vragen ook een belangrijke bijdrage geleverd in mijn professionele ontwikkeling.

Jeroen Veltman heeft me als mijn medisch begeleider ondersteund in mijn activiteiten in de kliniek. Onder anderen door de prettige manier van begeleiden heeft hij een omgeving gecreëerd waarin ik me op mijn eigen tempo kon ontwikkelen met hier en daar een klein duwtje in de rug om me aan te moedigen mijn grenzen te verleggen. Ik heb echter ook een groot deel van mijn begeleiding gekregen van de radiologisch laboranten en andere mammaradiologen. Hun vriendelijkheid, geduld en behulpzaamheid hebben er mede voor gezorgd dat ik een hele prettige periode heb gehad in de kliniek waarin ik veel heb geleerd over het vakgebied en nog meer waardering heb gekregen voor de groep mensen achter de medische plaatjes.

Ik wil ook mijn dank betuigen aan iedereen in de fotoakoestiek subgroep binnen M3I voor zowel het geven van hun input, feedback en leuke discussies tijdens en buiten de meetings. Met mijn medestudenten binnen de groep heb ik me in de studentenkamer enorm geamuseerd met alle serieuze gesprekken en inhoudelijke discussies, maar ik heb ook genoten van de momenten waarop de aandacht verschoof naar wat minder intellectuele onderwerpen. Er zijn twee mensen binnen de fotoakoestiek groep die ik specifiek wil noemen. Bruno Di Santi has been an amazing help with his contributions to the data analysis approach and the development of the MATLAB scripts. I also want to thank him for his willingness to preprocess my data with me in a noticeably short time. His confidence that we could manage it and his determination to succeed, made sure I stayed confident as well. Het fantoom zou er waarschijnlijk niet zo snel zijn gekomen zonder hulp en input van Johan van Hespen. Met zijn expertise is hij een enorme steun geweest in het ontwerpen en maken van mallen voor mijn fantoom. Ook waardeer ik het enorm hoeveel hij heeft geholpen met alle problemen rond de vacuümoven die toch wat minder plug-and-play bleek te zijn dan gedacht.

Als het komt op het realiseren van mijn opdracht wil ik ook een paar andere mensen bedanken die actief hebben bijgedragen aan het uitvoeren van mijn fantoomstudie. Zo wil ik Sip Jan Boorsma bedanken voor het maken van de uiteindelijke mal en Tom Knop voor zijn ondersteuning in de periode dat Johan ziek was. Daarnaast wil ik ook PA Imaging, en met name Laurens Alink, bedanken voor hun hulp met de fantoomexperimenten. Ik waardeer het enorm dat Laurens bereid was voor mij mijn data op te halen in Oldenzaal en mee te denken rondom de problemen met de data van de scans. Of course, I cannot forget Felix Lucka, without who I would not have any reconstructions of my phantoms to begin with. I greatly appreciate his enormous efforts to not just reconstruct my data once but twice in such a short time period. I had already accepted the latest setback, but he managed to reconstruct all my data in time.

Algemene inhoudsopgave

Part I: Professional Development

Verantwoording professionele ontwikkeling

1. Introductie

De afgelopen 15 maanden heb ik met veel plezier gewerkt aan mijn onderzoek en heb ik me daarnaast ook met veel voldoening ingezet in de kliniek op de afdeling radiologie in het ZGT in Hengelo. Gedurende deze periode heb ik me niet alleen beziggehouden met de inhoud, maar heb ik ook aandacht besteed aan mijn professionele ontwikkeling. Aan het begin van de afstudeerperiode heb ik enkele aandachtspunten voor mezelf opgeschreven waar ik extra aan wilde werken. Ik heb ervaren dat ondanks enkele voornemens, ik het lastig vind om niet terug te vallen in de bekende patronen. Desondanks dat ik er niet in geslaagd ben alle leerdoelen met succes te behalen, heb ik door te reflecteren op waarom het me niet is gelukt, wel veel over mezelf geleerd. Door nieuwe handvaten uit die ervaringen te creëren kan ik in de toekomst aan die leerdoelen blijven werken om mezelf stukje bij beetje verder te ontwikkelen. Naast dat ik veel heb geleerd door actief bezig te zijn met die leerdoelen, heb ik ook nieuwe inzichten gekregen op vlakken waar ik me niet specifiek op heb gefocust. Die inzichten hebben me veel geleerd over hoe ik als persoon ben en hoe mij dat als professional beïnvloed. In deze verantwoording heb ik voor het overzicht mijn leerdoelen en (leer)ervaringen opgedeeld in drie verschillende categorieën: Klinische ontwikkeling, Academische ontwikkeling, Algemene professionele ontwikkeling. In de volgende secties zal ik ingaan op mijn ervaringen, wat ik eruit heb geleerd en welke eventuele vervolgstappen ik zou kunnen nemen gedurende mijn verdere professionele carrière.

2. Klinische ontwikkeling

2.1. Zelfstandig functioneren op de afdeling

Ik heb het overgrote deel van mijn tijd op de afdeling radiologie meegelopen op de mammadiagnostiek. Binnen de mammadiagnostiek waren er verschillende nieuwe klinische vaardigheden waarin ik me kon ontwikkelen: het uitvoeren van ultrasound-onderzoeken, het beoordelen van mammogrammen en het uitvoeren van verschillende soorten puncties. Toentertijd waren mijn enige ervaringen met die vaardigheden het uitvoeren van ultrasoundscans op medestudenten en wat instructievideo's over ultrasoundgeleider puncties tijdens een vak in de master. Met mijn medisch begeleider had ik aan het begin van het afstuderen besproken dat we stap voor stap zouden kijken hoever ik zou kunnen komen in het zelfstandig uitvoeren van deze handelingen. Tijdens mijn klinische TG-schappen (de 10-weekse stages voor Technische geneeskunde) merkte ik dat die periodes voor mij te kort waren om mezelf in de kliniek echt in de richting van een zelfstandig functionerende professional te kunnen ontwikkelen. Tegen de tijd dat ik me een beetje vertrouwd voelde met de mensen op de afdeling, de ziektebeelden, de patiëntengroep en de klinische handelingen, was de stage alweer bijna afgelopen. Een belangrijk leerdoel deze periode was daarom om de stap gaan zetten van een student die slechts meekijkt, vragen stelt en opdrachten opvolgt, naar een beginnende zorgprofessional die tot een bepaalde hoogte zelfverzekerd en zelfstandig kan functioneren binnen de klinische afdeling.

Als ik nu terugdenk aan het begin van mijn afstuderen had ik niet verwacht te zijn waar ik nu ben. Destijds vond ik alles spannend en kon ik me nog niet echt voorstellen dat ik echt daadwerkelijk zelfstandig handelingen zou kunnen uitvoeren. Ik dacht toen alleen maar aan hetgeen wat ik allemaal wel niet fout zou kunnen doen en wat de patiënt, laboranten en radiologen dan wel niet van me zouden vinden. Ook al dacht ik niet dat er iemand zou zijn die verwachtte dat ik alles direct volledig goed zou kunnen doen, voelde ik toch een bepaalde druk om goed te presteren. Elke patiënt die in het ziekenhuis komt, komt tenslotte voor goede zorg en niet om zich een proefkonijn te voelen. Bovendien is weten dat een deel van je medisch consult door een student wordt gedaan, toch anders dan weten dat de persoon die een naald in je steekt nog ervaring op moet doen. Ik wilde daarom dat de patiënt minimale ongemak ervaarde als gevolg van dat ik nog lerende was.

Door veel te doen onder supervisie en gestructureerd te werk te blijven gaan, merkte ik dat ik steeds zelfverzekerder werd. Nu aan het einde van mijn periode op de mammadiagnostiek ben ik echter in staat om voor een groot deel zelfstandig een onderzoek te doen. En als er een punctie moet worden uitgevoerd waarvan ik het gevoel heb dat ik dat zelf kan dat dan ook zelf te doen. Toen ik steeds meer zelf mocht en ben gaan doen, merkte ik dat ik ook snel meer zekerheid in mijn houding naar de patiënt ervaarde. Dingen zelfstandig mogen doen, geeft toch blijk van vertrouwen van de radiologen. Dus waarom zou ik dan niet met vertrouwen naar de patiënt kunnen stappen met dat ik de punctie zal gaan uitvoeren als die daar toestemming voor geeft. De meeste patiënten hadden er geen problemen mee dat ze mij aan de onderzoekstafel zagen staan en niet de radioloog. Zeker omdat ik ook uitlegde dat ik werd begeleid door een radioloog en altijd de plaatjes nabesprak. Er is ook geen enkele keer geweest dat een patiënt sceptisch daarom ook nog de radioloog wilde spreken.

Wat mij aan het begin met name tegenhield was dus het feit dat ik bang was om een fout te maken of iets te doen waar de patiënt direct last van zou ondervinden. Dat is iets wat ik tijdens mijn TG-schappen ook ervaarde. Een kleine of onopvallende laesie niet vinden op een scan is minder direct een probleem als de radioloog vervolgens toch zelf ook nog even gaat scannen. Een punctie uitvoeren waarbij de patiënt ondanks de verdoving toch veel pijn ervaart, heeft meer impact op de patiënt. Er zijn enkele situaties geweest waarin ik wel echt het idee had dat ik iets fout had gedaan of waarin ik daadwerkelijk een fout heb gemaakt. Zo heb ik een keer een vacuüm biopt genomen met als doel om weefsel met kalk te biopteren. In de eerste zes weefselreepjes kon ik echter geen kalk vinden. Ik heb toen de radioloog erbij gehaald en die mee laten kijken met de instellingen van het apparaat en de tweede ronde van biopten. Ik voelde me heel schuldig naar de patiënt toe, omdat die een relatief vervelend onderzoek had ondergaan voor niks. Ik had verwacht dat de patiënt boos zou worden, maar die bleef eigenlijk erg nuchter. Ze had uiteraard gehoopt dat het goed zou zijn gegaan, maar ze begreep dat het soms door omstandigheden anders loopt. Ik heb achteraf ook de situatie met de radioloog besproken om erachter te komen wat er mogelijk fout kon zijn gegaan en hoe ik dat had kunnen voorkomen. Die vertelde me dat zolang alle stappen waren uitgevoerd zoals het zou moeten en er geen reden was om redelijkerwijs aan te nemen dat er iets fout zou gaan, had ik gehandeld zoals dat zou moeten.

De momenten waarop bij mij of bij de radioloog dingen anders gingen dan voorzien, hebben me er daarnaast bewust van gemaakt dat als er iets fout gaat in de kliniek, dat niet direct de ramp is die ik me voorstel. Soms gaan dingen fout en dat kan heel vervelend zijn, maar dan is het belangrijk dat er een goede communicatie is naar de patiënt en dat er kan worden beargumenteerd waarom er is gehandeld zoals dat is gebeurd. Zelfstandig kunnen functioneren in de kliniek betekent niet direct dat er nooit iets fout mag gaan, het gaat erom dat je jezelf kan verantwoorden.

2.2. Omgang met de patiënt

Een aandachtspunt waar ik gedurende de TG-schappen ook al aan heb gewerkt, maar waar ik ook tijdens deze afstudeerperiode aandacht aan wilde besteden, is de omgang met de patiënt. Dit is ook de eerste keer dat ik actief in aanraking kom met patiënten die de diagnose kanker gaan krijgen of hebben gekregen. Op de afdeling plastische chirurgie waar ik voorheen ook een periode heb gezeten, kwam ik ook in aanraking met borstkankerpatiënten. Maar die kwamen praten over de verschillende borstreconstructiemogelijkheden na de operatie. Er werd eigenlijk weinig tot geen aandacht besteed aan de reden voor de borstreconstructie.

Ik merkte dat ik het lastig vind om te beginnen aan of door te gaan met een punctie bij patiënten die overstuur zijn. Ook zijn er patiënten bij wie de eerste punctie toch pijnlijk was en die daardoor opzien tegen de volgende punctie. Ik vond het nog wel lastig om door te gaan als ik zag dat de patiënt het moeilijk had, maar geen teken gaf dat die niet wilde dat de punctie werd uitgevoerd. Moet ik dan de patiënt eerst uitgebreid gaan troosten of geruststellen, of moet je de procedure gewoon starten en er gedurende de procedure voor zorgen dat de patiënt zo comfortabel mogelijk is. Gewoon maar doorgaan met de procedure voelt persoonlijk dan zo harteloos, maar het helpt de patiënt ook

niet om juist helemaal mee te gaan in de emotie van die patiënt. De procedure wordt niet makkelijker als je het een dag later zou doen en er is geen garantie dat de patiënt er op een later moment wel meer klaar voor is. Daarnaast is overstuur zijn geen direct teken van weigering van de zorg die geleverd moet worden. Vanuit professioneel standpunt is het dus het beste om de patiënt ondanks dat die in de emotie zitten door de procedure te leiden. Maar ik moet nog wel even goed leren die knop om te zetten.

Om mezelf meer handvaten te geven voor hoe ik dat het beste kon doen, heb ik goed opgelet op hoe de radiologen en laboranten handelden in soortgelijke situaties. Soms vertellen de radiologen dat de punctie beter nu direct kan gebeuren dan dat het later nog eens moet gebeuren. En eigenlijk zijn patiënten het er altijd mee eens. Een methode die ik ook meerdere keren heb gezien bij de radiologen is dat ze de patiënt heel duidelijk vertellen dat ze gaan starten. De reactie van de patiënt daarop geeft je eigenlijk veel informatie over hoe de patiënt erin staat. Vaak reageren ze bevestigend en dan start je rustig de procedure, maar een enkele keer merkt je dat het te snel gaat. En dan wordt er nog wat extra tijd gegeven aan de patiënt om wat rustiger te worden. De laboranten probeerden ook door het gesprek aan te gaan met de patiënten ze weer rustiger te krijgen en een beetje af te leiden. Ik heb wel bewondering voor hoe zij dat soms hebben gedaan.

Voor mij is het denk ik belangrijk om goed de grens tussen persoon en professional in de gaten te blijven houden. Hoewel het belangrijk is om de patiënt niet uit het oog te verliezen, moet het meeleven niet ten koste gaan van het functioneren. Ik merkte aan mezelf dat ik gedurende mijn afstudeerperiode namelijk wel beter werd om mijn handelen te plaatsen binnen het kader van mijn professionele functie. Als professional moet je gewoon bepaalde dingen doen, ook al zijn die niet prettig om te doen en is er risico dat iemand pijn of ongemakkelijkheid ervaart. Dus op momenten waar ik als “leek” direct het ongemak voor de patiënt zou willen oplossen, heb ik geleerd als professional zo te handelen dat de patiënt ondanks het ongemak toch de beste zorg krijgt. Zo heb ik erop gelet dat ik duidelijk, rustig en stapsgewijs uitleg gaf en heb ik veel om bevestiging of feedback van de patiënt gevraagd. Uiteindelijk gaat het erom dat de patiënt het gevoel heeft gehad goede zorg te hebben gekregen en dat die ondanks de moeilijke situatie en de vervelende procedure toch goed is behandeld en is ondersteund.

2.3. Prostaten beoordelen

Naast dat ik me heb verdiept in de mammadiagnostiek, heb ik ook meegekeken bij verscheidene andere specialisaties. Een van de dingen die ik heb gedaan is het mezelf aanleren MRI-scans van de prostaat te beoordelen. Een physician assistant in opleiding moest voor zijn opleiding een onderzoek uitvoeren. Hij heeft gekeken naar de toegevoegde waarde van kunstmatige intelligentie bij het leren beoordelen van MRI-scans. De software die gebruikt wordt, heeft de mogelijkheid om automatisch verdachte plekjes te markeren in de scans. Hij heeft voor zijn studie enkele radiologen in opleiding gevraagd 200 scans te beoordelen, waarbij ze voor de middelste 100 scans gebruik mochten maken van kunstmatige intelligentie. De hypothese was dat je door de extra feedback, sneller en beter in staat bent verdachte plekken op te sporen en te classificeren. Hij had echter nog iemand nodig die de 200 scans volledig zelfstandig ging beoordelen. Ik vond het erg leuk om te doen, omdat ik het als een uitdaging zag om mezelf iets volledig nieuws aan te gaan leren. Maar ik vond het ook wel spannend dat alle beslissingen waren gebaseerd op wat ik dacht en vond. Ook al zat er geen enkele consequentie aan vast voor een patiënt, ik behandelde het beoordelen van de scans wel alsof het wel het geval was.

Ik heb ook meegekeken toen mijn antwoorden snel werden gecontroleerd voor een eerste indruk. En ik vond persoonlijk dat het slechter had gekund. Ik zag in het grote aantal fout-positieven wel dat ik het moeilijk vond om een mogelijk verdacht plekje af te schrijven als onschuldig. Dat is niet geheel verrassend voor mij aangezien dat ook wel iets is wat ik bij mezelf herken in andere situaties. Zeker als ik geen referentie heb om op terug te vallen, dan ben ik geneigd dan maar voor de zekerheid uit te gaan van het slechtste geval. Voor iemand die moeite heeft met keuzes maken en conclusies

trekken zonder alle informatie te hebben en zonder zeker te zijn van z'n zaak, was deze taak dus wel een goede uitdaging.

Ik vond het een heel leerzame ervaring zowel op medisch niveau als op het niveau van een beroepsbeoefenaar. Op medisch niveau, heb ik in principe volledig zelfstandig een begin gemaakt aan het leren beoordelen van prostaatscans. Ook van het analyseren van de fouten die ik heb gemaakt, heb ik veel geleerd waardoor ik nu beter weet waar ik in het vervolg op zou moeten letten. Ik heb nu ook echt bewust ervaren dat als je maar iets vaak genoeg doet, de ervaring die je opdoet ervoor zorgt dat je jezelf bijstuurt en daardoor ook beter wordt dan dat je was. Ik vond het interessant om te merken dat ik op een gegeven moment andere keuzes maakte, omdat ik bijvoorbeeld bepaalde patronen begon te zien. Bovendien was het dus een goede oefening in keuzes maken. Het zal tijdens mijn professionele carrière nog wel vaker voorkomen dat niet alle informatie beschikbaar is en dat er dan toch knopen doorgehakt moeten worden. Ik heb daar nu laagdrempelig en zonder gevolgen hierin kunnen oefenen.

3. Academische ontwikkeling

3.1. Mijn werk presenteren aan anderen (in het Engels)

Ik heb regelmatig tijdens de studie presentaties moeten geven aan medestudenten en docenten. Presenteren voor medestudenten of voor je docenten of begeleiders vind ik zelfs al wel spannend, omdat je jezelf openstelt voor de oordelen en kritiek van anderen. Maar die mensen zijn in ieder geval al tot een bepaalde hoogte bekent met wat je aan het doen bent. Presenteren voor nieuwe mensen van buiten de groep vind ik lastiger. Want die mensen hebben misschien wel bepaalde verwachtingen van mij of van wat ik presenteer. En als het dan ook nog in het Engels moet, maakt het dat nog spannender. Ik weet dat ik in een rustige situatie best een prima niveau van Engels heb. Maar ik vind improviseren en snel de juiste woorden moeten vinden in het Engels lastig.

Ik heb tijdens mijn afstudeerperiode meerder keren mijn werk gepresenteerd voor mensen die niet deel zijn van de fotoakoestiek groep. Zo heb ik een keer mijn werk gepresenteerd voor een groep studenten uit Japan en een keer voor twee onderzoekers uit Amerika. Die presentaties vonden in de tweede helft van mijn afstuderen plaats. Ik merkte dat ik er minder gespannen voor was dan ik had verwacht. Omdat ik er al ruim een half jaar aan had gewerkt, had ik het gevoel dat ik goed wist wat ik aan het presenteren was. De keuzes die ik heb gemaakt, zijn al besproken met anderen en kan ik beargumenteren. Daardoor was ik er zekerder van dat wat ik presenteerde inhoudelijk goed was. De presentatie goed voorbereiden draait er voor mij minder om dat ik bij elke slide weet wat ik ga vertellen en hoe, maar meer dat ik goed weet waarom ik iets vertel en wat erachter zit. Als ik inhoudelijk goed voorbereid ben, dan kan ik tijdens de presentatie zelf wel wat improviseren. Maar als ik de presentatie uit mijn hoofd ken, maar niet zeker ben van wat ik presenteer, dan klap ik sneller dicht.

Als het gaat om het Engels, merk ik bij mezelf dat ik wat losser ben geworden tijdens het presenteren. Ik heb geprobeerd om mijn perfectionisme een beetje af te zwakken, omdat ik in het verleden merkte dat het me tegenhield om mijn boodschap goed over te brengen. Doordat ik me zo zorgen maakte over het Engels, kwam ik minder zeker over op inhoudelijk vlak. Het besef dat het uiteindelijk draait om dat de inhoud goed is overkomen en minder in dat het Engels perfect was, is wel wat meer gedaald. Die knop omzetten kostte even wat werk, maar heeft er wel voor gezorgd dat ik toch wat meer ontspannen ben geworden. Wel betrap ik mezelf er nog op dat ik achteraf nog wel eens nadenk over hoe ik dingen heb verwoord en hoe dat beter had gekund. Maar ik ben er beter in geworden om dat tijdens het presenteren zelf een beetje los te laten.

3.2. Hulp vragen

Ik heb de neiging om als een "lone wolf" aan de slag te gaan en te proberen alles zelf te doen. Ik vind het gewoon fijn om me helemaal op iets te kunnen storten zonder rekening te moeten houden met iemand anders. Maar soms kan ik erin doorslaan, omdat ik het idee heb dat dat hoort bij zelfstandig

zijn. Bovendien wil ik niemand tot last zijn met mijn “triviale” problemen. Ik zal daarom niet snel om hulp vragen, tenzij ik echt volledig vastloop en niet meer weet wat ik moet doen. Een nadeel is dat het ervoor zorgt dat ik alleen maar kan terugvallen op mijn eigen kennis en kunde. Dit kan beperkend zijn en ervoor zorgen dat ik te lang bezig ben met iets waardoor er tijd verloren gaat. Idealiter zou ik alles zelf weten en zelf kunnen, maar dat is niet realistisch. Ik heb deze afstudeerperiode geleerd dat het daarom juist de kunst is om goed gebruik te maken van de kennis en kunde van anderen. Door de hulp te vragen van anderen die meer expertise hebben in een specifiek veld, ben ik tot nieuwe inzichten gekomen of heb ik makkelijker keuzes gemaakt.

Ik heb gedurende mijn afstudeerperiode gemerkt dat ik het steeds iets makkelijker vond om hulp of advies te vragen van anderen. Aan het begin was ik heel terughoudend. Ik vroeg alleen om advies als iemand actief vroeg of ik nog vragen had of nog tegen problemen was aangelopen. Tijdens de tussenevaluatie, kreeg ik dan ook de feedback dat ik wel heel behulpzaam ben, maar ook zelf wat meer aan de bel mag trekken als dat nodig is. Vanaf toen probeerde ik er wat meer op te letten of ik niet onnodig te veel probeer alles zelf maar op te lossen. Ik probeer nog steeds wel eerst dingen zelf uit te zoeken, maar ik vind het makkelijker om te accepteren dat ik er niet zelf makkelijk uit ga komen. Ook gebruik ik hetgeen wat ik al heb geprobeerd om echt gericht te kunnen vragen om nieuwe inzichten.

Voor het ontwikkelen van mijn mal heb ik bijvoorbeeld echt gebruik gemaakt van de kennis van Johan van Espen. Hij heeft me geholpen met welke materialen en ontwerpen mogelijk zijn. Als ik dat allemaal zelf had moeten doen, dan was ik steeds blijven itereren zonder echt iets uit te proberen, omdat er zo veel opties te verzinnen zijn. Bovendien had het me meer tijd gekost, omdat ik weinig ervaring heb met goede ontwerpen maken. Maar ik weet nog dat ik de eerste meeting met hem over mijn mal heel spannend vond. Want misschien vond hij wel dat ik het makkelijk zelf had kunnen doen en verzinnen. Maar ik merkte al snel dat die zorgen nergens voor nodig waren.

Ik merk dat ik soms bepaalde dingen zeg om mezelf een beetje in te dekken, zoals “misschien een domme vraag”, “ik loop tegen iets kleins aan”, “alles gaat goed, maar ik loop wel tegen iets aan”. Ook al zijn de dingen waar ik tegenaan loop misschien helemaal niet zo insignificant, ik probeer het toch kleiner te maken, omdat het dan naar mijn idee minder belastend over komt. Ook ben ik nog vrij voorzichtig in wat ik van iemand durf te vragen. Ik laat me snel afschrikken door een negatieve reactie, omdat ik het snel persoonlijk opvat wat helemaal niet het geval hoeft te zijn. Dus ik moet er nog aan werken om zelfs als ik hulp vraag aan anderen, zelfverzekerd over te blijven komen en assertief te blijven. Door onzeker over te komen, loop je juist sneller risico denk ik dat mensen over je heen lopen en je snel wegwuiven waardoor je niet verder komt.

3.3. Multitasken

Voor een afstudeerproject moeten er verschillende stappen worden uitgevoerd om de hoofdvraag volledig te kunnen beantwoorden. En ik vond het managen van al die stappen dat aan het begin van mijn afstuderen een uitdagende taak. Ik ben over het algemeen goed in het gestructureerd aan het werk gaan en overzicht houden van wat ik aan het doen ben en wat er nog moet gebeuren. Ik ben echter wat minder goed in multitasking en met verschillende dingen tegelijk rekening houden, vandaar dat ik daar een leerpunt van heb gemaakt. Het liefst rond ik iets af voordat ik aan iets anders begin, omdat ik dan in ieder geval de mogelijkheid heb om mijn volledige aandacht op iets te richten.

Ik merkte al snel dat ik, zoals ik al had verwacht, vrij veel moeite had om alle verschillende dingen taken die ik moest doen goed in te delen. Achteraf gezien, had ik bepaalde dingen sneller kunnen doen als ik andere prioriteiten had gesteld. Dat had me veel tijd gescheeld, omdat ik dan niet allemaal tijd had besteed aan testen die uiteindelijk onnodig waren.

Ik had eigenlijk te weinig een goed idee hoe alles met elkaar verbonden was. Ik zag alles als afzonderlijke onderdelen binnen het project, waardoor het lastig was om te zien wat in het grote plaatje echt prioriteit had. Ook vond en vind ik het lastig om in te schatten van hoelang iets zou duren of een grens stellen aan hoeveel tijd ik aan iets wil besteden. Hierin heb ik ook last van mijn perfectionisme.

Ik vind het moeilijk om een taak los te laten als het nog niet goed is en door te gaan naar een volgend onderdeel. Soms is het echter beter om te weten dat een geheel werkt, om vervolgens alles te optimaliseren, dan om alle individuele componenten eerst te perfectioneren.

Ondanks dat ik er niet echt in ben geslaagd om beter te worden in het uitvoeren van taken parallel aan elkaar, denk ik wel dat ik handvaten heb om daar in het vervolg wel stappen in te maken. Het is niet genoeg om de hoofd- en bijzaken van de individuele onderwerpen van elkaar te onderscheiden. Ik moet ook gaan proberen echt onderling linken te gaan leggen tussen al die hoofd- en bijzaken en het grote plaatje in het achterhoofd te houden. Ik verwacht dat het makkelijker is om een goede planning te maken als ik beter weet hoe alles met elkaar verbonden is. Ook is het dan makkelijker om knelpunten te ontdekken en daarop te anticiperen.

3.4. Knopen doorhakken

Ik weet van mezelf dat ik slecht ben in het doorhakken van knopen, zeker als de gemaakte keuzes cruciaal aan voelen en ik niet alle informatie heb. Ik zoek graag zaken zo precies mogelijk uit en ben ook bereid om daar veel energie en tijd in te steken. Het risico wat ik loop is dat ik daardoor verzand raak in de details en het doel uit het oog verlies. Mijn leerdoel voor deze afstudeerperiode was om beter te worden in knopen doorhakken en sneller keuzes maken. Soms is perfectie namelijk niet het belangrijkste, zolang het einddoel maar wordt bereikt en ik kan uitleggen waarom bepaalde keuzes zijn gemaakt.

Helaas bleek dit toch een moeilijker leerdoel te zijn dan verwacht. Ondanks mijn voornemens, heb ik gemerkt dat ik toch vrij snel in mijn valkuil viel. De keuzes die ik maak zijn goed onderbouwt en systematisch, maar ze zijn niet snel gemaakt. Hoewel ik achteraf makkelijk de momenten kan identificeren waarin ik te lang ben blijven hangen en waar ik sneller had kunnen zijn, heb ik ten tijde niet herkend dat dat het geval was. Ik zit dan zo in mijn eigen tunnel, dat het eigenlijk al te laat is. Pas al iemand anders erop hint dat ik voor het einddoel misschien al wel genoeg informatie heb om een keus te maken, ga ik erover nadenken. Ik denk dat, omdat ik het zo lastig vind om keuzes te maken, ik ook makkelijk te beïnvloeden ben door anderen. Als iemand vraagt of ik wel zeker weet of ik alles genoeg heb uitgezocht, zal ik ondanks dat ik eigenlijk wel zeker ben, toch kijken of ik niet iets heb gemist. Want als iemand dat zegt, dan zou dat wel niet voor niks zijn. Ook al heb ik echt alles uitgedacht of uitgeprobeerd, ga ik dan toch aan mezelf twijfelen.

Ik heb de laatste paar maanden gemerkt dat ik het makkelijker vind om een keuze te maken als even met iemand heb kunnen sparren of overleggen. Die persoon hoeft niet direct te helpen een keuze te maken en hoeft ook geen eigen voorkeur te hebben. Maar ik heb soms gewoon iemand nodig tegen wie ik expliciet kan vertellen wat het dilemma is en wat mijn twijfels zijn. Als ik het nu voor mezelf probeer te doen, gaat mijn eigen gevoel beïnvloeden hoe ik dingen zie. De vragen, suggesties en inzichten van anderen zorgen bij mij op de een of andere manier ervoor dat ik wat meer afstand neem tot het probleem en echt kijk naar de hoofdlijnen. Zo heb ik meermaals wel gemerkt dat ik soms wel een voorkeur voor een keus heb, maar dat gevoel niet volg omdat het naar mijn idee niet goed genoeg beargumenteerd is. Maar als ik het dan probeer te verantwoorden naar iemand anders waarom dat wel het geval is, dan kom ik eigenlijk heel ver. Omdat je niet altijd iemand hebt die een klankboord kan zijn, is het wel goed om te zien of er geen strategie is die ik kan gebruiken om het proces wel volledig zelfstandig door te lopen.

4. Algemene professionele ontwikkeling

4.1. Mezelf uitspreken

Ondanks dat ik moeite heb met keuzes maken, ben ik wel iemand die goed weet wat die wil en wat ik ergens van vind. Juist doordat ik veel over mijn keuzes nadenk, weet ik als ik eenmaal ergens voor ga wel waarom dat zo is. Ik ben alleen ook iemand die zaken vrij dicht bij zichzelf houdt. Ik zal niet zo snel

iets met anderen delen, zeker niet als er niet direct naar wordt gevraagd. Dit heeft zeker betrekking tot niet-inhoudelijke dingen, maar tot op een zekere hoogte op inhoudelijke dingen. Ik ben me ervan bewust dat het goed kan zijn om soms dingen echt uit te spreken zodat er geen onjuiste aannames worden gemaakt. Gedurende de TG-schappen ben ik al actief bezig geweest om verwachtingen wat meer te managen en minder onbesproken te laten. Ik heb ervaren dat dit voor meer rust bij mezelf zorgt, omdat ik dan minder geneigd ben om alles te overdenken. Dus ook deze periode heb ik geprobeerd duidelijk voor mezelf te krijgen wat er van me wordt verwacht. In de feedback die ik tijdens mijn tussenevaluatie terugkreeg, bleek dat ik soms wel wat assertiever mag zijn en wat meer van en uit mezelf mag delen. Daardoor kan ik meer sturing geven aan mijn onderzoek en ook aan mijn eigen leerproces. Maar ook is het goed voor begeleiders of andere betrokkenen te weten als ik ergens meezit, omdat ze anders ook niet weten wat er speelt.

Er zijn wel enkele momenten geweest waarop ik me echt zorgen begon te maken over dat ik ergens geen progressie in zag. Er zijn meermaals dingen niet helemaal zo makkelijk of snel gegaan als dat ik het graag zou willen. Ik neem niet zo snel uit mezelf genoegen met resultaten die minder zijn dat het doel was. Zeker als ik weet dat ik eigenlijk geen tijd heb om door te gaan met blijven proberen die optimale resultaten te behalen, kan elke tegenslag extra hard aanvoelen. Ik merkte aan mezelf dat alle frustratie gecombineerd met de tijdsdruk ervoor zorgde dat ik mezelf helemaal in de stress aan het werken was. Daarnaast kostte het veel energie mezelf gemotiveerd te houden en ondanks de tegenslagen toch nog iets te vinden waar ik wel trots op kon zijn.

Ik heb mezelf er toen toch, ondanks dat ik er tegenop zag, ertoe gezet de stap te zetten om het met een begeleider te delen. Ik vond het wel spannend om zo transparant te zijn en iets anders van mezelf te laten zien dan de persoon die alles onder controle heeft en weet wat die doet. Waar ik me zorgen over maakte was dat het zou lijken alsof ik de kantjes ervan af aan het lopen was of gewoon er maar de pet naar gooide. Terwijl ik van mezelf echt wel weet dat dat niet het geval was. Er was veel begrip voor hoe ik me voelde en er werd me verteld dat niet perfecte resultaten ook resultaten zijn. Het belangrijkste is dat ik in de verslaglegging volledig ben, kan beargumenteren waarom de resultaten mogelijk niet optimaal zijn en wat er kan worden gedaan om de resultaten te verbeteren. Toen ik dat hoorde, voelde ik me rustiger worden. De erkenning dat ik ondanks de resultaten wel mijn best aan het doen was en hard werkte om het best mogelijke eruit te halen deed me goed.

Ik ben best trots op mezelf dat ik die stap heb gezet om aan te geven dat ik even helemaal vastliep. Het is iets waar ik echt moeite mee heb. Maar het zou nog mooier zijn, als ik het ook zou kunnen als ik niet al zo ver in mijn stress ben als dat ik toen was. Nu speelden er ook nog andere dingen een rol, zoals het feit dat de scanner kapotging in de laatste maanden. Maar toch denk ik dat als ik al eerder mijn zorgen had besproken, ik mezelf stress had kunnen besparen. Er is dus nog genoeg ruimte voor groei met betrekking tot dit leerdoel.

4.2. Mezelf positioneren in de onderzoeksgroep

Een van mijn leerdoelen was dat ik na 15 maanden een eigen positie in de onderzoeksgroep zou hebben ingenomen. Initieel gezien dacht ik dat de beste manier om dit doel te halen was om veel het initiatief te nemen en te proberen mezelf actief onder de groep te voegen. En in theorie denk ik nog steeds dat dit een goede methode is om mensen snel te leren kennen en je in te mengen in de groep. Ik merkte echter al snel dat het voor mij niet de beste strategie was, want het gaat zo tegen mijn eigen persoonlijkheid in dat het alleen maar averechts werkte. Omdat ik steeds de interne druk voelde om maar sociaal te zijn en te integreren, werd de drempel om met anderen te interacteren alleen maar hoger en leek alles alleen nog maar ongemakkelijker om te doen. Ik had vooraf het gevoel alsof ik echt mezelf moest hebben geïntegreerd met de groep, omdat ik het idee had dat het iets zou zijn waar je naar zou moeten streven. Maar contacten leggen, gaat bij mij nu eenmaal niet snel, laat staan als ik niet direct veel met bepaalde mensen of groepen te maken heb. Als student in de fotoakoestiek subgroep is het voor mij veel relevanter en interessanter om mezelf te kunnen profileren binnen die

groep dan binnen de volledige vakgroep. Dat is namelijk de groep mensen met wie ik echt moet samen werken en met wie het belangrijk is om een goed contact te hebben.

Binnen de fotoakoestiek groep heb ik wel het gevoel alsof ik echt een eigen plekje heb kunnen vinden en dat juist door gewoon dicht bij mezelf te blijven. Tijdens de tussenevaluatie kreeg ik te horen dat ik een vriendelijk, meegaand en betrokken collega ben. Ik ben geïnteresseerd in anderen en ben binnen de onderzoeksgroep een vrij stabiele factor. Ik laat me goed tijdens meetings zien en neem actief deel met discussies. Wel mocht ik nog iets meer mijn positie binnen de groep mogen opeisen en me krachtiger positioneren. Ik denk dat ik in de eerste helft ook nog vrij veel in mijn hoofd had dat ik “maar een student” ben en dus per definitie een andere positie innam. Ik denk dat ik echter in de tweede helft me wat meer bewust ben geworden van welke meerwaarde ik heb.

Mijn tijd op de mammadiagnostiek heeft me veel geleerd over alle stappen in het diagnostisch proces rondom borstkanker. Voor mijn rol als onderzoeker waren deze inzichten zeer nuttig, omdat het me een beter begrip heeft gegeven over de relevantie van mijn afstudeeropdracht. Maar door die klinische kennis kon ik me binnen de fotoakoestiek groep positioneren als iemand met een medisch-technisch specialisatie. Binnen de fotoakoestiek groep was er in de periode dat ik er afstudeerde geen andere student of onderzoeker met een achtergrond in technische geneeskunde. Met de kennis uit de praktijk, kon ik soms tijdens besprekingen iets inbrengen waar de rest niet van op de hoogte was en wat voor verheldering zorgde. Tijdens mijn bedrijfsstage was ik ook een van de weinige studenten met een technische geneeskunde achtergrond. Toen heb ik ook wel gemerkt wat voor een toegevoegde waarde iemand met een meer medische achtergrond kan zijn in de ontwikkeling van nieuwe medische technologie en de bijkomende onderzoeken. Maar tijdens die stage had ik maar een beperkte ervaring vanuit de praktijk, dus was mijn bijdrage op dat vlak iets minder uitgesproken.

Ook op het gebied van fantomen heb ik, doordat het de focus was van het afgelopen jaar, een soort van kleine specialisme erin opgebouwd. Ik heb niet alleen kennis over mijn eigen ervaring, maar ik weet ook wat andere studenten hebben geprobeerd. Daardoor ben ik net wat beter op de hoogte van de materialen en methodes die zijn gebruikt dan iemand die alleen de presentaties en verslagen heeft zien langskomen. Ik denk dat ik daardoor goede input kan geven als iemand soortgelijke materialen wil gaan gebruiken voor fantomen als dat ik heb gedaan.

4.3. Mezelf positioneren in de kliniek

Naast dat ik me in de onderzoeksgroep als professional wilde positioneren, wilde ik dat ook in de kliniek. Nu is het zo dat mijn onderzoek echt voor een groot deel op de universiteit moest plaatsvinden vanwege de werkzaamheden in het chemisch lab. Bovendien zat ik als ik in de kliniek zat voornamelijk bij de mammadiagnostiek. Ik heb daarom met name focus gelegd op mezelf te positioneren binnen het mammoteam als beginnende professional.

Het vertrouwen van de radiologen en hun goede begeleiding is een enorme hulp voor mij geweest om te groeien in mijn rol en vertrouwen te krijgen en in mijn vaardigheden. Ze gaven me de ruimte om de weg naar zelfstandig handelen zelf vorm te geven qua tempo en qua welke stappen ik wilde nemen. Aan de andere kant, gaven ze me soms ook wel een beetje een duwtje in de rug om net dat ene stapje te nemen waar ik tegenaan aan het hikken was. Ze gaven tijdens de tussenevaluatie namelijk wel aan dat ik nog wat zekerder mocht zijn van mijn eigen kunnen, maar dat dat ook met ervaring komt.

Ik heb wel het idee dat ik me bij de laboranten en de radiologen door wie ik gesuperviseerd werd heb bewezen en dat ik een plek voor mezelf heb kunnen maken. Aan het einde van het afstuderen was het bij de meeste ongecompliceerde cystepuncties en stereotactische puncties niet eens meer de vraag of ik het ging doen of de radioloog. Alleen bij histologische puncties en markerplaatsingen heb ik er nog wel eens voor gekozen om de radioloog het te laten doen, omdat ik de casus net te lastig vond. Maar dat waren bewuste keuzes waar ik achteraf ook nooit spijt van heb gehad.

4.4. Dingen accepteren zoals ze zijn

Een van de dingen waar ik gedurende het project meerdere keren tegenaan ben gelopen is dat ik door mijn perfectionisme het lastig vind om soms zaken te accepteren zoals ze zijn. Ik wil graag aan mezelf en aan anderen kunnen tonen dat ik het beste uit mezelf heb gehaald en dat wat ik dan uiteindelijk produceer “goed” is. Rationeel gezien kan ik heel goed begrijpen dat als je met iets nieuws bezig bent of iets nieuws uitprobeert, je nooit kan verwachten dat alles direct gaat zoals je wil. Maar als alle resultaten niet in mijn eigen gedefinieerde plaatje van “goed” passen, dan vind ik het lastig om dat begrip om te zetten in acceptatie. Maar ik zal wel wat stappen moeten zetten om wat gemakkelijker dingen te accepteren zoals ze zijn. Dit is belangrijk, zodat ik in de toekomst beter om kan gaan met uitdagingen en problemen en tegenvallen niet mijn zelfvertrouwen laat aantasten.

Ik denk dat de reden dat ik nu tijdens mijn afstuderen er moeite mee heb gehad is, omdat ik toch wel snel een vergelijking maak met hetgeen wat andere onderzoekers laten zien. En in een gepubliceerd artikel ziet alles er zo netjes en afgerond uit. En omdat ik altijd wel de lat hoog leg voor mezelf, maak ik mezelf wijs dat er wordt verwacht dat mijn werk net zo netjes en afgerond is. Ik kan binnen de tijd die ik heb echter niet blijven itereren totdat ik mijn “perfecte” plaatje heb bereikt. Ik zal soms genoegen moeten nemen met datgene wat kan in de tijd die ik heb. Daarnaast zal ik ook moeten leren accepteren dat goed ook goed genoeg kan en mag zijn. Mijn begeleiders hebben me indirect ook wel geholpen met dat acceptatieproces. Zij hebben regelmatig herhaald dat in onderzoek dingen eenmaal vaak anders gaan dan verwacht. Ook ben ik er door hun wel wat bewuster van geworden dat het doel van het afstuderen niet is om een onderzoek uit te voeren wat perfect is, maar dat ik heb laten zien dat ik de vaardigheden en kennis bezit om een wetenschappelijk onderzoek uit te voeren.

Ik was aan het begin van mijn opdracht daarnaast vrij ambitieus in mijn doelen. Ik heb soms de tijd die ik voor bepaalde stappen nodig zou hebben en de hoeveelheid werk die iets ging kosten onderschat. En omdat ik de hoogte van de lat niet automatisch bijstel als ik mijn plannen moet wijzigen, blijf ik streven naar doelen die soms niet meer realistisch of relevant zijn. Ik denk dat het voor mij in de toekomst daarom goed zou zijn om wat vaker bewust mijn plannen en doelen te evalueren en op basis daarvan mijn vervolgstappen te bepalen. Ik heb namelijk ervaren dat als ik dat doe, dat ik dan meer rust heb en mijn resultaten beter in de actuele context kan plaatsen.

Ondanks dat ik heb ervaren dat dingen accepteren zoals ze zijn nog niet gemakkelijk is voor mij, heb ik wel het idee dat ik mezelf daarin heb ontwikkeld de afgelopen periode. Ondanks dat ik nog steeds het liefst streef naar perfectie, ben ik er naar mijn gevoel wel wat beter in geworden om de situatie te zien zoals die is, tevreden te zijn met wat er wel is behaald en door te gaan naar een volgende stap. Zo vind ik dat ik eigenlijk toch wel ondanks alle uitdagingen die er waren en de gebreken in mijn project, wel heb kunnen laten zien wat ik kan en dat ik toch wel wat werk heb verzet.

5. Conclusie

Al met al, terugkijkend op de afgelopen 15 maanden heb ik wel het gevoel dat ik door de nieuwe ervaringen en door actief bezig te zijn met de leerdoelen stappen heb gemaakt met betrekking tot mijn professionele ontwikkeling. Zelfs bij de leerdoelen die niet met groot succes zijn behaald of de problemen waar ik tegen aanliep, heb ik het gevoel dat ik er door er op te reflecteren wat nuttigs uit heb gehaald waar ik in de toekomst mee verder kan. Wat betreft de kliniek heb ik duidelijk gemerkt dat ik langzaamaan zelfverzekerder werd in mijn houding en dat ik ook steeds meer vertrouwen kreeg in mijn vaardigheden. Ook vind ik dat ik het niveau van zelfstandigheid in de kliniek heb behaald die ik voor mijzelf als realistisch ervaar. Ik ben namelijk toch gegaan van iemand die het spannend vindt om onder directe supervisie een echoprobe op iemand te zetten naar iemand die zelfstandig een echogeleide punctie kan uitvoeren. Wat betreft mijn academische ontwikkeling, is het allemaal met wat meer vallen en opstaan gegaan. Ondanks de goede voornemens om sneller keuzes te maken en goed mijn aandacht te verdelen tussen alle taken die gedaan moeten worden, blijven het struikelpunten waar ik zonder dat ik het door heb in mijn valkuilen stap. Dat blijven nog wel

aandachtspunten waar ik in de toekomst nog genoeg aan zal kunnen werken. Wel denk ik dat ik tijdens deze afstudeerperiode tot nieuwe inzichten ben gekomen die me kunnen helpen. Een van de successen waar ik persoonlijk wel trots op ben is dat ik er voor mijn gevoel in ben geslaagd om zowel binnen de mammadiagnostiek als de fotoakoestiek groep een plekje voor mezelf te creëren waar ik me goed in voel. Op mijn eigen tempo en op een manier die bij mij past, heb ik mensen laten zien wie ik als professional ben en wat ik kan.

Part II: Research Assignment

Abstract

Research Background: Currently, breast cancer has become the most commonly diagnosed cancer type. One up-and-coming imaging technique for breast imaging is photoacoustic imaging (PAI). At the University of Twente, a 3D photoacoustic breast tomography system has been developed, the Twente Photoacoustic Mammoscope (PAM) 3. Various research groups have studied how skin tone influences 2D PAI systems. While the results of these various studies are highly informative, no study has yet been published on the influence of skin tone on 3D PAI performance.

Aim: This study aims to investigate the influence of pigmentation on the imaging performance of the PAM3 system for photoacoustic breast imaging. These insights are important to better understand the limitations of the system and guide its further development towards clinical impact.

Methods: In this study, the influence of skin tone on the image quality of photoacoustic breast imaging was explored with the use of phantom experiments and in vivo experiments. Three novel breast phantoms with a skin-mimicking layer were developed. The skin layer of each phantom was imparted with an absorption coefficient, using a melanin-mimicking substance, to match a small selection of skin tones. These phantoms were imaged with the PAM3 system using six wavelengths in the range of 680 to 1060 nm. To assess the influence of skin tone on the imaging performance, the imaging depth, the signal-to-background ratio (SBR) of various targets the occurrence of artefacts and the photoacoustic spectra of the skin were determined. A similar analysis was conducted on the already available data of three volunteers with different skin tones in a volunteer case study.

Results: Copolymer-in-oil doped with alcohol-soluble nigrosine dye, mimicking melanin, dissolved in ethanol, was shaped into a 1 mm thick skin-mimicking layer. Different skin tones were obtained by adjusting the concentration of nigrosine. Each of the three breast phantoms has a hemispherical geometry and consists of a skin-mimicking layer covering a base material. For this base material, a mixture of native gel wax, paraffine and TiO_2 was used, to mimic fatty breast tissue. Four straight channels with a diameter of 3 mm run through the phantom and function as imaging targets. For the phantom study, these channels were filled with an inorganic blood-mimicking fluid (a mixture of nickel and copper sulphate solutions) with each a specific absorption spectrum. The phantom study and volunteer case study show that the imaging depth and the SBR seem to be significantly compromised by skin tone. For longer wavelengths, e.g. 797, 833 and 870 nm, the PAM3 shows a smaller decline in the imaging performance for darker skin tones.

Discussion and conclusion: In this study, the influence of skin tone on the imaging performance of the PAM3 system for breast imaging was explored. The results are highly suggestive for a significant decrease in imaging depth and SBR, and thus the detectability, of the imaging targets. The results also show that the use of longer wavelengths for imaging the breasts for darker skin tones might be advantageous. However, there were some major limitations in the phantom study and volunteer case study. The skin-mimicking layers of the phantoms were not homogeneous, and the base material of the phantom contained air bubbles. These flaws could have influenced the results. The three volunteers from the volunteer case study had different breast sizes and the breast tissue composition was most likely different for each volunteer. Consequently, it is not possible to directly compare the results of the volunteers. Nonetheless, this study showed how relevant the investigation of an inadvertent technical “racial” bias for PAI is and that compensation methods are necessary before photoacoustic breast imaging can be accessible for clinical practice.

Keywords: Photoacoustic, tomography, hemispherical, breast imaging, skin tone, phantom study, volunteer case study

Table of contents

List of figures

List of tables

Chapter 1

1. General introduction

Currently, breast cancer has become the most commonly diagnosed cancer type worldwide. One out of four new female cancer patients are breast cancer patients, and one out of six cancer-related deaths are caused by breast cancer [1]. Arnold et al. estimated that the increase in breast cancer incidence and the number of breast cancer-related deaths will persist [1]. It can be expected that with a rise in breast cancer cases, a rise in the burden of breast cancer care on the healthcare system will follow [1]. Efficient and effective diagnostic imaging for breast cancer is therefore an important and relevant research topic for the medical imaging field.

New imaging techniques to improve the diagnostic process for breast cancer are being studied and developed. One of these up-and-coming techniques is photoacoustic (PA) imaging, also known as optoacoustic imaging [2]. When PAI is used to obtain a 3D scan, it is known as photoacoustic tomography (PAT) [3]. The core value of PA imaging (PAI) in the identification of malignant tumours lies in the ability of PAI to exploit one of the hallmarks of cancer, increased angiogenesis [4,5]. By selecting specific wavelengths to maximise differences in optical absorption, PAI can visualise blood vessels with high contrast [5,6]. In cancerous tissue, there is often an abnormal stimulation of angiogenesis to provide the malignant tumour with nutrients and oxygen. In general, this rapidly formed microvascular network is highly disorganised and consists of abnormally shaped and leaky vessels [4,5]. By visualising and identifying these abnormal vessel structures in PA images, it is possible to locate a malignant tumour [4]. Not only can PAI visualise the vascularisation, but it also has the potential to provide quantitative information about the imaged tissue. An important example of quantitative PAI is the ability to create maps that are related to oxygen saturation (sO_2) [5,7]. The ability to provide both morphological and functional information is why PA is considered a promising imaging modality for various purposes within breast imaging, from diagnostics to treatment assessment [8,9].

Despite the promising outlook for PA in breast imaging, the influence of skin tone on the reconstructed image is not yet fully understood. Manohar et al. suggested in 2019 that while skin tone was estimated to have a marginal effect on PA breast imaging, it would be useful to investigate it further [4]. Since then, it has been discovered that the influence of skin tone on PAI is of more significance than expected. The influence of melanin, a major determinant of skin tone [10,11], on PA imaging can be divided into two components. As a strong absorber, melanin can cause a significant decrease in the optical fluence, in other words, the number of available photons, in the underlying tissue layers. As a result, the penetration depth and therefore the imaging depth decreases [12–15]. Additionally, in 2D PAI, melanin can cause the presence of indirect clutter artefacts, which reduce image quality [12]. The origin of clutter artefacts lies in high amplitude acoustic waves that can be produced when there is a combination of strong absorbers and a high fluence. These so-called clutter waves propagate and can be reflected by acoustic heterogeneities. Detected clutter waves can overpower the actual PA signals that come from the surface layers and influence image reconstruction [13,14,16]. As the difference in skin tone is largely determined by differences in melanin content and distribution, it can be imagined that skin tone does influence PA breast imaging leading to an unintentional racial bias.

Various research groups have studied how PAI systems are influenced by skin tone. Else et al. and Vogt et al. have studied its influence using phantoms with which they mimicked different skin tones

and analysed how the image quality of the PA scans was affected [17,18]. Else et al. also explored the effects of skin tone on quantitative PAI. Their study was not limited to only phantom experiments, but it also incorporated computer simulations and small-animal experiments [17]. Several other research groups that have focussed on studying the challenge skin tone poses for PAI have performed volunteer studies [12–15]. The in vivo results showed that a darker skin tone results in a decreased imaging depth. This decrease can result in a reduced visibility of blood vessels as well [12,15]. Mantri et al. also discovered that a reduced image quality and penetration depth can lead to unintended biases in the sO_2 measurements in subjects with a darker skin tone [12]. To characterise the skin tone of their subjects, Li et al. [15] and Mantri et al. used the Fitzpatrick skin phototypes (FSP). However, the use of the FSP for characterising skin tone has become controversial in part due to the subjectivity of the method. Furthermore, the validity and reliability of characterising skin tone with the FSP are criticised in several papers [10,19]. It is therefore preferable to characterise the skin tone objectively and quantitatively. Fernandes et al. for instance classified the skin tones of the volunteers in their study quantitatively with the use of the Individual typology angle (ITA°) [13,14].

The results of the various studies with 2D PAI systems and the virtual trials for 3D PA breast imaging are highly informative. They show clear evidence that 2D PAI systems require some compensation method to reduce the effects of skin tone on the reconstructed PA images. Nonetheless, the obtained insights cannot be translated directly to 3D PAT systems [12]. The occurrence of clutter-like artefacts due to the highly absorbing melanin in the skin for instance might only occur in linear array PA systems [12]. However, no study has yet been published in which the influence of skin tone on PAT has been investigated in either a phantom or a volunteer study. Thus far, only virtual trials, courtesy of Park et al., have been used to investigate skin tone on the detectability of lesions in PA breast imaging [20,21]. For further development of PAT and its translation to the clinic, it is therefore imperative that a good understanding is obtained of the influence of skin pigmentation on PAT.

At the University of Twente, a PA tomography system specifically for 3D breast imaging was developed called the Twente Photoacoustic Mammoscope (PAM) 3. In this study, the influence of skin tone on this 3D PA breast imaging will be explored with the use of phantom experiments and a volunteer case study.

Chapter 2

2. Clinical context

In this chapter of the thesis, some in-depth information will be given about the anatomy of the breast, breast cancer and the main medical imaging modalities used during the diagnostic process. The purpose of this chapter is to give some clinical context to the project since the PAM3 is a dedicated PAT system for the breast, with one of its major purposes being the imaging of breast cancer. While this project itself is not specifically focused on breast cancer imaging, it is part of a larger research project that aims to develop a new imaging device for breast imaging.

2.1. The breast

The breast consists mainly of fibroglandular tissue surrounded by adipose tissue (See Figure 1) [22]. The breasts have their own network of arteries, veins, and lymph vessels. The lymph is mostly drained towards the axillary lymph nodes. This is why these are the most important lymph nodes with regard to breast cancer and the development of metastases. Nonetheless, lymph with malignant cells might drain to other lymph nodes [22]. The fibroglandular tissue, the functional part of the breast in which the milk is produced [23], can be divided into glandular tissue and supporting fibrous tissue. The glandular tissue is attached to the skin for support via fibrous connective tissue called the suspensory ligaments [22]. While both women and men have breasts, the glandular tissue usually only develops fully in women [22]. The density of the female breast is defined by the ratio between fibroglandular tissue and adipose tissue. This ratio varies between individuals and is determined by different factors, such as age and hormone levels [22]. The nipple is located at the greatest prominence of the breast. The nipple as well as a circular area of skin around it, which is called the areola, are more pigmented than the rest of the skin [22].

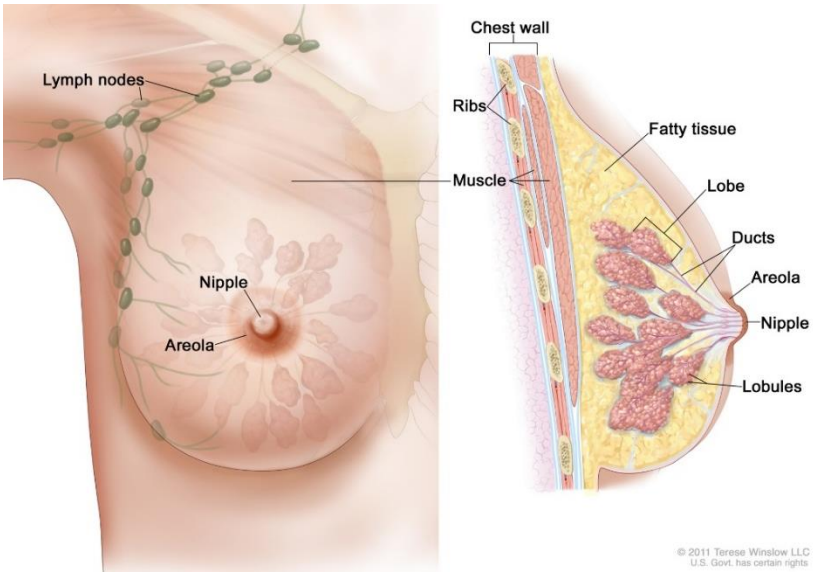

Figure 1: The anatomy of the female breast [24].

2.2. Breast cancer in the female population

Breast cancer is most often found in the upper outer quadrant of the breast, but it can occur anywhere in the breast where there is glandular tissue [25]. The majority of malignant breast tumours originate from the milk ducts in the glandular tissue [22]. These tumours, classified as invasive ductal carcinoma non-special type, occur in 50-70% of the cases. The second most common breast cancer type, with a prevalence of 5-15%, is invasive lobular carcinoma. Examples of rarer malignant breast tumour types are mucinous carcinoma and metaplastic carcinoma [25].

In many cases of breast cancer, the patient presents to the physician with complaints of a palpable lump in the breast [25]. However, the presence of various visual characteristics can also point towards the presence of a malignant breast tumour. Of these signs is the presence of abnormal breast contours caused by a tumour. Furthermore, there can be dimpling of the breast. This is due to the invasion of cancer into surrounding glandular tissue and fibrosis, which can cause tension on or shortening of the suspensory ligaments. When this occurs behind the nipple, it can lead to nipple retraction. Thirdly, if the tumour blocks the lymph drainage, fluid can build up in the subcutaneous tissue, resulting in lymphedema. This in turn can lead to deviations in the shape and location of the nipple and a thickened skin with prominent pores. In the medical field, this phenomenon is also known as the peau d'orange sign [22].

Breast cancer can invade nearby tissue types such as the fascia of the pectoral muscle underneath the breast. However, it can also spread throughout the body to locations further away from the breast. Generally, breast cancer initially metastasises via the lymphatic system. As mentioned before, most of the lymph is drained via the axillary nodes. This explains why lymph node metastases most commonly occur in the axilla. However, occasionally lymph node metastases can be found in other lymph nodes, such as the ones around the clavicle. Cancer cells can invade tissue further away from the breast through the lymphatic and blood vessels. When cancer spreads through the lymphogenic metastasis pathway, it often invades the organs in the abdomen and the contralateral (opposite) breast. Hemogenic metastasis occurs when the cancer cells are transported through the body after venous drainage via the posterior intercostal veins. The organs affected are usually the vertebrae, the brain, and the cranium [22].

2.3. Imaging modalities for breast cancer diagnosis

For the diagnosis of breast cancer, various imaging modalities can be used (See Figure 2). Mammography is the standard technique used for breast cancer screening and uses X-rays for the image formation. It is the initial modality used for diagnosis following an abnormal screening mammogram or a referral from a general practitioner for women older than 30 years with breast complaints [7,26]. However, this technique has some drawbacks. Some women experience the compression of the breast during the examination as uncomfortable or painful [27]. Another disadvantage of mammography is the strong decrease in diagnostic sensitivity for patients with radiodense breast tissue or strongly heterogeneous breasts [5,27].

A second imaging technique used for breast imaging is ultrasound (US). Clinicians generally use US as an additional imaging modality and rarely as a standalone modality. US allows an excellent view of the anatomical morphology of the breast [5,7]. This makes US an excellent modality to thoroughly examine regions in which the patient has complaints or where other imaging modalities have shown abnormalities. However, the small field of view strongly limits its suitability for screening the whole breast for lesions. It is, therefore, that with some exceptions US is in general not used as an alternative for mammography as an initial imaging modality. An exception is for instance made for female patients younger than 30 years. For this group, US is the standard primary imaging modality [26]. Other disadvantages of US besides the limited field of view are that US suffers from both a high false positive rate and a high inter-operative variability [5,7]. In 70% of the cases in which the mammography and US

are suggestive of malignancy (BIRADS classifications 4 and 5 [26,28]), the biopsy results are negative [5].

Magnetic resonance imaging (MRI) is another imaging modality that can be used for breast imaging. To better visualise breast lesions, gadolinium-based contrast agents are injected intravenously [4]. MRI is used in cases where mammography and US give inconclusive or conflicting results. It is also the imaging modality used when for treatment purposes more information is needed about the cancerous tissue. The benefit of MRI for breast imaging is that it has a high sensitivity and low specificity for detecting breast cancer [5,7]. A disadvantage, however, is that it is a relatively expensive modality that is not widely available everywhere. Furthermore, not all patients who have an indication for an MRI scan can undergo the examination. This is for instance the case for patients who are allergic to the contrast agent, suffer from or are at risk of impairment of their renal function, suffer from claustrophobia, or have regular pacemakers or certain metal objects in their body [4,27].

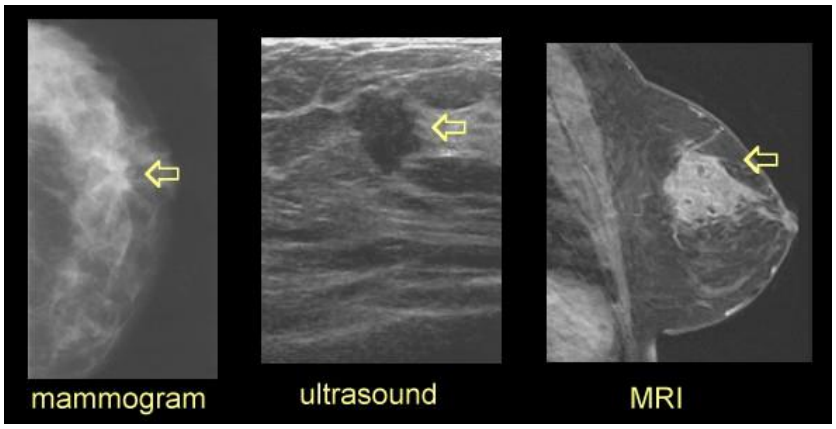

Figure 2: Visualisation of a breast mass on a mammogram, an ultrasound image, and an MRI view [29].

Chapter 3

3. Problem description

Various research groups are investigating new or alternative imaging methods for conventional breast imaging modalities due to their aforementioned respective disadvantages [30–32]. Other researchers are studying how adaptations of conventional imaging methods, such as contrast-enhanced mammography, dedicated breast CT, and transmission ultrasound tomography, can contribute to breast imaging [33–35]. As mentioned before, PAI is an up-and-coming imaging technique. Its application for breast cancer imaging has been studied extensively for the last few decades [36]. However, only in the last few years has there been recognition of the possibility of an unintended racial bias in PAI, due to the absorption of light by melanin in the skin. A paper showcasing the influence of skin tone on a hemispherical PAT system for breast imaging has yet to be published. The aim of this project is therefore to investigate the influence that melanin has on PAI of the breast using the PAM3 system. Considering the results of the studies in which linear or curved PA probes were used, there is a reasonable likelihood that skin tone will have an influence on the quality of the breast scans made with the PAM3 system. However, it is still important to thoroughly investigate this matter for this system to understand the extent of the influence. Thus, the research question of this thesis can be formulated as: *What is the effect of skin pigmentation on the imaging performance of a photoacoustic computed tomography system, most specifically for the PAM3 system, in imaging the breast?*

To answer the research question, the project has been divided into various phases. To give some structure to these phases a set of sub-research questions has been composed:

- *How can the human skin be mimicked adequately for photoacoustic imaging experiments with a physical phantom?*
- *How can a simplified physical breast phantom with a skin-mimicking layer be developed that is suitable for experimentation using the PAM3 system?*
- *What changes can be found in the image quality between 3D photoacoustic scans made of physical phantoms that represent women with different skin tones?*
- *What changes can be found in the image performance of the PAM3 system between 3D photoacoustic scans made of the breasts of volunteers with different skin tones?*

Chapter 4

4. Development of a skin-mimicking material

4.1. Introduction

During the COVID-19 period, new insights were gained into the possible presence of an unintended racial bias in optical medical devices such as pulse oximetry devices [12]. These insights have highlighted the necessity to investigate, in depth, how skin tone influences optical imaging techniques. This has spurred multiple research groups in the field of photoacoustic imaging (PAI) to also investigate the unintended racial bias for this particular modality [12,14,17,18,37]. One strategy that can be explored to investigate the performance of PAI is to perform phantom experiments with tissue-mimicking physical phantoms.

The last couple of years have seen great advancements in the development of both tissue-mimicking materials and phantoms that are compatible with PAI [38–41]. However, there is a lack of experience in how to merge these fields and develop well-characterised phantoms with skin-mimicking layers suitable for PAI experiments [18]. Phantoms in which the skin is mimicked have been developed for some time already for other imaging modalities [42,43], including other types of optical imaging systems [44–46]. However, the materials commonly used for the development of these skin phantoms are often not suitable for application in PAI experiments [18]. Hence, the development of an appropriate phantom material represents a major bottleneck in the advancement of skin phantoms for PAI.

Two studies have been published relatively recently in which a skin-mimicking layer was developed to investigate the influence of skin tone on PAI. Else et al. used agarose in combination with intralipid and synthetic melanin for their skin-mimicking material [17]. However, agarose has a short-term stability, which limits the reuse of the material [47]. Conversely, Vogt et al. have used polyvinyl chloride plastisol (PVCP) for the material of their phantom and added alcohol-soluble nigrosin and TiO_2 to tune the optical properties [18]. While PVCP is a much more stable material than agarose, there is as of yet no standard supply chain for the necessary ground materials. Moreover, plasticizers based on phthalates are under regulatory oversight due to their toxicity [47].

Not only is the development of an adequate phantom dependent on the suitable materials that are available but also on the shape of the phantom. A major goal of this project is therefore to develop an alternative skin-mimicking layer that can be used to fabricate a skin layer on phantoms compatible with the Twente Photoacoustic Mammoscope (PAM) 3 system. This part of the thesis will delve into the process of the development of the skin-mimicking material and elucidate the extent to which optical properties of the skin can be mimicked by the material.

Related sub-research question:

- *How can the human skin be mimicked adequately for photoacoustic imaging experiments with a physical phantom?*

4.2. Background

For the development of a skin-mimicking layer, it is important to have a good comprehension of the composition of the skin and how different skin tones can be distinguished from each other. In addition, to understand the essential parts in the development of a skin-mimicking layer, some basic knowledge about the underlying principle of PAI is essential. This is necessary to ensure that a material is developed that produces realistic signals for photoacoustic tomography (PAT). It is therefore that in this section some additional background will be given about the skin, the different methods to classify skin tone and the theory behind PAI.

4.2.1. The skin

The skin can be divided into three distinct layers: the epidermis, the dermis and the subcutis [48]. The properties and structure of the skin layers depend on several factors including age, sex, ethnicity, and body part [49]. The thickness of the skin for instance differs depending on the location of the skin on the body. Monnier et al. found that in the chest area, the total thickness of the skin can be 0.6-2.7 mm [38] and the thickness of the epidermis alone can be around 54.3 µm [50]. Oltulu et al. on the other hand found a mean total skin thickness of 4.8 mm and a mean epidermal thickness of 76.9 µm for the female breast [51].

In discussions about skin tone, a distinction must be made between facultative and constitutive skin tone. Constitutive skin tone is genetically determined, whereas facultative skin tone also depends on environmental factors such as sun exposure [10]. The skin tone is mainly dictated by the number of melanin-filled melanosomes in the epidermis and the haemoglobin in the dermis. However, the contribution of haemoglobin is minor in comparison to that of melanin. Moreover, the influence of haemoglobin is more apparent in lighter skin tones [52]. Other examples of pigments in the skin are bilirubin, carotenoids, and porphyrins [53].

Melanosomes are formed by melanocytes and then transported to keratinocytes, the principal cells of the epidermis [52]. The number of melanosomes in the skin can be expressed as a volume fraction. The volume fraction of melanosomes (M_f) in the human epidermis can be divided into three ranges: 1-3% for very light-pigmented skin, 11-16% for moderately-pigmented skin, and 18-43% for dark-pigmented skin [54]. In darker skin, melanosomes are not only present in larger quantities, but they are also larger and filled with a higher quantity of melanin than in lighter skin tones [12,52]. The increased size and melanin concentration in melanosomes leads to an increase in the absorption cross-section [12]. Additionally, the distribution of melanosomes in the dermis is different for a lighter skin tone compared to a darker skin tone. In a lighter skin tone, the melanosomes are mostly clustered together above the nucleus to protect the DNA from the ultraviolet radiation of the sun. In darker skin tones, on the other hand, the distribution of melanosomes is more widespread throughout the whole epidermis. Furthermore, the melanosomes are also more likely to be present in the extracellular matrix as well [52]. A schematic representation can be found in Figure 3.

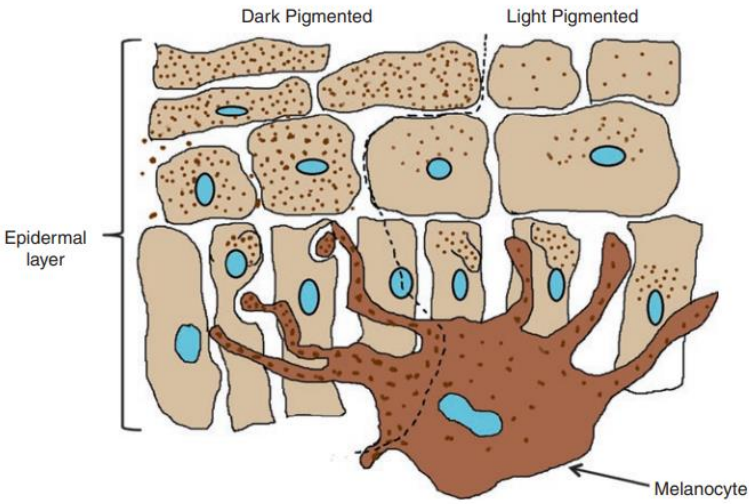

Figure 3: Difference in melanosome distribution between dark and light skin [52].

4.2.2. Skin tone characterisation

The differences in melanin content and other chromophores in the skin result in a broad range of different skin tones. The classification of these skin tones into different groups has been done for many years and various purposes. The characterisation of the skin tone can be accomplished using subjective and objective methods.

Subjective methods include the use of the Fitzpatrick skin phototypes (FSP) and colour charts. The FSP was originally developed to characterise light-coloured skin (FSP I up to IV) based on its behaviour towards sun exposure. It therefore not directly based on the actual pigmentation levels in the skin. To classify darker skin tones as well, FSP V and VI were added to the scale (See Figure 4). However, this illustrates an inherent problem of the FSP. While there is variation between darker skin tones, this broad range is grouped into just two types [55,56]. This causes a lack of subtlety in characterising darker skin colours.

Objective methods to investigate skin tone include optical measurements, histological analysis, and high-performance liquid chromatography (HPLC). Histological analysis and HPLC are invasive methods since they require skin samples to be taken to assess the melanin content. These methods are therefore regarded as unsuitable for clinical practice. An alternative, more practical, method to objectively classify skin tone is to use optical measurements. There are different devices available that can be used for these measurements. These devices can roughly be divided into colorimeters and spectrophotometers. Both types of devices are generally based on reflectance measurements of light in the visible and near-infrared spectrum [57]. Depending on the device and manufacturer, different metrics for the pigmentation level can be given as outputs. The most used metrics are the melanin index (MI), the CIE L*a*b* values, and the individual typology angle (ITA) values (which are specifically developed for skin tone assessment) (See Figure 5). The ITA values are derived from CIE L*a*b* values, and can be calculated with the following equation [55]:

$$ITA° = \tan^{-1}\left(\frac{L-50}{b}\right) \cdot \frac{180}{\pi}$$

While the MI values correspond to a certain melanin concentration in the skin, the precise definition of this metric is not standardised. The equation utilised to compute this metric can differ across devices and manufacturers [57]. One of the difficulties encountered in measuring the skin tone with these optical devices is the fluctuating level of erythema at the measurement site. The amount of blood in the skin could potentially influence the measurements. This is due to an overlap in the absorbance spectra of haemoglobin and melanin. The extent to which the MI values are affected depends on the

wavelengths used in the measurement [58,59]. However, some manufacturers claim that their device can correctly differentiate between melanin and erythema [59].

Figure 4: The Fitzpatrick skin phototype scale, a subjective classification method for skin tone [60].

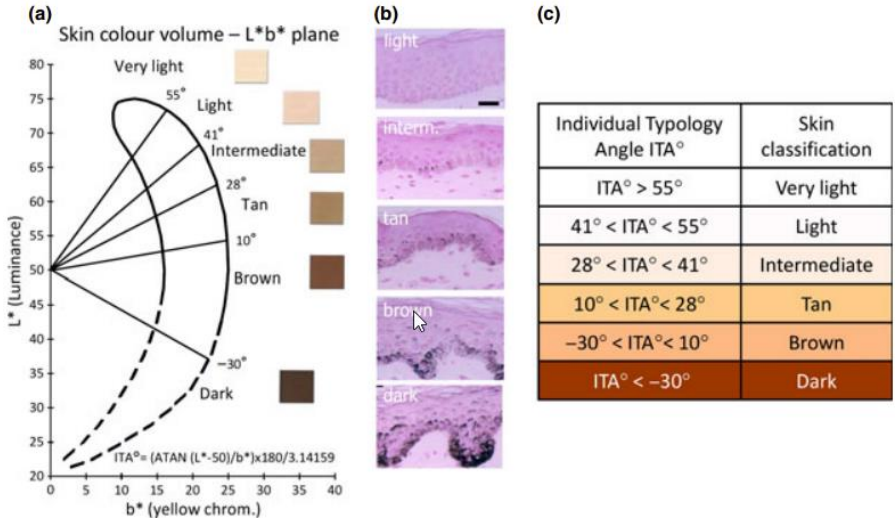

Individual Typology Angle ITA°	Skin classification
ITA° > 55°	Very light
41° < ITA° < 55°	Light
28° < ITA° < 41°	Intermediate
10° < ITA°< 28°	Tan
−30° < ITA°< 10°	Brown
ITA° < −30°	Dark

Figure 5: The ITA° values, used to characterise skin tone more objectively [61].

4.2.3. Theory behind photoacoustic imaging

PAI can be categorised as a hybrid imaging method since both light and ultrasound are involved in the formation of the images. The basis of PAI lies in the photoacoustic effect [3]. In PAI, tissue is irradiated with short-pulsed light, usually of a specific wavelength. The light is absorbed, which causes an initial rise in local temperature, which in turn induces a pressure rise and the formation of acoustic waves. These waves contain frequencies in the range of megahertz, which can be detected using ultrasound (US) transducers. Unlike light, which scatters strongly in tissue, acoustic waves can propagate relatively far in their original direction. This is why PAI retains a relatively high spatial resolution for deeper tissue layers in comparison to purely optical modalities [3]. In PAT, the object of interest is illuminated, and PA signals are acquired from different angles around the object. Using a reconstruction algorithm, such as universal back-projection or time reversal, a 3D PA image is generated [3,62].

For PA waves to be generated, the duration of the light pulse must meet two criteria. The duration needs to be shorter than both the thermal relaxation time (τ_{th}) and the stress relaxation time (τ_s). τ_{th} depends on the desired spatial resolution and the thermal diffusivity of the absorbing tissue. τ_s on the other hand depends on the speed of sound in the absorbing tissue and the desired spatial resolution [3]. With a pulse duration shorter than τ_{th} and τ_s, there is stress and thermal confinement within the absorbing tissue. This means that the fractional volume increase of the tissue is negligible, and the initial pressure rise (p_0) can be described as [3,62]:

$$p_0(\vec{r}) = \Gamma \eta_{th} \mu_a F(\vec{r})$$

This equation shows that $p_0(\vec{r})$ is proportional to the local optical fluence ($\mathrm{F}(\vec{\mathrm{r}})$), the absorption coefficient (μ_a), the efficiency in which the absorbed light is converted to heat in percentage (η_{th}), and the dimensionless Gruneisen parameter (Γ). Despite that Γ and η_{th} are tissue type specific, they are often assumed to be constants for practical reasons. This assumption has the consequence that, if F is known, μ_a can be recovered from the measured p_0 [3].

The propagation of the generated acoustic wave in tissue can be described by the general photoacoustic equation [3,63]:

$$\left(\nabla^2 - \frac{1}{v_s^2}\frac{\partial^2}{\partial t^2}\right) p(\vec{r}, t) = -\frac{\beta}{C_P}\frac{\partial H(\vec{r}, t)}{\partial t}$$

In this equation v_s is the speed of sound in the medium, C_P is the specific heat capacity at constant pressure, and β is the thermal expansion coefficient. $p(\vec{r}, t)$ is the acoustic pressure at position $\vec{r}$ at time t. $H(\vec{r}, t)$ is the heating function, which describes the amount of deposited thermal energy per unit volume and per unit time [3]. It is related to the deposited optical energy by the following equation [3]:

$$H(\vec{r}, t) = \eta_{th} \mu_a \phi$$

The fluence rate (φ) is the first time derivative of the optical fluence. In the photoacoustic equation, the source term for the acoustic wave is associated with the time derivative of H. This is why in practice PA waves can only be generated with a pulsed light source and not with a continuous light source [63].

The light used in PAI has a low intensity and is non-ionising. Consequently, PAI does not have the same health hazards as imaging modalities in which ionising radiation is used such as mammography [36]. Since the generation of the PA signal depends on μ_a, the contrast in the PA images is provided by differences in the absorption of the used wavelength(s). To image a specific tissue type or material, its absorption of the used light has to be sufficiently high to create a detectible signal. This means that by picking the correct wavelengths, in theory, any material that absorbs light can be imaged. In situations in which endogenous contrast is insufficient, exogenous contrast agents can be used to create or increase the contrast [3].

4.3. Requirements

The requirements for a sufficiently adequate skin-mimicking layer are directly associated with the material properties that stand at the basis of PAI: the optical properties and the acoustic properties. As described in Section 4.2.3, the formation of PA signals for a given imaging wavelength depends on the ability of a specific substance to absorb that particular light [3]. As mentioned in Section 4.2.1. the skin tone is mainly determined by the melanin content in the epidermis. While there are other chromophores present in the different skin layers, they can be assumed to be of less interest [52]. The minimal requirement for the skin layer is therefore that it mimics the melanin-containing epidermis. A benefit of only mimicking the epidermis is the reduced complexity of the skin-mimicking layer. This

reductionist approach can be seen as well in the phantoms of Else et al. and Vogt et al. [17,18]. For the development of a skin-mimicking material with similar properties as the epidermis, a careful selection of materials is necessary. This section will go into the different requirements for the melanin-mimicking substance, which is the substance that will mimic the absorption properties of melanin, and the basis material of the skin-mimicking material, which is the material in which the melanin-mimicking substance is embedded.

4.3.1. Requirements basis skin-mimicking layer

The basis material for the skin-mimicking material is important for the mechanical properties of the final material and how the material can be further processed into a phantom. And for it to realistically mimic the properties of the epidermis at the site of the breast it has to comply with a few requirements.

The requirements itself, the rationale and the consequences for the practical implementation can be found in Table 1. As can be seen in the table, there are two methods to implement the requirement that the total absorption of light by the skin-mimicking material has to be similar to the total absorption by the epidermis in vivo. Developing a material capable of creating a layer with a realistic thickness, which at the site of the breast is 76.9 ± 26.2 µm [51] has the preference. With a skin-mimicking material with the same thickness and μ_a as the epidermis, the PA signal detected from this skin-mimicking layer will be similar to the signal detected in vivo. If the chosen skin-mimicking material is too stiff or not viscous enough to achieve the desired layer thickness, approach 2 has to be implemented. By compensating for the deviation in achievable layer thickness, the total absorption of light is mimicked. The downside is that the lower μ_a will result in lower PA signal intensities for the fabricated layer than is expected from the epidermis. The second requirement about the scattering properties is less important than the requirement for the absorption properties. For near-infrared light, it is expected that the dermis is the main contributor to the scattering properties of the skin [64]. Mimicking the scattering properties of the epidermis perfectly is therefore of less importance. Especially since for PAI, the scattering properties of the tissue do not directly influence the image formation.

Some criteria have less priority and could be seen more as preferences. For instance, the acoustic properties of the materials should ideally be close to those of the skin. However, the acoustic properties are of less importance for this research as it is the difference in optical properties of different skin tones that is investigated. The preferences can be found in Table 2.

Table 1: Requirements for the basis skin-mimicking material.

Requirement	**Rationale**	**Consequence for implementation**
Total absorption of light by the skin-mimicking layer is similar to the total absorption of light by the epidermis.	To mimic the effect of the skin tone on the fluence distribution below the skin and thus the decrease in PA intensity for underlying imaging targets.	Two possible approaches are: 1. A skin-mimicking material capable of creating a layer with the same thickness and μ_a as the epidermis. 2. A skin-mimicking material with which a skin-mimicking layer can be created with a thickness that deviates from the epidermal thickness in combination with μ_a in which there is compensation for the deviation in thickness.
Scattering properties in the range of the real epidermis or skin.	Main motivations for this requirement are: 1. The skin is an important scatterer of light. While most photons are scattered in the	Depending on the inherent scattering properties of the chosen material, TiO_2 can be added to increase the scattering properties [17,18].

	forward direction (the anisotropy factor is 0.8-0.95), some of the incoming light does get lost due to scattering [64]. 2. If a colorimetric device is used for the characterisation of the skin-mimicking layer, the layer should scatter light because the device is based on reflectance measurements [57].	
Long-term stability of the material.	The chosen skin-mimicking material should not degrade within a few months, and the optical properties should not change within that time period, so it is possible to do new measurements on the same material.	Water-based materials should be avoided [47].
The mechanical properties promote the fabrication of thin layers in a controlled manner.	Producing a layer of a specific thickness should be reproducible.	The viscosity of the material should be low enough as this promotes the fabrication of thin layers.
Easy fabrication process of the material.	The more straightforward the process, the higher the likelihood of high reproducibility and the lower the risk of differences in the optical properties of skin-mimicking material due to differences in the basis of the skin-mimicking material.	Materials that have fabrication methods with steps that take up a long time (multiple hours) should be avoided. As well as materials that necessitate the use of dangerous constituents.
Long-term stability of the material.	The long stability of the skin-mimicking material depends mostly on the stability of the basis of the skin-mimicking material.	Water-based materials should be avoided [47].
Close to negligible inherent optical absorption of the basis skin-mimicking material within the wavelength range of interest (680-1060 nm).	Mimicking the absorption spectrum of the epidermis is more straightforward if the inherent absorption properties of the basis skin-mimicking materials do not have to be considered.	It should be verified using spectrophotometric measurements that the chosen material is optically transparent for the wavelength range of interest.

Table 2: Preferences basis skin-mimicking material.

Preference	**Rationale**	**Consequence for implementation**
The material is reusable after the material is fabricated.	To be able to split the development of the material and the development of a phantom into two phases, the material should be reusable at a later time point.	The material should become malleable and/or liquid again by reheating the material.
Easy scalability of the fabrication of the material to different volumes.	It should be possible to make the skin-mimicking material regardless of how much material is needed for a specific end goal.	The steps in the fabrication of the material should not take up significantly more time for larger volumes despite the use of suitable equipment.

The inherent acoustic properties of the material should be similar to the values of skin, or it should be possible to tune these properties.	To better mimic the in vivo situation, the acoustic properties of the skin-mimicking material should match those of the skin.	The acoustic properties should be within the range of soft tissue values.

4.3.2. Requirements melanin-mimicking substance

In the development of skin-mimicking layers with different skin tones, the melanin-mimicking substance is vital. Consequently, there are a few requirements that have to be met for a substance to be considered adequate for this application. They can be found in Table 3. Some papers mention that melanosomes add to the scattering properties of the skin for wavelengths in the range of 600-700 nm [65]. However, other sources state that the influence of the scattering properties of melanosomes on the scattering properties of the skin is insignificant in visible and near-infrared (NIR) light [65–67]. This, together with the fact that scattering properties are less important for PAI, is why mimicking the scattering properties of melanin and melanosomes is not considered a requirement.

Table 3: Requirements melanin-mimicking substance.

Requirement	**Rationale**	**Consequence for implementation**
Similar shape of the absorption spectrum of the melanin-mimicking substance as for the absorption spectrum of the epidermis for the wavelength range of interest (680-1060 nm).	The skin-mimicking material should mimic the skin for the whole wavelength range of 680-1060 nm to properly investigate how skin tone influences the imaging performance of the PAM3 system.	The absorption spectrum of the melanin-mimicking substance should follow the equation that describes the absorption coefficient of the epidermis (shown in the text below the table).
Compatibility of the melanin-mimicking substance with the basis skin-mimicking material of the skin-mimicking material.	To obtain the optimal absorption properties, the melanin-mimicking substance has to be incorporated well with the basis skin-mimicking material and in a stable fashion.	It should be ensured that the substance dissolves properly in the material and that over time the substance does not leach from the material.
Homogeneous distribution of the substance throughout the skin-mimicking material.	The optical properties of a skin-mimicking layer should not differ spatially.	The substance should be dissolved properly, and no aggregation should occur.

The absorption coefficient of the epidermis ($\mu_{a,epi}$) for a specific wavelength (λ) as a function of melanin content can be described as [46]:

$$\mu_{a,epi}(\lambda) = M_f \mu_{a,mel}(\lambda) + \left(1 - M_f\right)\mu_{a,0}(\lambda)$$

The first term depicts the contribution of the melanosomes in the epidermis to $\mu_{a,epi}$ and depends on the aforementioned melanosome volume fraction (M_f) and the absorption coefficient of the melanosomes ($\mu_{a,mel}$). The second term depicts the contribution of the "base" absorption of unpigmented epidermis. This equation can be simplified by neglecting the base absorption of the epidermis. Jacques has approximated $\mu_{a,mel}$, which results in the following equation for $\mu_{a,epi}$ [18,68]:

$$\mu_{a,epi}(\lambda) = M_f(519\ [\mathrm{cm}^{-1}])\left(\frac{\lambda}{500\ [\mathrm{nm}]}\right)^{-3.53}$$

4.4. Methods

In this section, the development and characterisation of the skin-mimicking material will be described. The properties that were characterised are the optical and acoustic properties of the skin-mimicking material. The optical properties of interest are the reduced scattering and absorption coefficients, and the acoustic properties of interest are the acoustic attenuation and the speed of sound.

4.4.1. Material development

Copolymer-in-oil (CiO) has been chosen as the basis skin-mimicking material for the skin-mimicking layer. This is a material that has been chosen by consensus by the International Photoacoustic Standardisation Consortium (IPASC) as the most suitable material for making photoacoustic phantoms since its optical properties can be easily tuned. For our purpose, it is convenient to obtain different skin tones by adding different absorbers or scatterers. It is also a reusable oil-based gel material that allows the separation of the material fabrication from the development of a phantom. This will allow flexibility in the time management during the development of a phantom with this material. To mimic the different skin layers alcohol-soluble nigrosin (211680-25G, Sigma-Aldrich) was used as the melanin-mimicking substance. While nigrosin is not able to fully mimic the optical absorption of melanin, the error margin is within the acceptable range [18]. A full overview and comparison of the different materials that have been considered for the skin-mimicking material and melanin-mimicking substance can be found in Appendix A.

The CiO basis skin-mimicking material can be made by adding high molecular weight polystyrene-block-poly(ethylene-ranbutylene)-block-polystyrene (SEBS) (200557-250G, Sigma-Aldrich) and low-density polyethylene (LDPE) (43949.30-250G, Thermo Scientific) to light mineral oil (330779-1L, Sigma-Aldrich) in concentrations of respectively 12% w/w and 5% w/w. During the trial phase of this part of the project, it was unfortunately found that this material cannot be moulded easily, or with sufficient accuracy and reproducibility into homogeneous layers with thicknesses of around 100 µm. However, based on different small experiments performed on the material and other similar materials it was hypothesised that it should be possible to achieve a layer thickness of 1 mm with this material. As mentioned in the requirements section, when the achievable layer thickness of the skin-mimicking material is larger than the thickness of the epidermis, the absorption properties should be adjusted to account for this deviation in thickness. Else et al. [17] performed a phantom study on a cylindrical phantom with a 1 mm thick skin-mimicking layer. And similarly, they too took this increase in the thickness of a factor 10 into account in the optical properties of the material [17].

With a layer thickness of 1 mm in mind, the concentrations of alcohol-soluble nigrosin were tuned to obtain similar total optical absorptions for the different skin-mimicking materials as for epidermal layers with different melanin content. The melanosome volume fractions (M_f) that were being mimicked are 0%, 3%, 9% and 27%. The four different variations of the skin-mimicking material were developed by adding nigrosin in concentrations of 0.0% w/v, 0.001 % w/v, 0.003 % w/v and 0.009 % w/v (based on the volume of mineral oil). These concentrations of nigrosin were carefully selected, based on calibration measurements in a transparent oil-based gel material. For the fabrication of the skin-mimicking material, the protocol of Hacker et al. was slightly adapted based on the approach of Vogt et al. for making skin-mimicking phantoms based on polyvinyl chloride plastisol (PVCP) [18,41]. The nigrosin was first dissolved in ethanol (9.1 % v/v based on the volume of mineral oil used) before adding it to the mineral oil, instead of adding nigrosin directly to the mineral oil. Vogt et al. showed for PVCP that this approach improved the absorption properties of the skin-mimicking material [18]. For the skin-mimicking material with no nigrosin, pure ethanol was added to avoid differences in acoustic and optical properties. The full protocol for the fabrication of the skin-mimicking material can be found in Appendix B.

4.4.2. Optical characterisation

The optical properties, i.e. the reduced scattering and absorption properties, of the skin-mimicking materials were determined at the Institute for Laser Technologies in Medicine and Metrology (ILM) at the University of Ulm. They determined these properties by performing measurements on slabs of material of 60x50x5 mm with a custom-made single integrating sphere and applied advanced Monte Carlo simulations [69,70]. The results were compared to the theoretical absorption and scattering properties of epidermal layers with different M_f values [46,67]. A compensation for the difference between the actual thickness of the epidermis and the thickness of the skin-mimicking layer was applied to the theoretical data to allow for a fair comparison. The optical properties of the skin-mimicking materials were also determined in our group following the inverse adding doubling (IAD) method [71]. The full description of the methods and the obtained results can be found in Appendix C.

4.4.3. Acoustic characterisation

For the measurement of the acoustic attenuation and speed of sound of the skin-mimicking material, a block of material was made with the use of a sample holder with known dimensions and a stable geometry. The holder has a thin (d_1) and a thick side (d_2), of 3 and 5 cm, respectively. The acoustic characterisation was performed using an adaptation of the insertion method [72]. A schematic image of the set-up for the acoustic characterisation can be found in Figure 6. The set-up consists of a rail system with on one side an ultrasound transducer and on the other a hydrophone needle (SN3753 NH1000, Precision Acoustics). The holder can be placed directly onto the rail to ensure good alignment of the material and measurement instrumentation. This improves the accuracy and reproducibility of the measurement. The whole measurement set-up, except for the electronics was submerged in water. By simply rotating the sample holder 90° in the set-up, a measurement can be performed through either the thick or the thin side of the sample. For the measurements, two transducers with centre frequencies of respectively 1 MHz (V303 0.5" unfocussed, Olympus IMS) and 2.25 MHz (V306 0.5" unfocussed, Olympus IMS) were used. The temperature of the water was measured with a thermometer during the measurements. The speed of sound of the sample (c_s) was determined using the following equation:

$$c_s = \frac{\Delta d}{\Delta t + \frac{\Delta d}{c_w}}$$

In this equation, Δd is the difference between d_1 and d_2, c_w is the speed of sound in water and Δt is the difference in time of arrival of the signals measured through the thick and thin side of the sample. The Δt is determined by calculating the cross-correlation of the two signals. The acoustic attenuation (α) as a function of frequency (f) was estimated with the use of the power spectra of the signals (I) with the equation:

$$\alpha_s(f) = \alpha_w(f) + \frac{20}{\Delta d}\log_{10}\left(\frac{I_2(f)}{I_1(f)}\right)$$

The acoustic attenuation of water (α_w) is low in comparison to the attenuation caused by the material. Therefore, this term can be neglected [38,73]. The frequency range for which the acoustic attenuation was calculated was determined by selecting the full width half max of the peak at the centre frequency. The acoustic attenuation generally follows a power function:

$$\alpha(f) = a_0 f^n$$

To obtain the α_0 and n, the estimated values of $\alpha(f)$ were fitted to a power function using a nonlinear least square regression.

The volume of the block of material used for the acoustic measurements was determined from a scan with a C-arm (ARTIS Pheno, Siemens Healthineers). The density of the material (ρ_s) was calculated using the determined volume and the weight of the block. The acoustic impedance (Z_s) of the material follows from ρ_s and c_s by using the equation [38]:

$$Z_s = \rho_s c_s$$

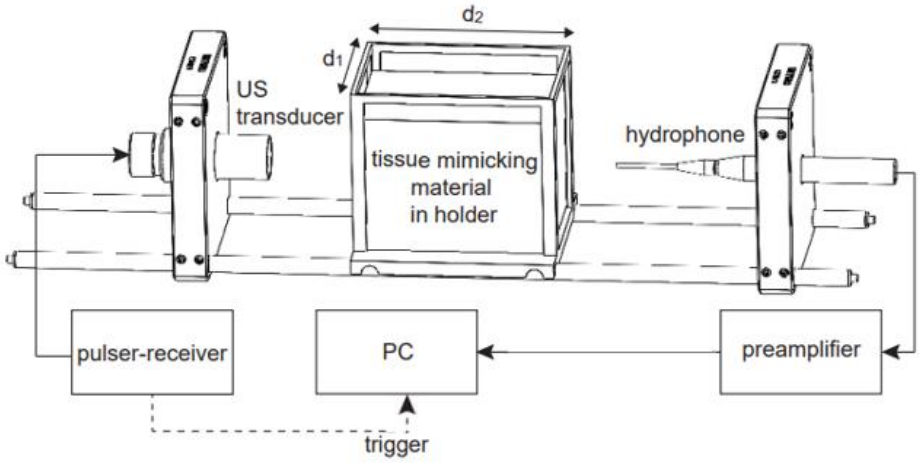

Figure 6: Schematic overview of the acoustic set-up. Image adapted from [38].

4.5. Results

Four skin-mimicking materials have been produced, one control material with no nigrosin and three materials that mimic a light, medium and dark skin tone. The optical characterisation has been performed on all materials. As mentioned in the methods section, the optical properties of the skin-mimicking materials were also measured by us following the IAD method. However, it was found that there are significant differences between the results obtained by ILM and those obtained with the IAD method, which also vary over time. Similar discrepancies in the optical properties of phantom materials were found in previous experiments. Consequently, there were some concerns about the reliability and accuracy of the results obtained with the IAD method. Henceforth, only the results derived by ILM are used for verification and validation. Our IAD methods and the results are included in Appendix C for the sake of completeness. Since the concentration of nigrosin is the only difference between the materials, the acoustic characterisation has only been performed on the control material.

4.5.1. Optical characterisation

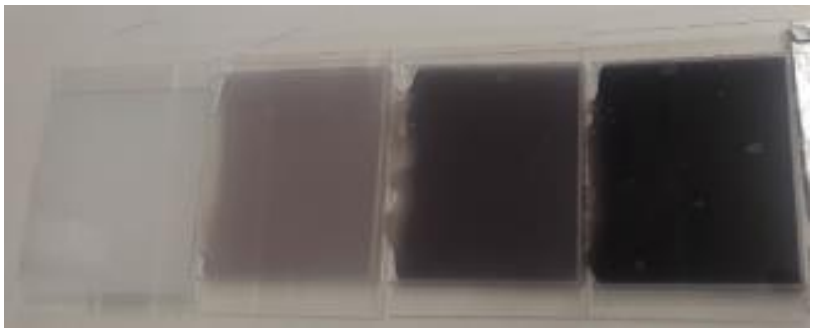

Figure 7: Photograph of four samples of the four skin-mimicking materials, with from left to right the control, the light skin tone, the medium skin tone, and the dark skin tone.

In Figure 7, the 5 mm thick samples of the four skin-mimicking materials used by ILM for the optical measurements are shown. Going from left to right, the colour becomes darker. The by ILM determined absorption coefficient of these four different skin-mimicking materials can be found in Figure 8 on the left. For the materials with nigrosin, the corresponding epidermis layers would have M_f values of 0%, 3%, 9% and 27%. In the results for the material without nigrosin, it can be appreciated that the optical absorption of CiO itself in the wavelength range of interest is negligible. For these four materials, the sum of squares errors (SSE) in the wavelength range of 600-1100 nm was 0.020, 0.020, 0.031 and 0.232, respectively. In Figure 8 on the right, the reduced scattering coefficient of the four different skin-mimicking materials determined by ILM can be found. The reduced scattering coefficients are consistently above the theoretical curves for the epidermis from Afshari et al. and Jacques et al. [46,67].

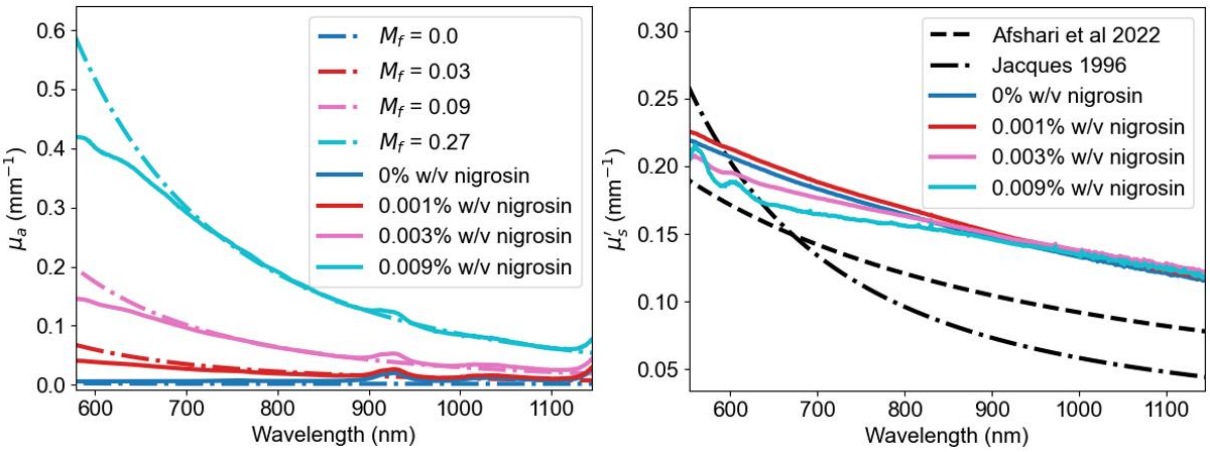

Figure 8: Absorption coefficients (left) and reduced scattering coefficients (right) of the four different skin-mimicking materials determined by ILM. The absorption coefficients of the materials are compared to the desired theoretical absorption coefficients of the epidermis with different melanosome fractions (M_f). The reduced scattering coefficients of the materials are compared to the desired theoretical reduced scattering coefficients of the epidermis.

4.5.2. Acoustic characterisation

In Figure 9, the time signals for the acoustic measurements for the skin-mimicking material can be found. The calculated speed of sound is 1452.7 m/s at a water temperature of 21 °C. The density of the material is 858.62 kg m^{-3}, which results in an acoustic impedance of 1.25 MRayl. The frequency-dependent acoustic attenuation follows the power law with $\alpha_0 = 0.298$ and $n = 1.615$, as shown in Figure 10.

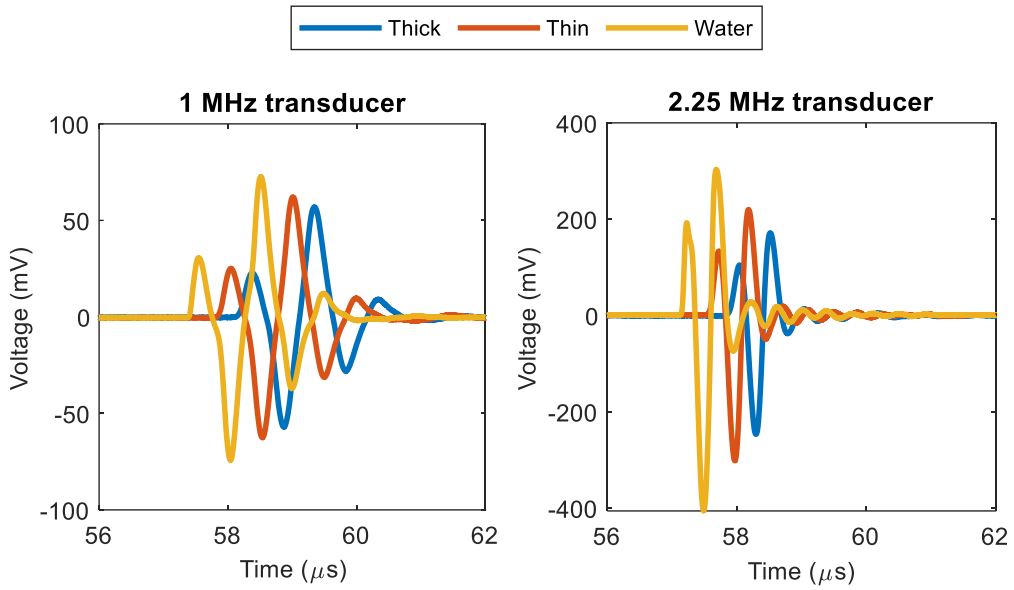

Figure 9: Time signal of the transmission measurement for just water and through the thin and thick side of the sample for a 1 MHz and 2.25 MHz transducer.

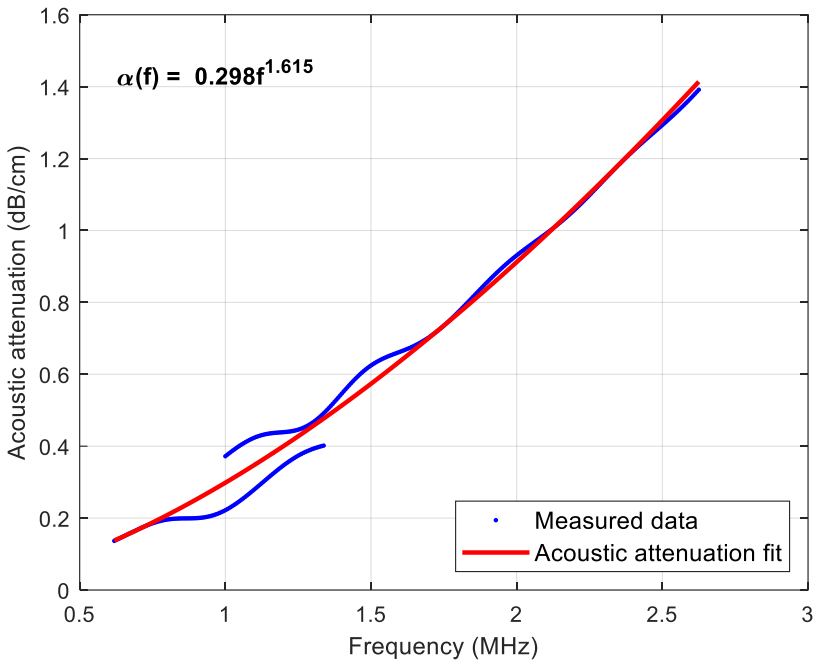

Figure 10: The frequency-dependent acoustic attenuation determined from the measured data is shown in blue, while the exponential fit is shown in red.

4.6. Discussion

The aim of this subsection of the whole research project is to develop a skin-mimicking material that can be used to develop a physical phantom for PAI experiments. Four CiO-based skin-mimicking materials were developed in which the concentration of alcohol-soluble nigrosin was varied to obtain three materials that mimic different skin tones and one control. The absorption and reduced scattering coefficients of samples of these materials were determined. The speed of sound and acoustic attenuation for a frequency range around 1 MHz were also determined.

It can be seen in the results that the absorption coefficients of the materials follow the theoretical curves of the absorption coefficients of an epidermal layer of 1 mm well (See Figure 8).

From the small SSE values, it can be concluded that the absorption coefficients match well with the theoretical absorption curves for the intended M_f values. The results for the obtained reduced scattering coefficients show that the values for the skin-mimicking materials deviate from the theoretical curves for the scattering properties of the epidermis (See Figure 8). Since mimicking the scattering properties of the epidermis was of lower importance for this project, the deviation is in the acceptable range. The speed of sound of the skin-mimicking materials is 1452.7 m/s and the frequency-dependent acoustic attenuation follows the power law with $\alpha_0 = 0.298$ and $n = 1.615$. These values are close to the values found by Hacker et al. for a CiO sample with slightly different concentrations of SEBS and LDPE [74]. The acoustic properties of the skin-mimicking materials are closer to fatty tissue than to skin tissue [73], which was to be expected from an oil-based material. However, as was mentioned in the requirements section, it is sufficient if the acoustic properties of the skin-mimicking material are in the range of tissue values. The acoustic properties of just one out of the four developed materials were determined due to time constraints. Since the only difference between the materials is the amount of nigrosin, it can be assumed that the properties of one material are representable for the other materials as well.

This project is not the first study in which a skin-mimicking material for physical phantoms for PAI is developed. However, it is the first attempt in which CiO is used to develop this skin-mimicking material. Moreover, no other research group has thus far used CiO to mimic a specific tissue type. Else et al. used a water-based base material, which allowed the use of synthetic melanin as a melanin-mimicking material. Synthetic melanin is a better equivalent of human melanin than nigrosin. However, in the wavelength range of interest for this project, nigrosin shows a sufficient mimicry of melanin. In addition, CiO is stable for a longer period of time [47]. Furthermore, it is a reusable material. Vogt et al. also used alcohol-soluble nigrosin as a melanin-mimicking material. However, their skin-mimicking material was based on PVCP [18], which has the disadvantage that the raw materials are not standardised, which fortunately is the case for CiO. Further, while PVCP is also stable for an extended period of time, it is not reusable [47].

As mentioned above, for the wavelength range of interest, the developed material is able to mimic skin. However, for wavelengths below 600 nm, the deviation from the spectrum of melanin becomes significant. This means that the material developed in this project cannot be used for experimentation with light-based imaging applications that use wavelengths below 600 nm. Then, it would be necessary to use other absorbers. Grillo et al. have investigated the development of CiO with glycerol instead of LDPE. They show that the addition of glycerol could potentially allow hydrophilic absorbers to be integrated in the CiO [75]. It would be interesting to investigate this further, as it could allow the use of melanin or derivatives of melanin.

Another important downside of this material is that it is relatively viscous in comparison to water-based materials. As mentioned before, this has the consequence that it is notably challenging to create a homogenous layer with this material with a thickness in the range of 100 µm. For this material to be suitable for the development of a phantom, being able to control the thickness of a layer of material is important. Moreover, the results should be reproducible. These requirements can be achieved for layer thicknesses of 1 mm, which is a factor 10 larger. Consequently, absorption and reduced scattering coefficients have to be a factor 10 lower than desired. So, while the total absorption of light is similar to what would be for a realistic epidermal layer, the optical properties are in essence not similar. The PA signals produced by a skin-mimicking layer of 1 mm of this material will therefore have significantly different amplitudes compared to the signals produced by the skin. The effect of the increased thickness on the reconstructions might be relatively small. In in vivo situations, there is a partial volume effect due to the factor 4-8 difference between the resolution of the system (which is normally around 786 µm and 426 µm at best [76]) and the thickness of the epidermal layer. The envisioned layer thickness of the skin-mimicking layer is about at most a factor 2 larger than the resolution. As a result, there is no partial volume effect, and the layer might have a similar thickness in the reconstruction as the real epidermis would have. Furthermore, we are less interested in absolute values and more in relative changes in the signal of the skin-mimicking layer and/or imaging targets

between the mimicked skin tones. And for that, the total absorption by the skin-mimicking layer is of more importance.

Despite the inherent limitations of CiO, the results show that for the wavelength range of 600-1100 nm, the developed CiO-based material can, with some compensation for the intended layer thickness, mimic the skin. The mimicked skin tone can be easily tuned by adjusting the concentration of alcohol-soluble nigrosin dissolved in ethanol. Important advantages of using CiO as the basis skin-mimicking material for the skin-mimicking layer are the long stability, reusability, and relatively easy preparation. With this in mind, it can be concluded that the developed skin-mimicking material is an excellent candidate as a material for a physical phantom for PAI.

4.7. Conclusion

This part of the study aimed to develop a material that could mimic the skin and could be used for a physical phantom for PAI. By adjusting the concentration of alcohol-soluble nigrosin added to the basic ground materials for CiO, three different skin tones have been mimicked. The mechanical properties of CiO make it difficult to create a thin layer of material with a similar thickness as a real epidermis. However, it is possible to compensate for the difference in thickness of the skin-mimicking layer compared to the epidermis. The results show that with this compensation taken into account, the optical properties of the materials are close to those of the epidermis. However, it should be mentioned that the acoustic properties of the material are closer to those of fatty tissue than to those of skin tissue. Not only is the developed material able to mimic the skin, but it also has a long stability and is reusable. Overall, the developed material shows great potential for its application in the development of a phantom with a skin-mimicking layer for PAI.

Chapter 5

5. Development of photoacoustic phantoms with a skin-mimicking layer

5.1. Introduction

Over the years, continuous research has led to significant progress in tissue-mimicking materials for photoacoustic imaging (PAI) [40,77,78]. Examples of materials with tuneable optical and acoustic properties that have been commonly used are polyvinyl chloride plastisol (PVCP), polyvinyl alcohol (PVA), hydrogels, and copolymer-in-oil (CiO) [40,47,74]. In the last couple of years, there has been an increased interest in the subject of how skin tone influences PAI. This has led to the development of various phantoms with a skin-mimicking layer.

In general, phantoms developed for PAI, while often mimicking the optical and acoustic properties of tissue, have a simplistic geometry [40,75,77]. The geometry of the phantom is usually tailored to the geometry of the transducer of the photoacoustic (PA) system that is used for the study. This is also the case for phantoms with a skin-mimicking layer [17,18]. Else et al. have developed a cylindrical phantom from which they made cross-sectional scans with a curved array covering an arch of 270° [17]. Vogt et al. on the other hand used a linear array for their study. Therefore, they developed a planar phantom [18]. As of yet though, there has not been a dedicated phantom mimicking skin on a breast-sized object developed for a hemispherical geometry photoacoustic tomography (PAT).

The Twente Photoacoustic Mammoscope (PAM) 3 is a PAT system with a hemispherical configuration specifically developed to image the breast. The illumination and detection geometry of the system are optimised to obtain good-quality images of the breast [79]. Consequently, the geometry of the phantoms developed for this system needs to be compatible with this system to obtain relevant results. For the PAM3 system, an anthropomorphic breast phantom and various more simplistic phantoms have been developed [38,79]. However, none of these phantoms included an adequate skin-mimicking layer. One of the main goals of this project is therefore to develop phantoms with a skin-mimicking layer with which it is possible to investigate the influence of skin tone on PA breast tomography. With the complexity of the phantom on one hand and the clinical relevancy of data obtained with the phantom on the other, a simplified breast phantom mimicking breast tissue and the skin was developed. This part of the thesis will address the development, fabrication, and characterisation of these phantoms.

Related sub-research question:

- *How can a simplified physical breast phantom with a skin-mimicking layer be developed that is suitable for experimentation using the PAM3 system?*

5.2. Requirements

The main purpose of the simplified breast-mimicking phantom with a skin-mimicking layer is to provide a mechanically and chemically stable object that can be used to evaluate and validate the performance

of the PAM3 for different skin tones. For the development of the phantom, various requirements for the phantom itself have been formulated. Based on the requirements of the phantom several criteria for the fabrication method of the phantom have been defined as well. The requirements for the phantom can be divided into the requirements for the materials and the requirements for the design of the phantom. The former has been discussed in the previous chapter, and only the requirements for the material of the base of the phantom, the part underneath the skin-mimicking layer, will be addressed in this chapter.

5.2.1. Requirements phantom base material

The requirements for the phantom base material can be found in Table 4. One of the requirements is about the acoustic properties of the base material. It would be ideal if the acoustic properties of the base material were similar to the ones of breast tissue. Since the PAM3 is designed to image the female breast, results from the phantom could be more easily translated to results obtained from patients or volunteers. However, since the main purpose of this phantom is to analyse the effect of skin tone on the imaging performance of the PAM3 in general, properly mimicking the breast is of less importance.

Table 4: Requirements phantom base material.

Requirement	**Rationale**	**Consequence for implementation**
Low inherent optical absorption for the wavelength range of interest (680-1060 nm).	Enough light will reach the imaging targets for the production of well-detectable signals.	It should be verified using spectrophotometric measurements that the chosen material allows light to penetrate deeply for the wavelength range of interest.
Minimal notable absorption peaks in the wavelength range of interest.	This can cause significant spectral colouring effects. To be able to observe just the influence of different skin-mimicking layers, the base material has to be of minimal influence on the fluence.	It should be verified using spectrophotometric measurements that this is not the case.
Optically and acoustically homogeneous (within and between batches).	To avoid non-reproducible variations in the fluence or measured signals not caused by the skin-mimicking layers or targets.	Check if the fabrication of the material itself can introduce inhomogeneities (e.g. the freezing and thawing procedure of polyvinyl alcohol [47]).
Stable over at least a few months.	It could be possible that there is a period of a few weeks between fantom fabrication and measurements that have to be bridged. The base material should be stable over a similar time period as the skin-mimicking layer to keep the whole phantom stable.	Water-based materials should be avoided [47].
The acoustic properties of the base material mimic soft tissue in general.	To keep the results somewhat clinically relevant.	Perform acoustic measurements to verify that the values are within the range of normal tissue values.

5.2.2. Requirements phantom design

The requirements for the design of the phantom (See Table 5) also include requirements for the imaging targets. Imaging targets are parts of the phantom that will result in a very high or very low signal intensity compared to the background to provide a well-recognisable area or volume that can be used to analyse or compare scans. In the case of PAI, imaging targets are parts of the phantom that absorb the optical wavelengths of interest well so a high PA signal can be detected. These imaging targets can be structures of the same base material but with different optical absorption properties, or compartments that can be filled with a liquid or solid substance. With the last approach, the optical properties of the imaging targets can be adjusted easily if specific absorption properties are desired for different scans. The first requirement for the imaging target is related to the possibility of assessing with this phantom the imaging depth, which was also done in previous studies regarding the effect of skin tone on PAI [12,18].

Table 5: Requirements phantom design.

Requirement	**Rationale**	**Consequence for implementation**
Compatibility with the illumination and detection geometry of the PAM3 system.	A homogeneous light distribution limits the spatial variation of the PA signals at similar depths and can result in an increased field of view [79].	The size and shape of the phantom should be chosen in such a manner that the illumination profile on the skin-mimicking layer is as homogeneous as possible.
A consistent thickness of the skin-mimicking layer for the part of the phantom surface that is imaged.	Differences in thickness over the surface of the phantom will result in variations in the absorption of the light and thus the fluence. The consequence would be that for some common metrics such as imaging depth and signal-to-background ratio, there is a non-depth-related spatial variation.	The chosen fabrication method should facilitate control over the thickness of the layer.
The skin-mimicking layer and the base part of the phantom should be well attached to each other.	Main motivations for this requirement are: 1. Acoustic coupling should be adequate. 2. The skin-mimicking layer should not detach from the base material to improve the morphological stability of the phantom.	The phantom should preferably consist of a single component.
Imaging targets placed at different depths.	To analyse the imaging depth with a phantom it is necessary to have imaging targets at different depths.	Multiple imaging targets at different depths should be included in the phantom or one or more longer imaging targets to span a range of depths.
The path for the incoming light is roughly the same for each target.	There should be minimal variation in signal intensity between imaging targets with the same optical properties at the same depths.	Different imaging targets are positioned rotationally symmetrical.

5.2.3. Requirements phantom fabrication method

An important aspect of the successful development of the phantom is that the fabrication method is reliable and reproducible to avoid undesired variations between phantoms. In practice, this means that the fabrication method for the phantom should result in a consistent skin-mimicking layer for different phantoms and identical positioning of the imaging target(s) between phantoms.

5.3. Methods

In this methods section, various topics will be discussed. The development of the materials used for the phantoms and the characterisation of these materials are described. After that, the development of the phantom itself is brought into focus with a summarisation of the phantom design and phantom construction. Lastly, the characterisation of the skin-mimicking layers of the phantoms regarding their thicknesses and skin tone classification is discussed.

5.3.1. Base material

The base material of the phantom has been chosen to consist of native gel wax (NGW) (SFX Gel Wax, British Wax). This non-scattering and optically transparent material is oil-based just like the skin-mimicking material, facilitating material compatibility. Furthermore, because it is oil-based it is hypothesised that the optical and acoustic properties can be easily tuned to mimic (fatty) breast tissue. An overview of the different materials that were considered for the base material can be found in Appendix A. To tune the acoustic properties of the material and improve the mechanical durability of the material, 8% w/w paraffin (Alec Tiranti) was added to the NGW. Since NGW is inherently optically non-scattering, 0.15% w/v TiO_2 (248576-100G, Sigma-Aldrich) was added to increase the scattering properties of the base material to more resemble the scattering properties of breast tissue. To improve the dispersion of the TiO_2 in the base material, 1.6% v/v ethanol was used as a carrier liquid. The full protocol for the fabrication of the base material can be found in Appendix D.

The optical properties of one batch of the base material of the phantom, i.e. the reduced scattering and absorption properties, were determined at the Institute for Laser Technologies in Medicine and Metrology (ILM) at the University of Ulm just like for the skin-mimicking materials. The results were compared to the theoretical absorption and scattering properties of fatty breast tissue [38]. The optical properties of the base material were also determined in our group following the inverse adding doubling (IAD) method [71]. These results can be found in Appendix E.

Similarly, to characterise the acoustic properties of the base material, the same methodology as for the skin-mimicking material in Chapter 4 (Section 4.4.3, page 41) was used. A block of material was made in the sample holder and the transmitted acoustic pressure was measured for different acoustic frequencies. With the measurements, the speed of sound and acoustic attenuation of the base material was determined. To determine the acoustic impedance a separate block of material was made. For more information about the set-up and the data analysis, see Chapter 4 (Section 4.4.3, page 41). The results were compared to the acoustic properties of fatty breast tissue [38].

5.3.2. Skin mimicking material

The in Chapter 4 developed skin-mimicking material was used to fabricate the skin-mimicking layer of the phantoms. For the phantoms with medium and dark skin tones, the same materials as were produced in Chapter 4 could be used. However, for the light-skinned phantom new material was made. The same protocol was used as for the light skin tone mimicking material in Chapter 4 (Section 4.4.1, page 40). To have a rough estimation of the optical properties of the new light skin-mimicking material batch the optical properties were determined using the IAD method. The results can be found in Appendix E.

5.3.3. Phantom design

The phantom consists of a hemispherical part with a radius of 6 cm, which is connected to a 3 cm thick cylindrical supporting part with slanted sides (See Figure 11). The hemispherical part of the phantom will be the part that is to be imaged. With a hemispherical phantom, the design is kept simplistic but still compatible with a hemispherical PAT system. The size of the phantom is based on two papers about the PAM3 [76,79]. In the study described in these papers, it is shown that the breast immobilisation cups with a maximum depth of 5.2 and 5.8 cm respectively received the most homogeneous illumination on the surface [79–81]. It was also demonstrated that with the PAM3 system imaging depths of up to 4.8 cm could be reached [76]. It was hypothesised that with a radius of 6 cm for the hemispherical part of the phantom, maximal depth information can be obtained while having a rather homogeneous illumination. Moreover, until 6 cm depth, the PA signals are also not yet dominated by noise and interference signals [76].

The supporting part of the phantom has as the name suggests multiple auxiliary functions. It contains a 3D-printed component that can be used to secure the phantom to a mounting system (See Figure 12). This is necessary to correctly position the phantom in the measuring set-up. Additionally, the supporting part of the phantom functions as a transition zone between the part of the phantom that is imaged and the air in the room. If the transition is in or just outside the field of view, there is a risk that acoustic reflections formed at this transition cannot be filtered out of the raw data and are thus present in the reconstructions. By placing the transition farther outside the field of view, signals caused by back reflections from this transition can be more easily filtered out, resulting in improved reconstructions.

Four straight wall-less channels with a diameter of 3 mm are positioned rotationally symmetric in the phantom and function as the imaging targets (See Figures 11 and 12). They are positioned in different directions just off the centre and are oriented downwards with an angle of 53.6° with respect to the central axis through the phantom (See Figure 11). The opening is located at the base of the supporting part of the phantom and the tip is located a few mm from the surface of the hemispherical part. With these imaging targets, signals at different depths can be analysed to assess imaging depth. Furthermore, because each channel can be filled with a specific solution, the optical properties of the imaging targets can be adjusted to the desired values.

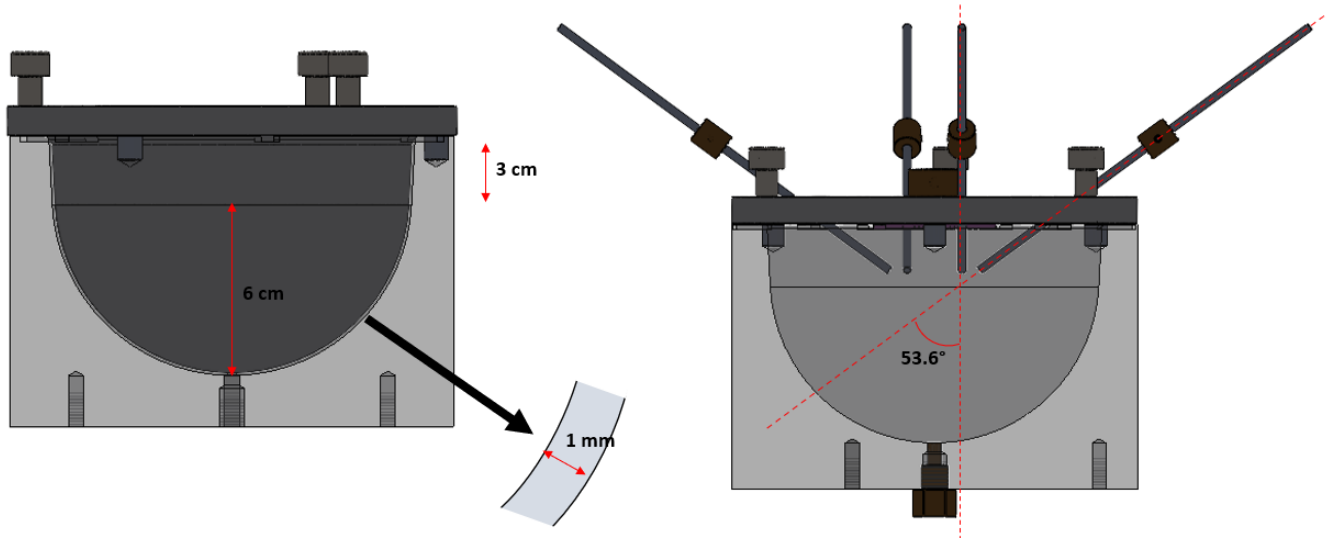

Figure 11: Schematic overview of the mould and the dimensions of the phantom. On the left, the mould configuration for the first step of the phantom fabrication (the skin-mimicking layer) is shown, with the bottom component and the top component. On the right is the configuration for the second step, with the 2nd top component and the four rods.

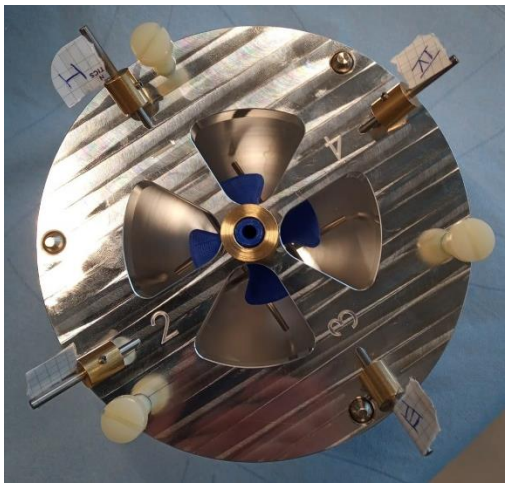

Figure 12: Photograph of the mould configuration for the second step of the phantom fabrication, with the four rods and the 3D printed component.

5.3.4. Phantom construction

The phantom is constructed in two steps. The fabrication method is inspired by the phantom of Garret et al. for microwave breast imaging since their phantom had a similar shape and design [42]. However, their phantom material allowed them to use 3D-printed moulds, which was not feasible for the phantom developed in this project. The full protocol for the phantom fabrication can be found in Appendix F.

First, the skin-mimicking layer of CiO is made using a custom-made aluminium mould with a bottom part, which functions as a container, and a top part, which functions as a lid. When the two components are combined, a thin 1 mm space between the two components is left. When this space is filled with phantom material, a 1 mm outer layer is created. The two mould components are heated up in a vacuum oven (3608-6CE, Thermo Scientific) at a temperature of 150 °C. This is to slow the cooling down and subsequent setting of the CiO, which is also around 150 °C, when it is poured into the bottom part of the mould. The lid component of the mould is coated in a thin silicon layer (Silikon-spray, Toolcraft) before it is put in the oven. Once the CiO is poured into the bottom mould part, the top part is placed on top and completely pressed down. Two dowel pins ensure the correct alignment of the two mould components. Excess CiO can flow out of the mould via four small channels at the top of the container part of the mould. The top part of the mould can be lifted after the CiO has set, using three nylon screws.

After the skin-mimicking layer is created, the remainder of the phantom is constructed. A second top component of the mould is placed on the bottom part of the mould. This component contains inserts for four stainless steel rods of 3 mm in diameter that will create the four channels. It also contains an opening that can be used to fixate the 3D-printed support for the phantom during the fabrication process at a specific height. The base material is heated in an oil bath (HBR 4 control, IKA) until it is liquified and degassed in the vacuum oven. The phantom mould is filled with the base material by carefully pouring the material on top of the skin-mimicking layer. To stimulate air bubbles still present in the material to rise, the bottom of the mould is gently tapped on the workbench.

Once the material is fully cooled down, first the four rods are removed and then the top mould component is lifted. The whole phantom is then carefully removed from the outer mould by softly pulling on the supporting structure. To aid the process of removing the phantom from the mould, pressurised air is blown into the mould from the bottom.

5.3.5. Skin layer thickness characterisation

To verify that the skin-mimicking layer is 1 mm thick, an ultrasound (US) scan was made of the phantoms with a clinical US system (Acuson S3000 Ultrasound System, Siemens Healthineers) at different locations on the hemispherical surface of the phantom. The phantom was scanned with a linear array probe (14L5 linear Array probe, Siemens Acuson, Siemens Healthineers) at a frequency of 14 MHz. The thickness of the skin-mimicking layer was measured directly in the obtained US images using the calliper function. The US scans were performed twice at 5 different locations. The hemispherical surface of the phantom can be divided into four quadrants with four lines. The first four locations were positioned about halfway along each line (the locations are denoted with a red x in Figure 13). The fifth location is at the crossing point of the four lines.

5.3.6. Skin tone characterisation

A colorimeter was used (SkinColorCatch, Delfin) to determine the individual typology angle (ITA°) values for each phantom. The purpose of these measurements is to determine if it is possible to link the optical properties of the phantoms to an ITA°-based skin tone classification. This might allow better comparison of results obtained in phantom experiments to those obtained in in vivo experiments. The colorimeter was placed gently on the surface of the phantom. The ITA° values were determined three times at five different locations. Four of those locations were at the centre of each quadrant (the locations are denoted with a green + in Figure 13). The fifth location was just like for the layer thickness measurements at the crossing point of the four lines.

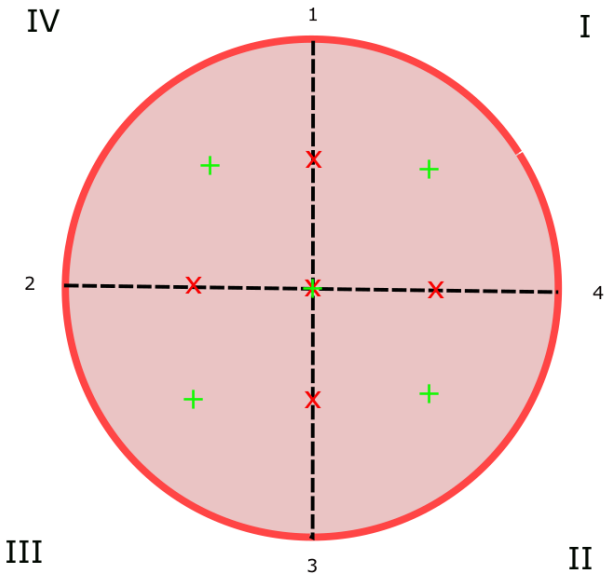

Figure 13: Schematic representation of the top view of the phantom. Four lines divide the surface into four quadrants. The green + signs are the locations for the colorimetric scans and the red x signs are the locations for the ultrasound scans. At the centre of the phantom, both a green and a red sign are located.

5.4. Results

Three phantoms have been developed that mimic a light, medium and dark skin tone. The results of the assessment of these phantoms are shown in this section after the results of the characterisation of the base material. As mentioned in Chapter 4 Section 4.5 page 42, there are concerns about the reliability and accuracy of the results obtained with the IAD method. Therefore, the results for the

optical characterisation of the base material and the new batch of light skin-mimicking material can be found in Appendix E.

5.4.1. Characterisation base material

Figure 14: Photograph of a sample of the base material for the phantom.

A photograph of a sample of the base material can be seen in Figure 14. The base material is a mixture of NGW, paraffin and TiO_2. Consequently, while the material is optically scattering, it should have minimal optical absorption in the visual spectrum. The results for the absorption coefficients confirm this (See Figure 15 on the left). The material has relatively low absorption coefficients for the whole wavelength range of interest (680-1060 nm). However, there are some peaks in the spectrum, which are characteristic of materials based on oil. One of these characteristic peaks is the one around 920 nm, which is the most striking one. In Figure 15 on the right, a decrease in reduced scattering coefficients for increasing wavelength can clearly be seen. The values are within the range of normal tissue.

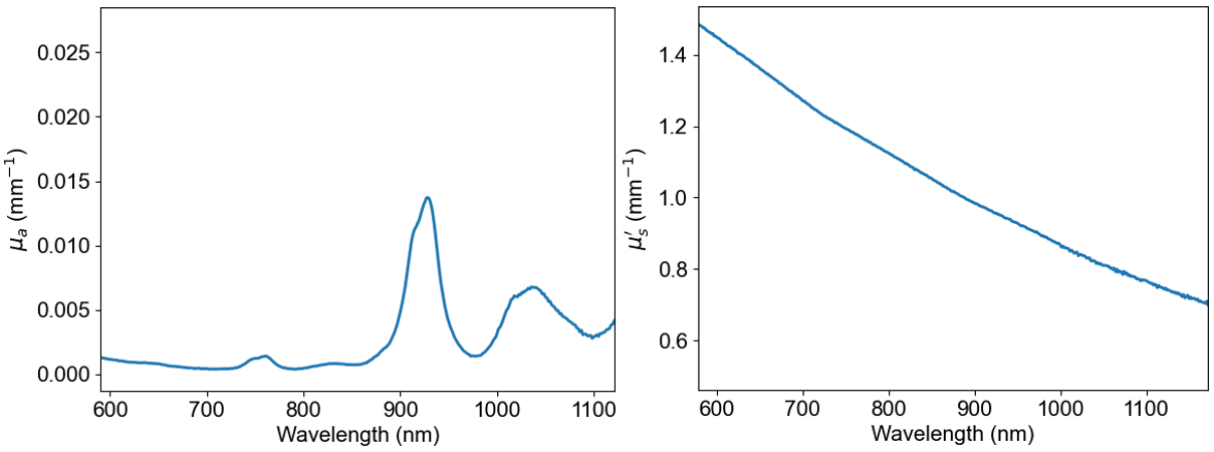

Figure 15: Absorption coefficients (left) and reduced scattering coefficients (right) of a sample of the base material determined by ILM.

In Figure 16, the time signals for the acoustic measurements can be found for the two transducers. The calculated speed of sound is 1441.1 m/s and the determined parameters of the power law for the frequency-dependent acoustic attenuation are α_0 = 0.585 and n = 1.582 (See Figure 17) at a water temperature of 21 °C. The acoustic impedance is 1.23 MRayl and follows from the speed of sound and the density, which is 855.28 kg m^{-3}.

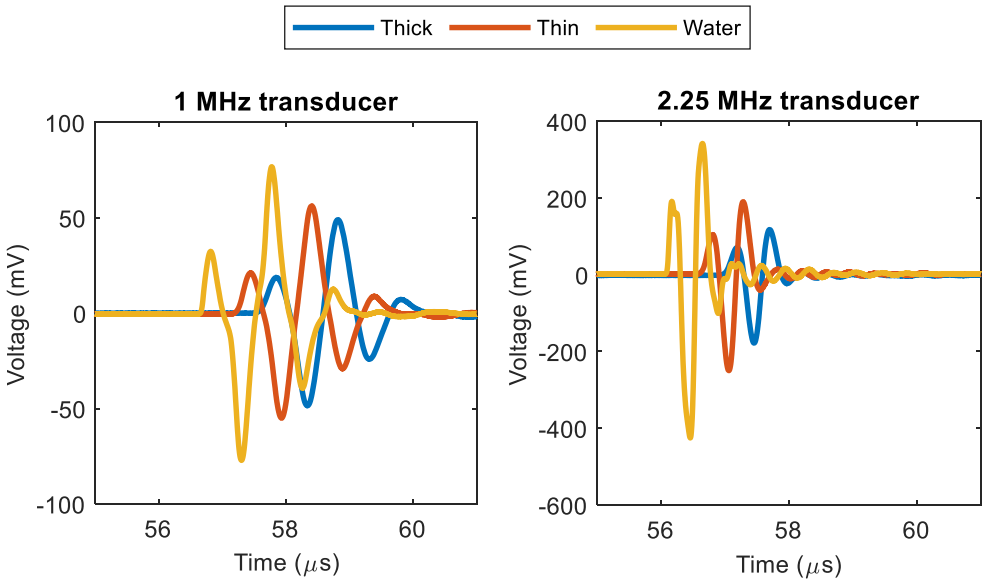

Figure 16: Time signal of the transmission measurement for just water and through the thin and thick side of the sample for a 1 MHz and 2.25 MHz transducer.

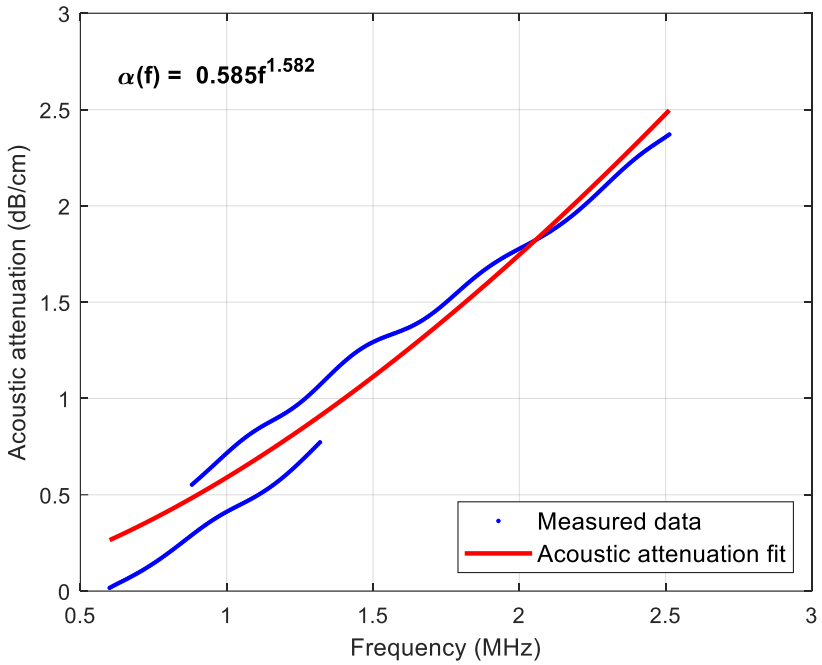

Figure 17: The frequency-dependent acoustic attenuation determined from the measured data is shown in blue, while the exponential fit is shown in red.

5.4.2. Phantoms

Figure 18: Photograph of the three phantoms from left to right mimicking a dark, medium, and light skin tone.

Three phantoms have been made (See Figure 18 for a photograph of the phantoms). With these phantoms, three different skin tones have been mimicked: light, medium, and dark. The skin-mimicking layers on the hemispherical part of the phantoms and the base material just underneath the layer have been assessed visually. The layers are not completely homogeneous due to some irregularities in or underneath the surface. From the outside, it is difficult to distinguish if these irregularities are air bubbles between the layers or locations where the material has folded or has been displaced from other locations. There are also some lighter and darker areas. In Table 6, an overview of the most notable findings can be found.

A cone beam computed tomography (CBCT) scan (kVp of 109 kV and an isotropic resolution of 467 µm) has been made of each phantom with a C-arm (ARTIS pheno, Siemens Healthineers) (See Figure 19 to 21). These scans were used to assess the interior of the hemispherical part of the phantoms for the presence of air bubbles and other particularities and to assess the status of the four channels. The channels were all open and the surfaces were relatively smooth. There were air bubbles present in all phantoms. For the phantoms with light and dark skin tone, these bubbles were less than 1 mm in diameter and mostly present at the border between the skin-mimicking and the base material. In the phantom with the light skin tone, there are fewer bubbles than in the phantom with the dark skin tone. The phantom with the medium skin tone not only has these bubbles at the border between the two materials but also in the bulk of the phantom. These air bubbles were also larger, with diameters of in general 1-1.5 mm.

Table 6: Overview of the findings after visual inspection of the three phantoms.

	Phantom light skin tone	**Phantom medium skin tone**	**Phantom dark skin tone**
Quadrant I	There seems to be a black thread of about 1 cm in or just underneath the skin-mimicking layer 2-3 cm from the centre. At the outer edge of the hemispherical part towards quadrant II and quadrant IV there are some spot irregularities.	No peculiar findings specific to this quadrant.	Several small spots on the surface are the result of air pockets underneath the CiO during the fabrication of the skin-mimicking layer.
Quadrant II	At the outer edge of the hemispherical part, there are some irregularities.	There is an elongated area, which is noticeably lighter, but the edges are darker. As if the CiO material was displaced outwards.	No peculiar findings specific to this quadrant.

Quadrant III	There is a small dent in the shape of a small air bubble, which was stuck underneath the skin-mimicking layer during the fabrication.	Some thin branched irregularities follow a circular pattern.	Several small spots on the surface are the result of air pockets underneath the CiO during the fabrication of the skin-mimicking layer.
Quadrant IV	No peculiar findings specific to this quadrant.	Some thin branched irregularities follow a circular pattern.	No peculiar findings specific to this quadrant.
Overall	The colouration of the layer at the hemispherical part is even. The most apparent blemishes are the thread and the occasional irregularities.	The colour of the layer is not homogeneous, with at the centre a dark spot and in quadrant II a light spot.	The colouration seems to be even, apart from a lighter spot at the centre. However, the irregularities found in the other two phantoms are present in this phantom spread out over all quadrants.

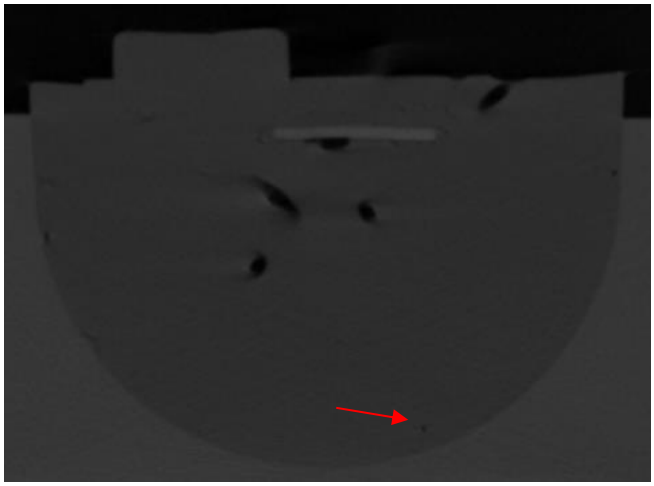

Figure 19: A cross-sectional image of the CBCT scan of the phantom mimicking a light skin tone. Various small air bubbles are present in the hemispherical part of the phantom (red arrow).

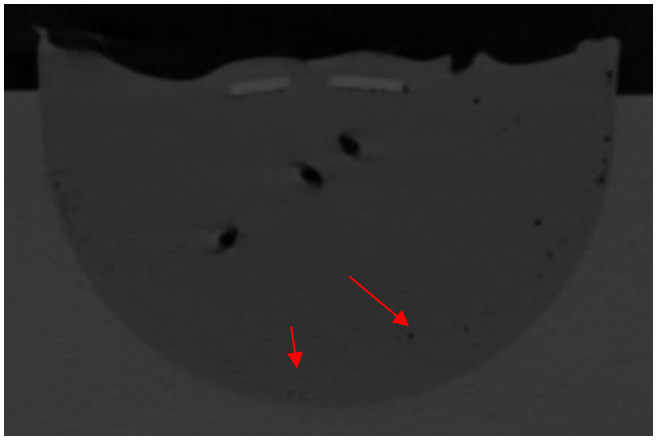

Figure 20: A cross-sectional image of the CBCT scan of the phantom mimicking a medium skin tone. Multiple small air bubbles are present in the hemispherical part of the phantom, both in the bulk at towards the surface (red arrow).

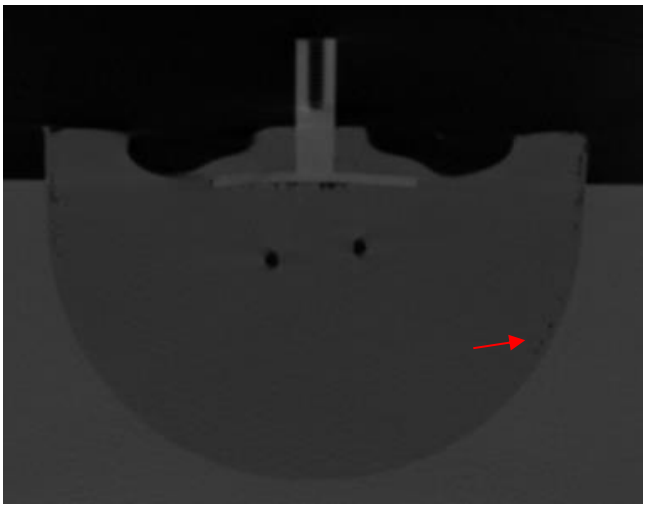

Figure 21: A cross-sectional image of the CBCT scan of the phantom mimicking a dark skin tone. Several small air bubbles are present in the hemispherical part of the phantom towards the surface (red arrow).

5.4.3. Skin layer thickness

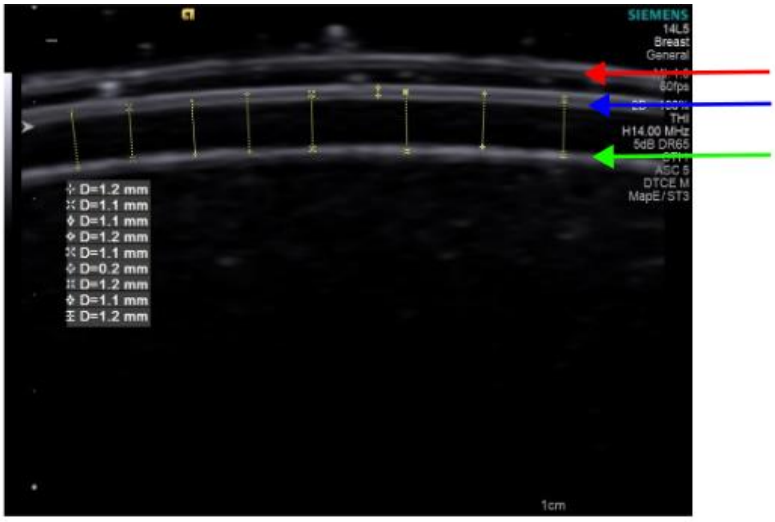

Figure 22: An ultrasound image from the surface layers of one of the phantoms. The different boundaries are marked by arrows: red for the protective foil, blue for the outer surface layer, and green for the transition from CiO to the base layer. The thickness of the skin-mimicking layer is measured at different locations.

The thickness of the skin-mimicking layer of the phantoms was determined at different locations within a scan (See Figure 22). The minimum difference in distance that could be measured was 0.1 mm. In the image shown above there are three different boundaries visible (marked by the arrows). The first boundary (red arrow) is the foil covering the probe. Above and beneath this boundary is ultrasound coupling gel (Aquasonic 100 Ultrasound gel, Aquasonic). The second boundary (blue arrow) is the transition from the ultrasound gel to the skin-mimicking layer. This boundary consists of two white lines with a black line in between. The distance between the white lines was measured and it was determined to be about 0.2 mm. The transition of the skin-mimicking layer to the base material can be seen as a fuzzier boundary (green arrow). The distance of the skin-mimicking layer was determined by measuring the distance between the centre of the third boundary and the black intermediate line of the second boundary. From the different measurements the mean and standard deviation per location and for the phantom as a whole were calculated. They can be found in Table 7. The layer for the light phantom has an overall thickness that is close to 1 mm. The overall layer thickness of the other two phantoms is larger, 1.2 and 1.1 mm, respectively. While there is some variation between measurement

locations, globally, the layer thickness is relatively constant. The largest deviation can be found for the phantom with the medium skin tone.

Table 7: Thickness of the skin-mimicking layers of the three phantoms based on ultrasound scans in mm. The mean and standard deviation of the different measurements are given for the five different locations and for the phantom overall are given.

	Phantom light skin tone	**Phantom medium skin tone**	**Phantom dark skin tone**
Location 1	1.03 ± 0.043	1.14 ± 0.049	1.15 ± 0.062
Location 2	1.04 ± 0.064	1.09 ± 0.063	1.13 ± 0.044
Location 3	1.01 ± 0.029	1.18 ± 0.053	1.10 ± 0.050
Location 4	1.06 ± 0.049	1.23 ± 0.066	1.11 ± 0.068
Location 5	1.03 ± 0.070	1.21 ± 0.086	1.12 ± 0.041
Overall	1.03 ± 0.056	1.17 ± 0.083	1.12 ± 0.057

5.4.4. Skin tone characterisation

The mean ITA° value values rounded to whole values for each phantom and each measurement location can be found in Table 8, as well as the respective skin tone categories corresponding to those values. There is a decrease in ITA° value with an increase in nigrosin concentration. The skin tone categories for the light and dark phantom are in agreement with the intended category. The phantom with the medium skin tone has some deviation for two measurement points but can overall be classified as tan. For all phantoms, there is a deviation in the ITA° value for the centre compared to the values at the quadrants. For the medium skin tone phantom, there are local variations in the measurements. Quadrant 4 is significantly lighter, and the centre is significantly darker than the rest of the phantom.

Table 8: ITA° values of the skin-mimicking layers of the three phantoms measured with the SkinColorCatch. The values as well as the corresponding skin tone classes are given for the five different locations [61].

	Phantom light skin tone	**Phantom medium skin tone**	**Phantom dark skin tone**
Quadrant 1	50 (light)	30 (intermediate)	-84 (black)
Quadrant 2	51 (light)	23 (tan)	-83 (black)
Quadrant 3	50 (light)	28 (tan)	-87 (black)
Quadrant 4	49 (light)	47 (light)	-86 (black)
Centre	66 (very light)	-30 (black)	-77 (black)

5.5. Discussion

The objective of this part of the project was to develop a simplified physical breast phantom that has a skin-mimicking layer and is suitable for experiments with the PAM3 system. The phantoms that were developed in this project consist of a base that mimics breast tissue covered with a layer of skin-mimicking material of around 1 mm thick. The base is made from a mix of NGW, paraffin and TiO_2. The skin-mimicking material on the other hand consists of CiO doped with alcohol-soluble nigrosin (the details can be found in Chapter 4). Each phantom has four channels that can be filled with an absorbing fluid and function as imaging targets.

The optical absorption of the breast-mimicking tissue is similar to the optical absorption of fatty breast tissue [38] (See Figure 15). And even though the reduced scattering coefficients are closer to those of fibroglandular tissue than fatty breast tissue, they are well within the range of normal tissue values [38] (See Figure 15). And since mimicking breast tissue was not the main concern of this subproject, these results were deemed acceptable. The speed of sound of the material is close to that of fatty tissue and the acoustic attenuation is also in the range of values found in the literature for fatty breast tissue [38]. To verify the acoustic properties, the results were compared to the values found for NGW with 8% paraffin by Maneas et al. and they closely match [78].

The skin-mimicking layers of the phantoms mimicking a medium and dark skin tone are thicker than 1 mm, as they are 1.2 and 1.1 mm respectively (See Table 7). The layer for the light phantom does have a thickness of 1.0 mm(See Table 7). The accuracy of the distance measurements is in the order of 0.1 mm, which means that a slight difference in measurement points can give a relatively large difference in the thickness measurement. The SOS values used for the US reconstructions are most likely also higher than the SOS of the skin-mimicking material, resulting in a discrepancy between the actual distance and the distance in the scan. Furthermore, the measurements are based on a cross-sectional image, and it is possible that the distance between the surface and the CiO-base transition is not the shortest. For instance, the probe might not have been completely perpendicular to the surface of the phantom. In addition, there is a chance that the measurements themselves might not have been taken completely perpendicular to the surface. With a measurement accuracy of 0.1 mm, this can result in significant differences. Unfortunately, it was not possible to use an imaging modality that could make a volumetric scan. Magnetic resonance imaging (MRI) and computed tomography had difficulties separating the CiO and the base material due to a lack of contrast. MRI also has a relatively low resolution, which renders it unsuitable for these small distances. Another modality that was investigated is optical coherence tomography. However, the available device can only be used for layers less than 0.1 mm thick and cannot measure a large surface area [82].

The ITA° values show a clear difference between the phantoms and the assigned skin tone classes are in general consistent with the intended skin tone classes (See Table 8). Since the phantoms do not contain melanin or a derivative of it, melanin-index (M-index) values were not used in the assessment. In the visible light part of the optical spectrum, the difference between nigrosin and melanin is significant. It is not known based on which wavelength or wavelengths the M-index is determined. It is therefore difficult to assess if the measured M-indices would accurately represent a real-life situation. And since there are only three different phantoms, it is difficult to link nigrosin concentration, M-index values, and ITA° values. For this to be possible, a broader range of nigrosin concentrations would have to be evaluated.

Limitations:

The results show a few important flaws in the developed phantoms (See Table 6). One issue is that the skin-mimicking layer is not fully smooth over the whole surface. In some locations, there are (micro)bubbles present due to air left in the material despite degassing the material. In addition, there are some irregularities on the surface. Some are most likely caused by difficulties with the release of the top mould component during the fabrication of the layer. These irregularities and bubbles will most likely be visible in PA scans and might cause visible artefacts. Unfortunately, due to time constraints, it was not possible to perform more iterations during the fabrication process to obtain more smooth and homogeneous layers. An explanation for the issues with the release of the mould could be that the spray can for the silicon coating was nearly empty. So, while during the fabrication the coating seemed to cover the whole mould evenly, it might be that the amount of silicon was unevenly distributed. A more even coating might result in an improvement in the results.

Another limitation is the inter-phantom variability of the layer thickness. The mould should have ensured that a constant 1 mm thick layer was fabricated, provided that an excess of material was poured into the mould. It is possible that during the fabrication of the layers, the mould was not fully closed, which resulted in a slightly thicker layer. More careful inspection of the mould while it was closed could perhaps have led to earlier detection of this occurrence. On the other hand, the measurement method itself could have resulted in distances being measured that were not the shortest distance through the skin-mimicking layer. Moreover, the resolution of the US device is also not high enough to accurately measure submillimetre distances to detect subtle deviations in thickness. So, while there is legitimate evidence for a deviation in layer thickness from the desired 1 mm, it is possible that the deviation could be smaller than was measured.

A limitation of the base material is that while the mixture of NGW and paraffin is a solid material at room temperature, at higher temperatures its viscosity greatly decreases. As a result, the TiO_2 can sink to the bottom and aggregate. By stirring the mixture vigorously, it was attempted to

minimise this occurrence. However, stirring can introduce air into the material, which necessitates degassing the material. During the degassing process, the TiO_2 has time to sink again. This process cannot easily be controlled. As a result, the scattering properties of the base material can vary between phantoms. Unfortunately, it was not possible to verify for each phantom what the scattering properties of the base material of that particular phantom were.

Lastly, during the fabrication process, air bubbles can be introduced in the base material during the mixing of the mixture. Despite efforts to remove air bubbles and prevent new air bubbles from forming, there are still air bubbles present in the hemispherical part of the phantoms (See Figure 19 to 21). They are especially present in the phantom with the medium skin tone. In the other two phantoms, the air bubbles are mostly in the border between the skin-mimicking layer and the base of the phantom. However, in the medium skin tone phantom, there are also a significant amount of air bubbles in the bulk of the base material. There is a high likelihood that the irregularities seen underneath the translucent skin-mimicking layer are related to the air bubbles seen in the CBCT scan. But from the outside, this cannot be fully confirmed. An explanation for these bubbles could be that when the hot base material is poured on top of the cold skin-mimicking layer air bubbles are formed at locations in which there are already small irregularities on the inner surface of the skin-mimicking layer. Due to the lower temperatures at the outer parts of the phantom, the base material at that part will cool down faster than the rest of the material and will solidify. As a result, the air bubbles that are present in the outer layer are trapped and cannot be removed from the base material. In addition, the interaction between the cool skin-mimicking layer and the hot base material could have led to the formation of some deformation of the inner surface of the skin-mimicking layer, which in turn could have resulted in air bubble formation and trapping of air bubbles. Degassing the base material longer, letting it cool down more before pouring it in the mould and pouring the base material even more carefully, could potentially reduce these irregularities and air bubbles.

Strength and advantages:

While the results show that improvements are necessary to fabricate phantoms of better quality, these phantoms are, to our current knowledge, a new development in the field of phantom development for PAI. They are the first phantoms, in which a skin-mimicking layer is integrated in a phantom of this size with a geometry suitable for a hemispherical PAT system. In the past, other phantoms have been specifically developed for the PAM3. Dantuma et al. have for instance developed multiple non-tissue-like phantoms for the PAM3 to investigate various device parameters such as the PA spatial resolution and light fluence distribution [79]. And Dantuma et al. have made a breast phantom, which mimicked different tissue types. While this phantom did have a skin layer, this layer was mostly for aesthetics and did not properly mimic the optical properties of the epidermis [38]. Since the article of Mantri et al showcased that variations in skin tone do influence PAI, various phantoms for PAI that mimic the skin have been developed [18,83]. An important limitation of the phantoms developed by other research groups is that the geometry of their phantom is not suitable for a hemispherical PAT system such as the PAM3. This necessitated the need to develop our own phantom.

An advantage of this phantom is that its application might not be limited to just hemispherical systems. While it is developed specifically for experimentation with the PAM3, the geometry of the phantom does allow other types of scanner geometries to be used. A linear US probe has been used on the phantom already. Moreover, imaging the breast with PAI has already been studied with linear array transducers and full-ring array transducers [9]. The similarities in geometry between the developed phantom and the breast would suggest that this phantom can therefore also be scanned with these types of PAI systems. In theory, this would mean that the same set of phantoms can be scanned by different systems. This would allow the comparison of results between scanners and a better understanding of how skin tone can affect different systems when they are used for the same application.

A second advantage is the presence of four imaging targets. Each imaging target runs through the whole phantom and can be used to investigate how the PA intensity of the target changes with

depth. Therefore, it is possible to investigate four different absorbing solutions at the same time. This can reduce the number of scans and consequently the amount of data necessary for the experiment.

While there are currently some flaws in the developed phantoms, the method itself shows great potential to fabricate this type of phantoms with a high reproducibility. The channels can be positioned with the same orientation and depth each time, due to the pins. The use of the mould also ensures that in the fabrication of the skin-mimicking layer, the effect of outside factors on the results is minimised as much as possible. And while the current results show quite some variation in the results, with more care and patience in the fabrication of the skin-mimicking layer more homogeneous and even layers can most likely be obtained.

A last advantage of these phantoms is that it opens the door to other phantoms with the same geometry. While the current design is rather simplistic, there is potential to alter the design to add more complexity or make it more realistic. The inside of the phantoms could be made of materials with different acoustic and optical properties to mimic both fatty and fibroglandular tissue. Or different targets can be added to investigate the influence of skin tone on other parameters. The mould itself can also be used to fabricate phantoms without a skin-mimicking layer by leaving the skin layer fabrication step out.

5.6. Conclusion

Three phantoms suitable for experimentation with the PAM3 have been developed. These three phantoms are a simplified representation of the fatty breast with three different skin tones: light, medium and dark. The thickness of the skin-mimicking layer is around 1 mm and is relatively homogeneous over the whole surface. With four imaging targets, the phantom could potentially allow the opportunity to investigate different absorbing solutions at the same time. This could increase the efficiency of the experimentation. Unfortunately, there are some major flaws in the currently developed phantoms. Most of these flaws are most likely related to the fabrication of the phantoms. It is necessary to perform some iterations in this fabrication process to perfect it and obtain a method that gives good and consistent results. Nonetheless, while improvements are necessary, the phantoms show a promising prospect for phantom experimentation to investigate the influence of skin tone on the imaging performance of a PAI system.

Chapter 6

6. Influence of skin tone on photoacoustic breast imaging: phantom study

6.1. Introduction

Due to an increased interest in the subject of how skin tone influences photoacoustic imaging (PAI), several phantom experiments have been conducted. A phantom study can be used to bridge the gap between in silico and in vivo experiments and can therefore be of great value. A phantom experiment is an excellent method to investigate the performance of a system or the influence of a specific factor in a realistic setting, while also having the freedom to tune specific conditions. Another advantage of phantom studies is that the experiments can be standardised to ensure repeatability and to allow comparison to similar phantom studies.

The two phantom studies investigating the influence of skin tone on PAI were conducted using 2D photoacoustic (PA) systems. Else et al. and Vogt et al. both found that with increasing skin tone there was an increase in PA signal intensity from the skin-mimicking layer and an increased presence of artefacts. Furthermore, they show that there is a clear deviation in the PA measurements of the oxygen saturation between skin tones [17,18]. However, the results from their studies can in all likelihood not be generalised for all PA systems or even for all measurement sites. Differences between illumination and detection geometry might cause differences in the precise effect skin tone has on the images. The same might be possible for differences in optical and acoustic properties of the tissue types in the imaged site. Vogt et al. and Else et al. simulated arbitrary tissue [17,18]. PAI is regarded as a promising imaging modality for breast imaging [8,9,84]. Therefore, addressing the effect of skin tone specifically on breast imaging is of great value for the translation of this modality to the clinic.

A major end goal of this project is to gain insights into how skin tone influences the image quality of PA breast images made with the Twente Photoacoustic Mammoscope (PAM) 3 system with a phantom experiment. An important difference between this study and the already conducted ones is that the PAM3 will give 3D information instead of 2D. There are no other studies that investigate the influence of skin tone on PAT. This too shows the major value of this study. This chapter of the thesis will focus on the conducted phantom experiment. The parameters that will be investigated are the imaging depth, the signal-to-background ratio (SBR) of various targets the occurrence of artefacts and the PA spectra of the skin-mimicking layer. The SBR can give an impression of the detectability of the imaging targets.

Related sub-research questions:

- *What changes can be found in the image quality between 3D photoacoustic scans made of physical phantoms that represent women with different skin tones?*

6.2. Background: The photoacoustic mammography system

The PAM3 system is a hybrid PA and ultrasound (US)-transmission tomographic system dedicated to 3D breast imaging (See Figure 23) [76]. While there have been clinical studies with the device [76], it is still in its development phase. With the US-transmission part of the system, it is possible to obtain a 3D speed of sound map of the imaged object. This map can be used in the PA reconstruction to correct for differences in the speed of sound between materials or tissues. As a result, the reconstructions can be more accurate [76]. The reconstructed images have an isotropic resolution with a maximum of 426 µm, which rivals the resolution of magnetic resonance imaging (MRI) images [76].

The PAM3 system consists of a hemispherical photoacoustic tomography (PAT) system built into a custom-built examination table. In the tabletop is an aperture beneath which is a water-filled compartment, the imaging bowl. To create an image of the breast, the patient has to lie in a prone position on top of the table and put one breast through an aperture in the table. With the breast pendant in the imaging bowl, the tissue can be illuminated over a solid angle of 2π steradians. Similarly, generated PA waves can be detected over the whole hemisphere as well. As a result, the breast can be reconstructed with limited to no limited view artefacts. This is one of the reasons why the breast is an ideal organ for PAT [76].

During the measurements, the pendant breast is immobilised in the imaging bowl with a breast-supporting cup. This cup positions the breast in the centre of the imaging bowl while at the same time keeping the breast stabilised to minimise motion during the measurement. The cup is made of optically and acoustically transparent polyvinyl chloride (PVC) and has a thickness of approximately 180 µm. There are holes in the cup to allow water to enter the cup to improve the acoustic coupling between the breast and the transducers [76,81].

The system has 40 laser outputs with a high beam divergence that are arranged over the hemispherical imaging bowl. As a result, the breast is illuminated homogeneously with a radiant exposure below the Maximum Permissible Exposure (MPE) [76]. The wavelength of these lasers can be tuned to be in the range of 680 to 1060 nm to allow spectral imaging. With measurements obtained at different wavelengths, quantitative imaging could in theory be achieved [80]. The output energy of the lasers is wavelength-dependent as it varies between 450 mJ for 680 nm and 230 mJ for 1060 nm [76].

The generated PA waves can be detected with 512 US detectors [85,86]. These detectors are highly sensitive as the minimal detectable pressure is on average 0.3 Pa [76]. The centre frequency of the detectors is about 1 MHz with a wide fractional frequency bandwidth of 123% [76,85,86]. These detector arrays can receive US waves within an acceptance angle of 34 degrees at -6 dB [80]. Due to the specific arrangement of the US detectors, there is a physical focusing effect toward the centre of the imaging bowl. It was found that the resulting enhanced sensitivity can lead to an increase in the intensity of the PA signal for structures deeper than 40 mm. However, at depths larger than 60 mm, the images will be dominated by noise and interference signals [76]. The PAM3 system with its quality of illumination, detection, and analog front-end electronics modules has been shown to receive signals from deeper in the breast than hitherto reported, reaching 48 mm in a specific case [76,85].

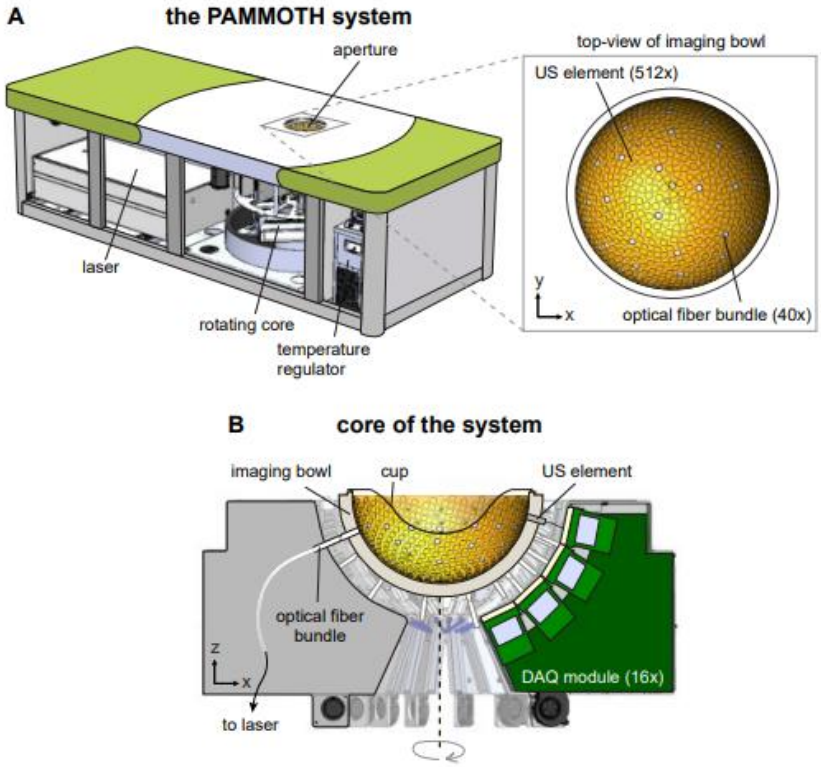

Figure 23: A schematic overview of the PAM 3 system with the 40 laser fibres and 512 ultrasound transducers in the imaging bowl [80].

6.3. Methods

For this phantom study, the three phantoms that were developed in Chapter 5 were used. The four channels in the phantoms were filled with a blood-mimicking fluid (BMF) to ensure good visualisation of the imaging targets while keeping the optical absorption within the physiologically realistic range. To have the possibility to assess differences in effect between veins and arteries, the four channels were filled with BMFs that mimic different blood oxygen saturation levels. All phantoms have been scanned with the PAM3, and the reconstructions have been performed using an iterative least-squares fit model-based reconstruction with a time-of-flight speed-of-sound correction. The radiofrequency (RF) data and reconstructed scans are analysed using MATLAB (Release 2024a, MathWorks). The data analysis is described in Section 6.3.3.

6.3.1. Imaging targets

The BMFs consist of an aqueous solution of the hydrated form of $CuSO_4$ (10695482, Fisher Chemical) and $NiSO_4$ (AC415611000, Thermo Scientific Chemicals). The $CuSO_4$ is a surrogate for oxyhaemoglobin and the $NiSO_4$ for deoxyhaemoglobin. These sulphates cannot be considered direct substitutes for these endogenous chromophores. However, there are similar characteristics in the absorption spectra in the near-infrared range. Additionally, these sulphates have a long-term photostability, which makes them suitable as chromophores in PAI [87,88].

Four different BMFs were made that mimic four different blood saturation levels of whole blood with a haemoglobin concentration of 150 g/L [88]. The absorption coefficients of the BMFs were matched to those of blood at 797 nm [87]. The protocol of S. Karremans was followed to produce the BMFs (See Appendix G), with a slight alteration to the molarity of the $NiSO_4$, which was 2.3 M as opposed to 2.2 M. The optical absorption properties of the solutions were determined with transmission measurements performed with a spectrophotometer (UV-2600i, Shimadzu) and the Beer-

Lambert law. The absorption coefficients of the different BMFs and those of blood for the corresponding saturations can be seen in Figure 24. The oxygen levels that have been mimicked and the corresponding concentrations of $CuSO_4$ and $NiSO_4$ can be found in Table 9, as well as the absorption coefficients at 797 nm and the deviation from the measured values to the desired values.

Table 9: Overview of the four different blood-mimicking fluids with the saturations they have to mimic, the concentrations of $NiSO_4$ and $CuSO_4$ as well as the target absorption coefficients, the measured ones, and the difference between the two.

Target # in analysis	Mimicked saturation (%)	C_{CuSO4} (M)	C_{NiSO4} (M)	$\mu_{a,blood}$ @ 797 nm (mm^{-1})	$\mu_{a,BMF}$ @ 797 nm (mm^{-1})	Difference μ_a (%)
4	55	0.094	1.048	0.4260	0.4237	0.55
3	70	0.119	0.699	0.4264	0.4262	0.03
2	85	0.145	0.349	0.4267	0.4286	0.45
1	100	0.170	0	0.4270	0.4305	0.81

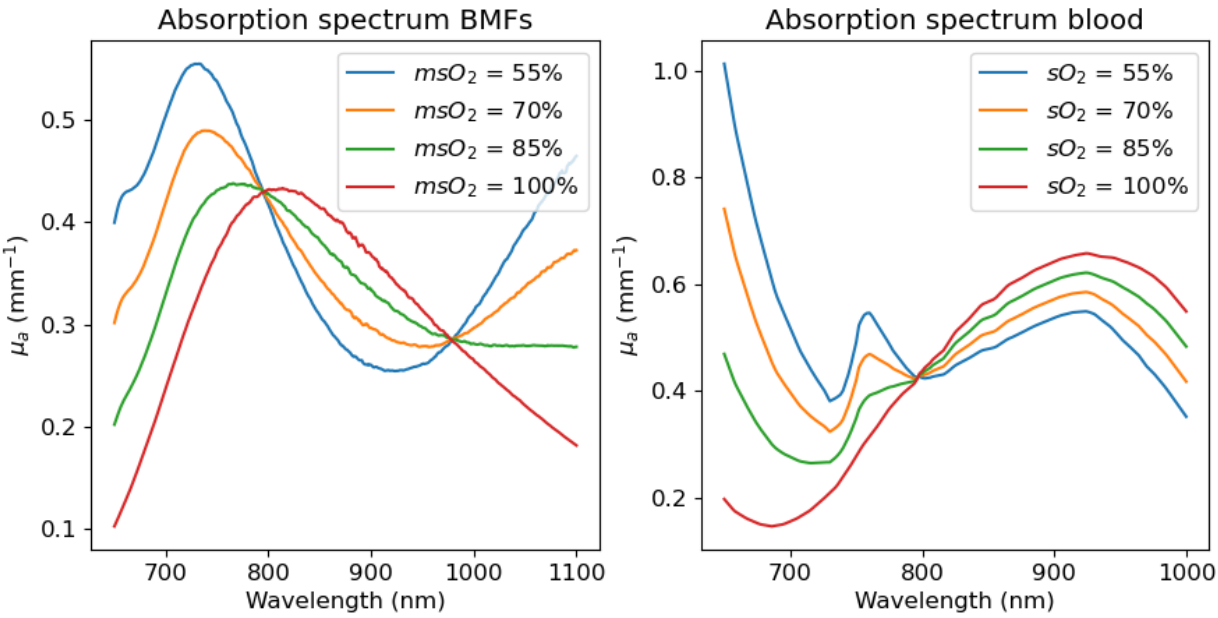

Figure 24: On the right, the absorption coefficients of the four different BMFs with a mimicked blood oxygen saturation (msO_2) of 55%, 70%, 85%, and 100%, respectively. On the left, the absorption coefficients of four different blood oxygen saturations (sO2) of 55%, 70%, 85%, and 100% respectively for blood with a haemoglobin content of 150 g/L. The graph is based on data compiled by S. Prahl [89].

6.3.2. Data acquisition

The phantoms were positioned in the centre of the imaging bowl with the hemispherical part of the phantom under the water line. The orientation of all three phantoms was similar. A wavelength sweep was performed from 680 nm to 1060 nm in steps of 5 nm. During the wavelength sweep a single scan is made for each wavelength and the imaging bowl remains in the starting position. In addition, six full scans were made for the following wavelengths: 755, 797, 833, 870, 920, and 1060 nm. For a full scan, 101 scans are made per wavelength and the imaging bowl rotates in between scans to cover 360° in 100 steps. These 101 scans can be reconstructed into a volumetric dataset. The full protocol for the data acquisition can be found in Appendix H. The reconstructions were performed with the use of time-of-flight speed-of-sound maps in the reconstruction process.

6.3.3. Data analysis

Signal-to-background ratio
A Hessian filter was applied to the reconstructions to enhance the signal from the imaging targets and reduce the signal from the background. A mask was used to isolate the signals from the regions in which the imaging targets were located. This mask was made for each phantom specifically and was based on where the imaging targets could be visually distinguished from the background. This means that while the imaging target may extend further in the phantom, its presence cannot be visually detected in the scan. The SBR for the imaging targets was determined for different depth layers [90]. The depth layers were defined from the surface of the phantoms radially inwards to account for the decrease in the fluence and thus the decrease in signal amplitude (See Figure 25). Each depth layer encompasses about 2 mm of phantom material. For each depth layer, the average value of the voxels corresponding to the imaging targets was calculated as well as the average value of the voxels corresponding to the background. The background is defined as all voxels that do not correspond to the imaging targets.

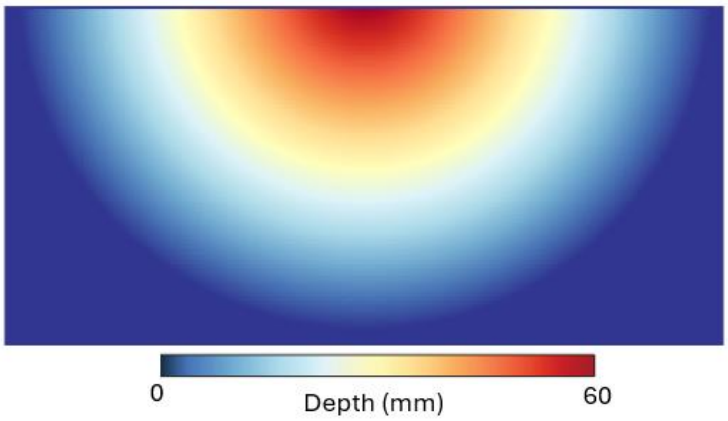

Figure 25: A schematic overview of how the depth layers are defined.

Imaging depth
For each wavelength, a measure of reached imaging depth was extracted from the reconstructions by locating the maximum depth at which the imaging targets can still be distinguished from the background. A cut-off value of 6 dB for the SBR is used to define the reached imaging depth [18]. For each imaging target, it is determined per phantom whether and at which depth the SBR first crosses the cut-off value. Due to the positioning of the imaging targets and the size of the phantom, the maximum depth at which an imaging target could be present in the reconstruction is 51 mm. However, it is possible that for certain phantoms higher imaging depths could have been reached. Should this be the case, the cut of value will not be crossed. While in theory it could be estimated by extrapolation at which depth the SBR crosses the cut-off value, it was chosen not to do this to avoid speculation. Therefore, in such occasions, the maximum reached imaging depth was set to 51 mm.

Signal from the skin
The signal from the skin-mimicking layer is determined from both the data from the wavelength sweep and the reconstructed data from the five full scans. The analysis of the raw time signals was performed semi-automatically. The skin-mimicking layer is the first phantom component that can produce a detectable PA signal. An estimation of the distance between the imaging bowl and the phantom was used to determine in which range of the time signals the signal of the skin-mimicking layer should be located. The first significant peak in the time signals within this data range was assumed to be the signal produced by the skin-mimicking layer. Since between transducers slight differences in the location of this signal are possible, locating this peak had to be performed for each transducer individually. For a specific transducer, the location and amplitude of this peak were determined manually in the time

signal obtained at 680 nm. For the other wavelengths, the amplitude of this specific peak was subsequently determined automatically using the location of the peak at 680 nm. After the signal amplitudes were obtained for all measured wavelengths, a post-processing step was applied. This post-processing step consists of a compensation for the known wavelength dependence of the laser output energy, as a higher laser power will result in a higher PA signal. Since selecting the location of the peak is a manual task, only the data of a small selection of transducers was analysed. The raw time signals of the wavelength sweep of 41 out of the 512 transducers were analysed. The transducers were strategically selected to ensure sufficient coverage of the whole surface of the imaging bowl while keeping the number of transducers within reason. One of the selected transducers is the one at the very bottom of the imaging bowl (transducer number 448). The position of all of the 41 transducers in the imaging bowl can be found in Figure 26.

To determine the signal from the skin-mimicking layers from the reconstructed data, the voxels corresponding to the skin-mimicking layer were isolated. Then, of these selected voxels, the average voxel value was determined for all six scans. Unlike for the results from the wavelength sweep, no compensation for the variation in laser output energy was applied to the results obtained from the reconstructed data.

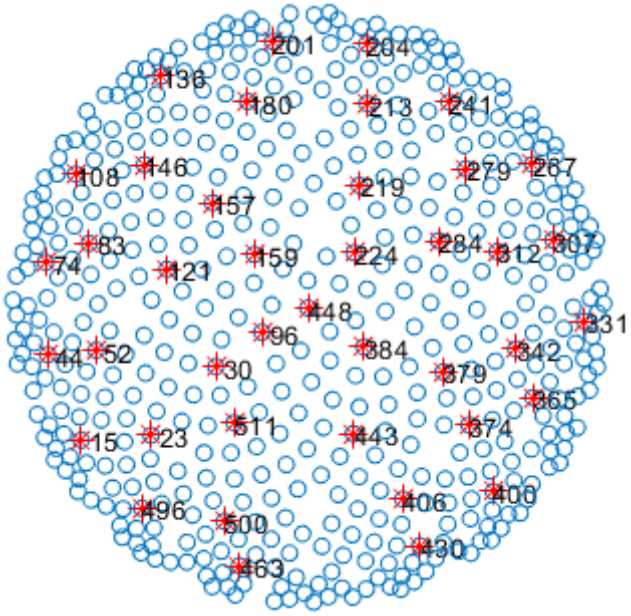

Figure 26: Position of the transducers in a cross-sectional projection. Since it is a projection, the distance between the 512 transducer positions in the image is not representative of the actual distance between the transducers.

6.4. Results

To assess the changes in the imaging performance of the PAM3 system for different mimicked skin tones, the imaging depth, SBR of the imaging targets and signal of the skin were assessed and the results are described in this section. First, the pre-processed data from the reconstructions of the three phantoms were visualised to obtain an initial impression of the data. The SBR and imaging depth were obtained from the reconstructed data by analysing the signals from the imaging targets. The change in the signals from the skin-mimicking layer was determined from both the raw time signals from the wavelength sweep and the reconstructed data.

6.4.1. Volumetric maximum intensity projections

In Figures 27 and 28, a bottom and side view of the volumetric maximum intensity projections (MIP) of the reconstructed scan at 870 nm of each phantom can be seen before and after the application of a filter to isolate the imaging target. The higher the PA intensity the brighter the colour in the MIPs is. For simplicity, hereafter the phantoms will be referred to as light, medium and dark phantoms.

The volumetric MIPs of the unprocessed reconstructions (Figure 27) clearly show an increase in the signal from the skin between the light phantom and the medium phantom. In the light phantom, for three of the imaging targets, the part closest to the surface can already be distinguished. This is not the case for the medium and dark phantoms. Contrary to the expectations, the MIPs between the medium and dark phantom show little difference. Since the absorption coefficients of the skin-mimicking layer of the dark phantom are thrice as high as those of the medium phantom, it was expected that some difference would be visible in the reconstructions as well. Especially in contrast to the visible difference between the light and medium phantom, the similarity between the medium and dark phantom is striking.

From the MIPs of the processed reconstructions, it can be appreciated that the visibility of the imaging targets decreases for increasing nigrosin concentration. It can also be seen that the MIPs contain more background signals for increasing nigrosin concentrations. This observation is the first indication that the contrast between the imaging targets and the background is enhanced in phantoms that simulate a lighter skin tone. For the light and medium phantom, all four imaging targets can be located easily. For the dark phantom, on the other hand, while the imaging targets are still somewhat discernable, they are more difficult to distinguish from the background. For the dark phantom, the imaging targets can also not be followed as deeply as for the other two phantoms. While in the MIPs of the unprocessed reconstructions, there is little difference between the medium and dark phantom, in the MIPs of the processed reconstructions there is a clear difference. This observed difference aligns with the expectations.

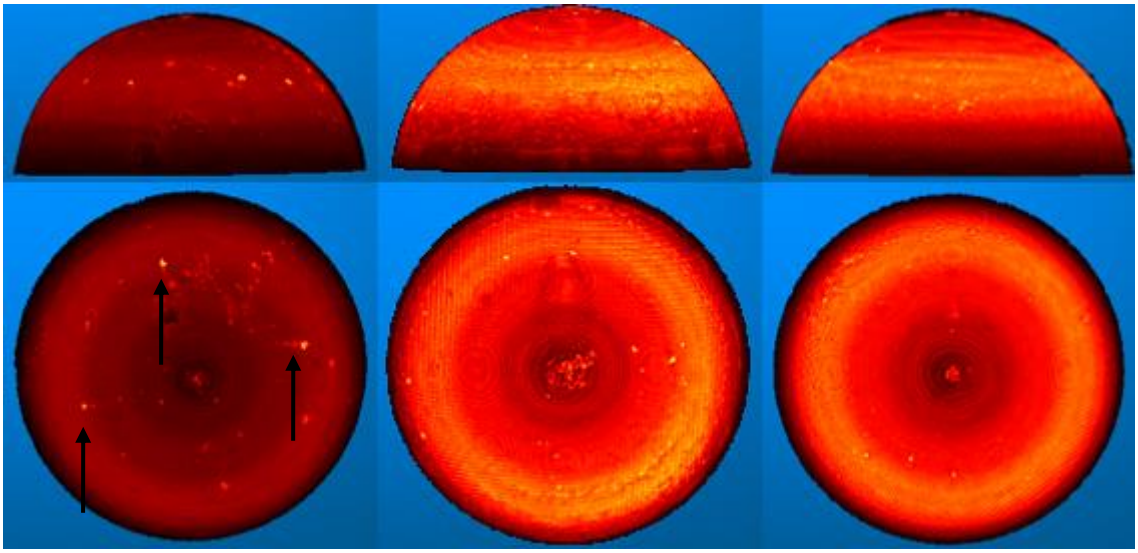

Figure 27: Bottom and side views of volumetric MIPs of unprocessed reconstructions at 870 nm for the three phantoms from left to right: light, medium, and dark. The black arrows point towards where parts of the imaging targets are visible in the MIP of the light phantom.

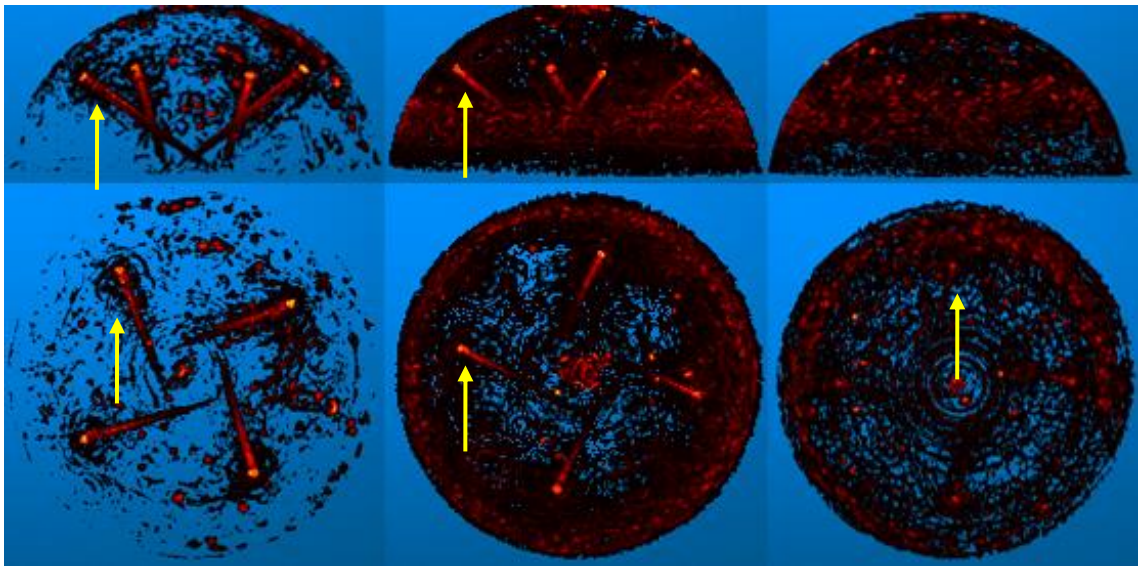

Figure 28: Bottom and side views of volumetric MIPs of processed reconstructions at 870 nm for all three phantoms from left to right: light, medium, and dark. The yellow arrows point towards where one of the imaging targets can be located in the three phantoms.

6.4.2. Signal-to-background ratio imaging targets

The SBR for imaging target 1 for the different depth layers is shown in Figure 29 for the three phantoms. The grey horizontal line marks the 6 dB cut-off value, which was used to determine the measure for the reached imaging depth. For the other three targets, the results are qualitatively similar and can be found in Appendix I Figure 58. It can be seen the SBR varies across different wavelengths. Between the phantoms, the decrease in the SBR over depth generally becomes steeper from light phantom to dark phantom and appears to approximate a linear trend. For all three phantoms, the values for the SBR for 797, 833 and 870 nm are very similar to each other for all depths. However, the SBR values for 755 nm are noticeably lower than those for the aforementioned three wavelengths, in particular for the medium and dark phantom, though they still follow the same general trend. The SBR values for 920 nm and 1060 deviate significantly from the others. The phantom material itself exhibits a higher optical absorption around 920 nm (See Section 4.5.1. page 42 and Section 5.4.1. page 54). This leads to a significant decrease in optical fluence at the site of the imaging targets for this wavelength in comparison to the other wavelengths. This accounts for the sharp decrease in SBR. For 1060 nm, the SBR values are lower for the light phantom in comparison to those for the shorter wavelengths. However, with a darkening in the skin tone, the SBR values for 1060 nm become more similar to those for the shorter wavelengths. It can be observed in the graphs that the SBR values can become negative, indicating that the background intensity exceeds that of the imaging targets.

To facilitate the comparison of the differences in SBR values for the different targets for various wavelengths at a specific depth layer, the SBR of the four targets at depth layer 10-12 mm is shown for the three phantoms in six separate bar charts for the six wavelengths (See Figure 30). For most of the wavelengths, the SBR values of the light phantom are in general higher than those for the medium and dark phantom. However, the SBR values for the dark phantom appear to be similar to slightly higher than those for the medium phantom. For 1060 nm, the difference between the phantoms is minimal. For the medium skin tone, the SBR values between targets are relatively consistent for all wavelengths except for 1060 nm. For this wavelength, there is a notable drop in the SBR for target 3 in comparison to the other targets. For the dark phantom, the values for targets 2 to 4 are relatively similar for 797, 833, and 870 nm, whereas the SBR for target 1 is higher. For all phantoms, the effect of the fat peak at 920 nm is noticeable in the SBR for all imaging targets. Generally, with increasing wavelength the SBR values appear to increase for the medium and dark phantom. However, for the light phantom, the SBR values remain relatively stable.

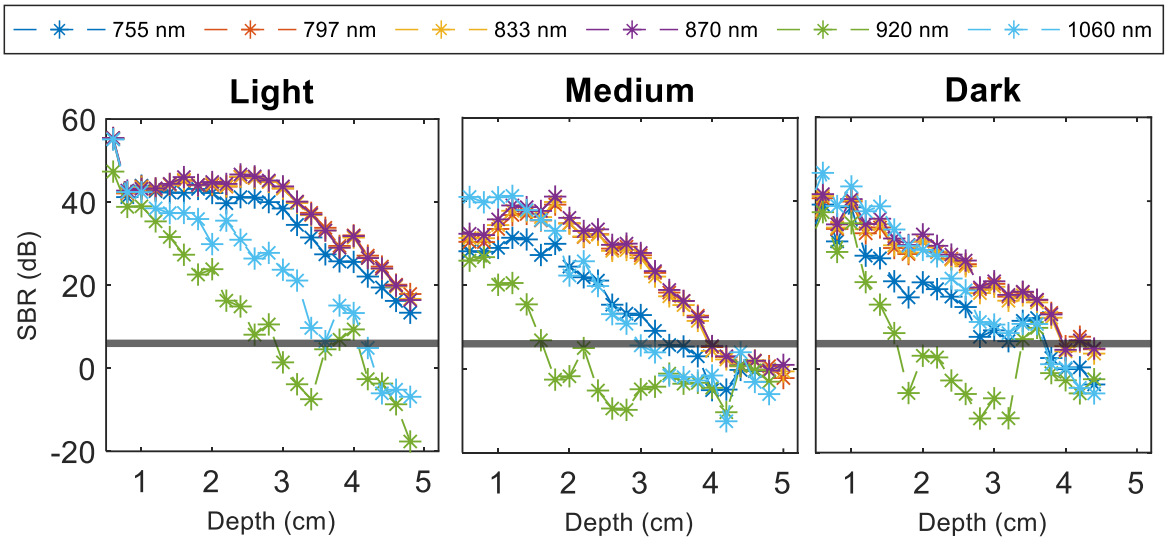

Figure 29: The SBR for the six different wavelengths for target 1 for the different depth layers. The grey horizontal line marks the 6 dB value. Be aware that a data point at "depth" 2 cm represents the SBR value for the parts of the imaging targets within the depth layer 2.0-2.2 cm.

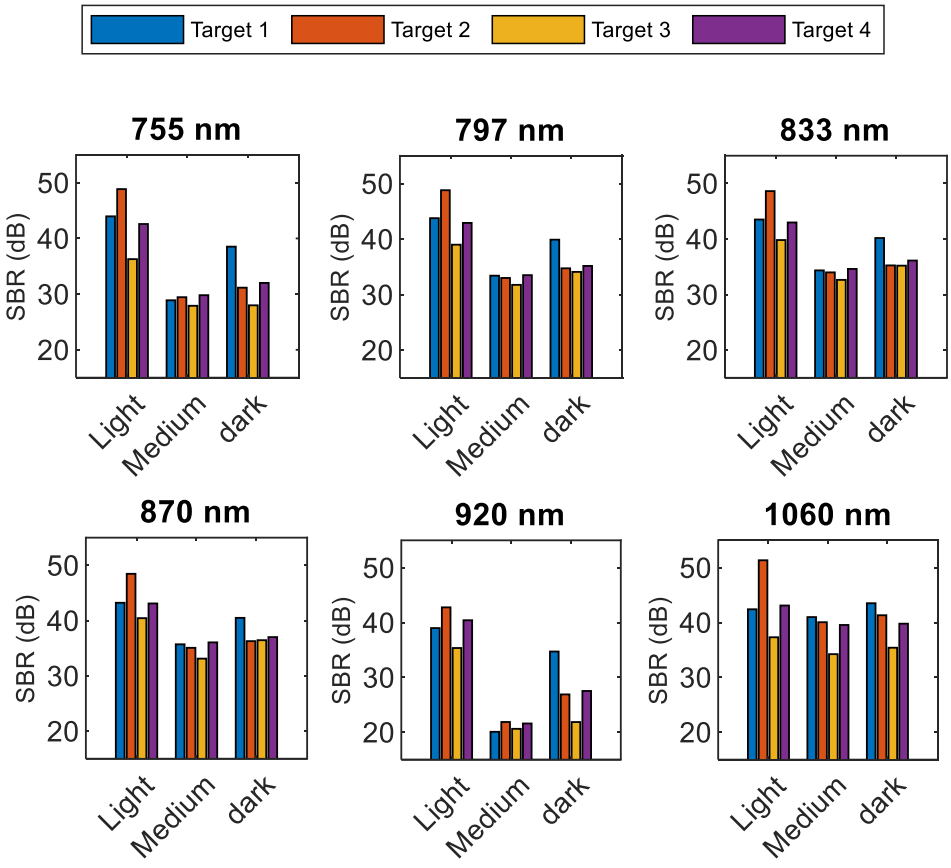

Figure 30: The SBR for the depth layer 10-12 mm for the four imaging targets for the three phantoms shown for the six wavelengths.

6.4.3. Imaging depth for different wavelengths

For the six wavelengths (755, 797, 833, 870, 920, and 1060 nm) a measure of the reached imaging depth has been determined from the reconstructed data. As mentioned before, a measure of the

imaging depth, from hereon referred to as imaging depth, was obtained by determining for which depth the SBR first crosses the threshold of 6 dB. In Figure 31, for each target, the imaging depth at different wavelengths for the three phantoms is shown in a bar chart. In Appendix I Figure 59 to 61, the difference in the visibility of the imaging targets can already be appreciated by visual inspection of the volumetric MIPs of the three phantoms for the six wavelengths. The imaging depth that can be reached by the PAM3 system for the light phantom, when considering only the first four wavelengths, varies between 47 mm and 51 mm, depending on the wavelength. For the medium phantom, the imaging depth varies between 33 mm and 47 mm, while for the dark phantom, it ranges between 33 mm and 45 mm.

For the light phantom, the imaging depth for the four targets is generally close to or equal to the maximum imaging depth that can be assessed with the applied approach. However, at 920 nm and 1060 nm, the imaging depth is decreased, most likely due to the increased optical absorption by the phantom material. For the medium phantom, from 755 nm to 797 nm the imaging depth increases, plateaus, and then decreases again for 920 and 1060 nm. A similar trend can be observed for the dark phantom. There is a distinct difference between the light phantom and the medium and dark phantoms. In particular, for targets 1 and 3, where there is a significant decrease from light to medium phantom. Conversely, there is no difference in imaging depth for targets 1 and 3 between the medium and dark phantom for 797, 833, 870 and 920 nm. For targets 2 and 4, there is a gradual decrease in imaging depth from light to dark phantom, which follows the expected trend. The greater imaging depth for 755 and 1060 nm for the dark phantom compared to the medium phantom is unexpected. For the light phantom, the maximum possible imaging depth that could be assessed in this study was reached relatively easily for almost all four imaging targets. This can also be appreciated in the graphs for all four imaging targets found in Appendix I Figure 58. In general, for all three phantoms, the imaging depth decreases, increases, and then decreases again from target 1 to target 4.

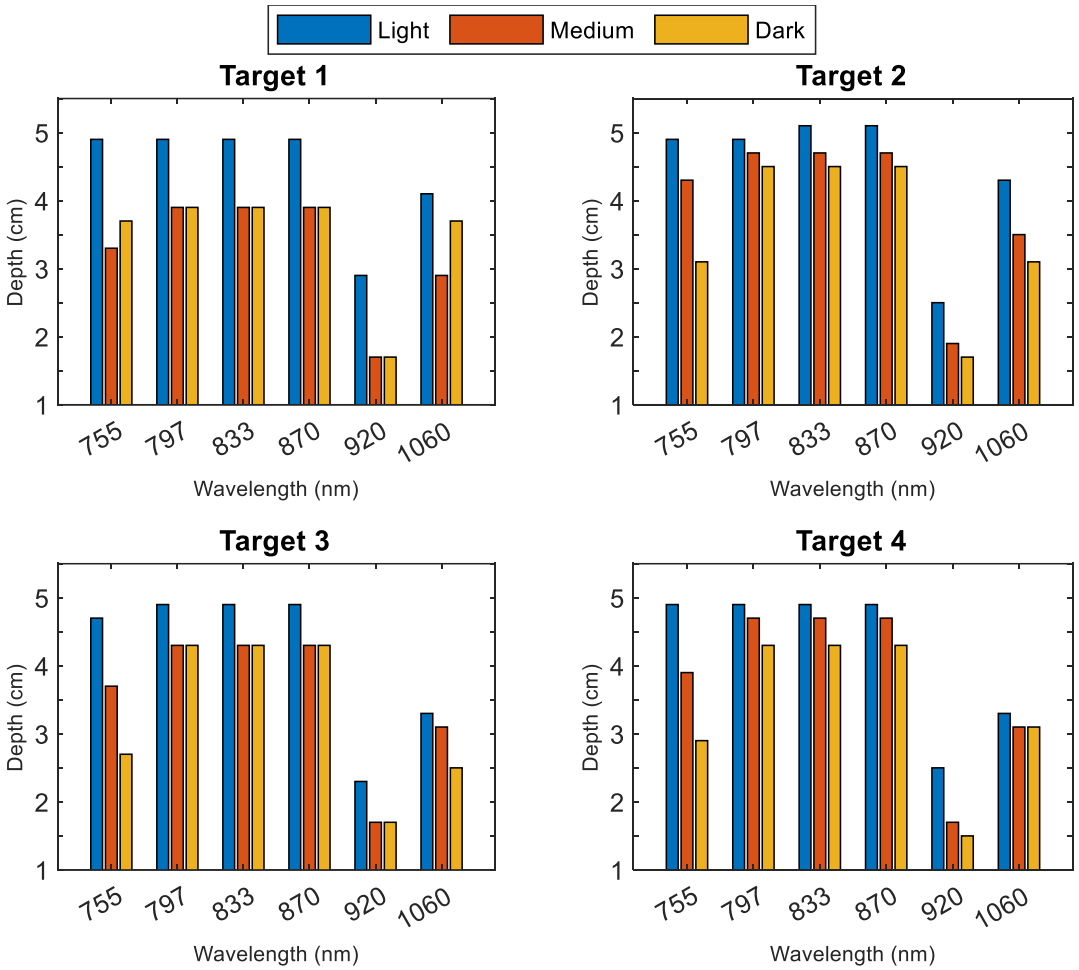

Figure 31: A measure of the imaging depth for the six wavelengths visualised in a bar chart comparing the three phantoms for each target separately.

6.4.4. Signal from the skin-mimicking layer

The MIPs of just the skin-mimicking layers for all three phantoms show at least one location on the phantom surface with a visible blemish (See Figures 32 to 34). This blemish can also be seen with the eye on the physical phantom. Visual inspection of the MIPs for the light phantom for the different wavelengths shows that the signal of the skin-mimicking layer first increases for 797 nm and then decreases again for increasing wavelength (See Figure 32). For the medium phantom, it appears that the signal from the skin-mimicking layer is similar for the first four wavelengths. Only for 920 and 1060 nm, there is a significant difference visible (See Figure 33). For the dark phantom, the differences between the wavelengths are even smaller (See Figure 34). In Figure 35, the graph displays the skin-mimicking layer signals directly retrieved from the reconstructions. As mentioned above, the results are not corrected for the wavelength-dependent laser output energy variations of the system. The graphs confirm what could already be seen in the MIPs. For the light phantom, the graph follows the expected curve, with a decrease in signal for increasing wavelength with a peak at 920 nm. However, the graphs for the medium and dark phantoms show unexpected results. Firstly, the values for the first four wavelengths for the medium phantom are higher than for the dark phantom. Secondly, there is no clear decrease in the signal of the skin-mimicking layer for these wavelengths. For the medium phantom, the signal of the skin-mimicking layer is decreased for 920 and 1060 nm. However, for the dark phantom, the decrease is minimal in comparison to the decrease for the medium and light phantom. If the compensation for the laser output were to be applied, the results are expected to be even less in agreement with the expectations. The presence of air bubbles in the phantom material

and the other in Chapter 5 mentioned inhomogeneities in the phantoms may be the explanation for some of these unexpected results.

The mean and standard deviation of the 41 signals of the three skin-mimicking layers are shown in Figure 36 for the wavelength range 680-1060 nm. The signals from the skin-mimicking layers that are based on the wavelength sweep data show a clear decrease in signal intensity for increasing wavelength. The higher the mimicked pigmentation level the higher the PA intensities are. This aligns with the increase in absorption coefficients due to higher concentrations of alcohol-soluble nigrosin. Between the light and medium skin-mimicking layer and the medium and dark skin-mimicking layers the signal intensity about doubles around 800 nm, whereas the absorption coefficients triple (See Figure 37). For the data of the dark phantom, the time signals showed for a majority of the selected transducers a clipping of the signals from the skin-mimicking layer for the shorter wavelengths (between 680 nm and 745 nm). As a result, the mean PA intensities for the peak of the skin-mimicking layer are not accurate for these wavelengths and have therefore been excluded. For all three phantoms, the effect of the increased absorption around 970 nm by the water in the imaging bowl can be seen as a sudden drop in PA intensity between 950 nm and 1020 nm (Continuous arrow in Figure 36). After the water peak, the PA signal intensity for the skin-mimicking layers increases again. This showcases a so-called spectral colouring effect that the water in the imaging bowl has on the signals originating from the phantom. In Appendix I Figure 62, a figure showcasing the signal of water for the three phantom measurements can be found, with a peak around 970 nm. In the data from the light skin-mimicking layer, a small increase in the signal intensity can be found around 920 nm. This most likely corresponds to the fat peak, attributed to the oil in the skin-mimicking material (which can also be seen in Figure 8, Section 4.5.1. page 43). The darker the skin-mimicking layer, the less noticeable this fat peak becomes.

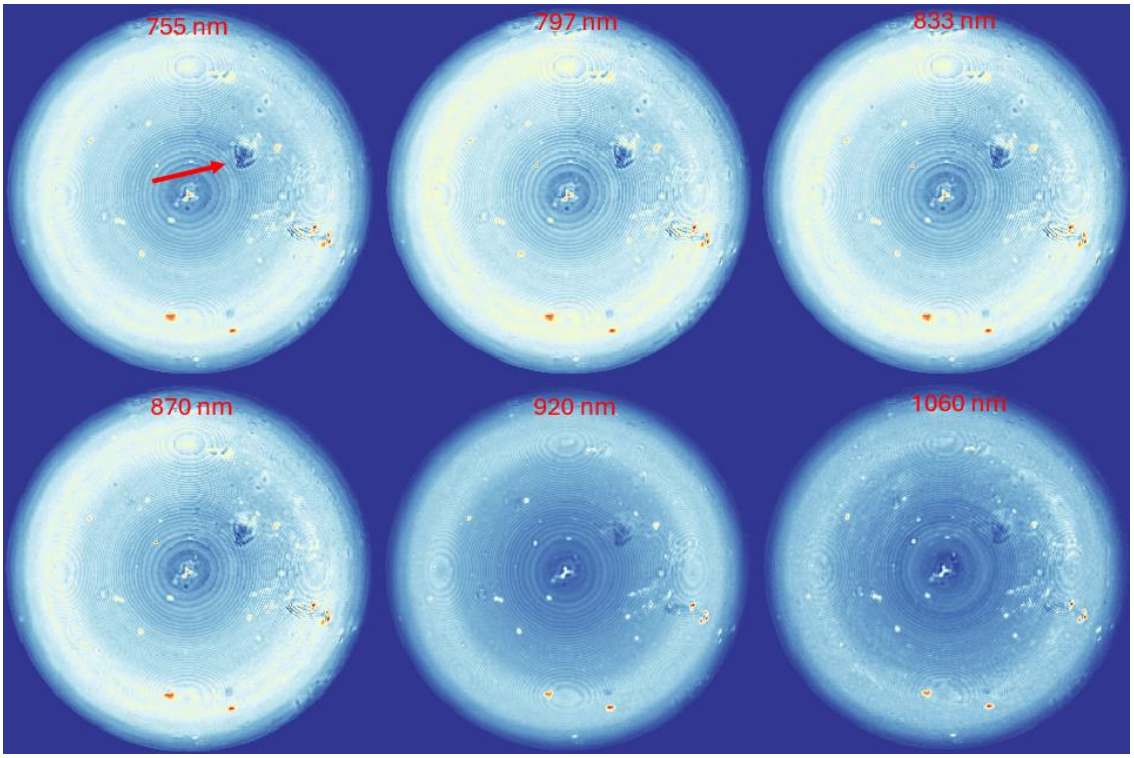

Figure 32: MIP for just the skin-mimicking layer for the light phantom for the different wavelengths. The red arrow points toward a region where there is a visible irregularity in the skin-mimicking layer.

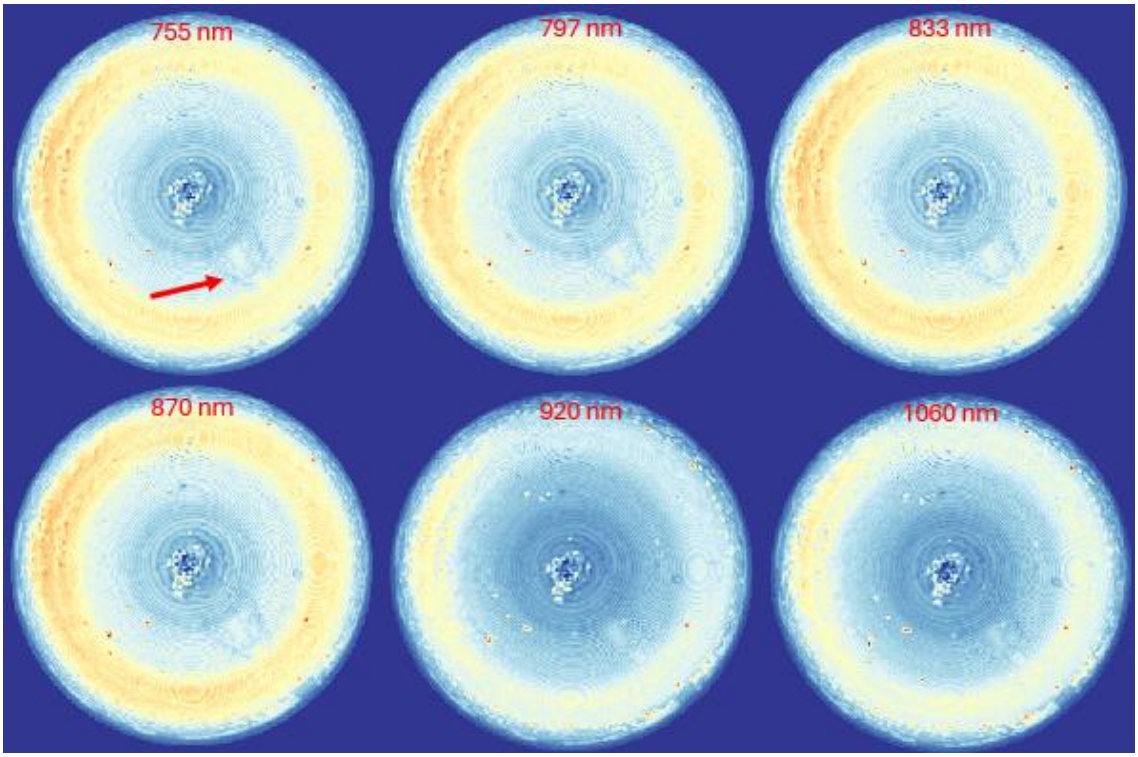

Figure 33: MIP for just the skin-mimicking layer for the medium phantom for the different wavelengths. The red arrow points toward a region where there is a visible irregularity in the skin-mimicking layer.

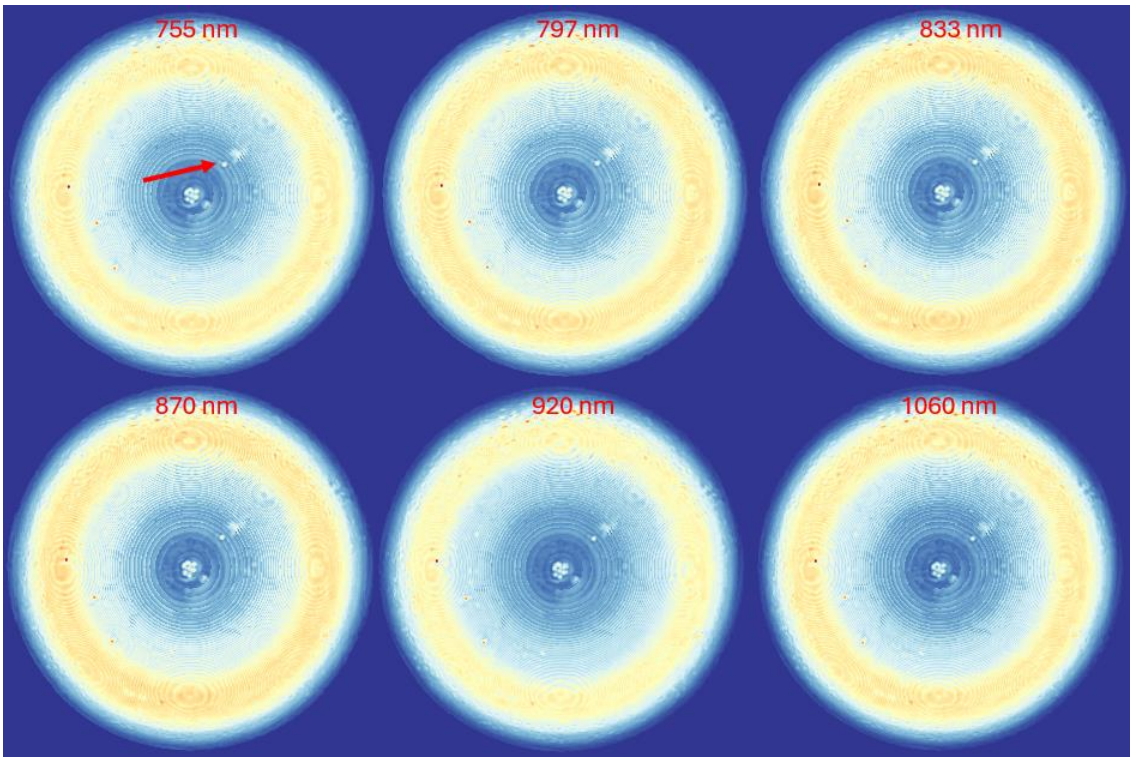

Figure 34: MIP for just the skin-mimicking layer for the dark phantom for the different wavelengths. The red arrow points toward a region where there is a visible irregularity in the skin-mimicking layer.

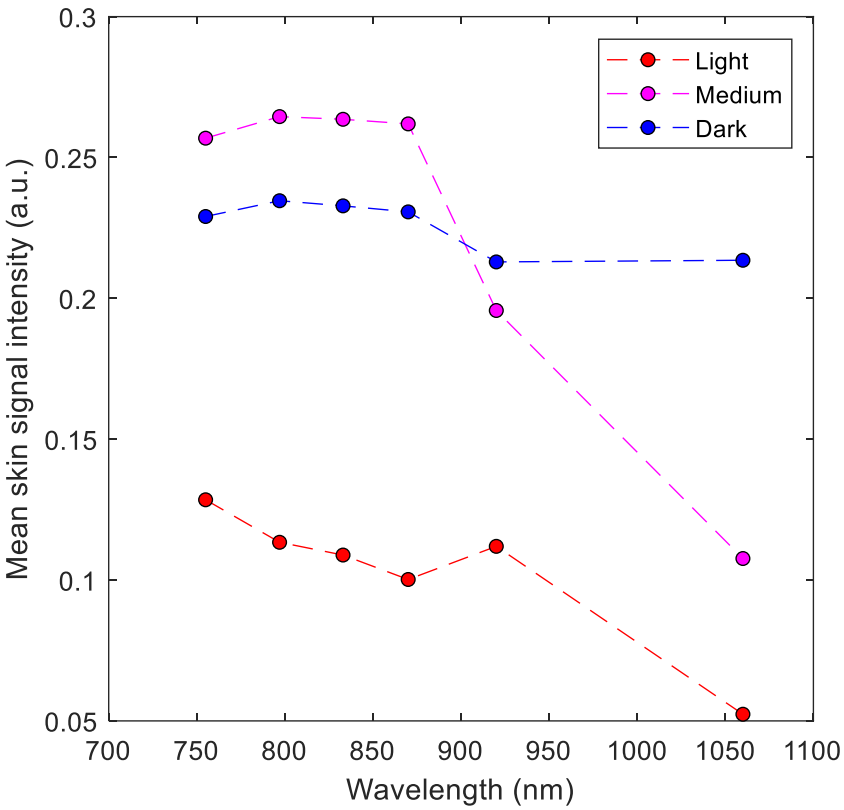

Figure 35: Uncompensated average skin-mimicking layer signal intensity for the six wavelengths for the three phantoms. The dotted lines are simply to guide the eye.

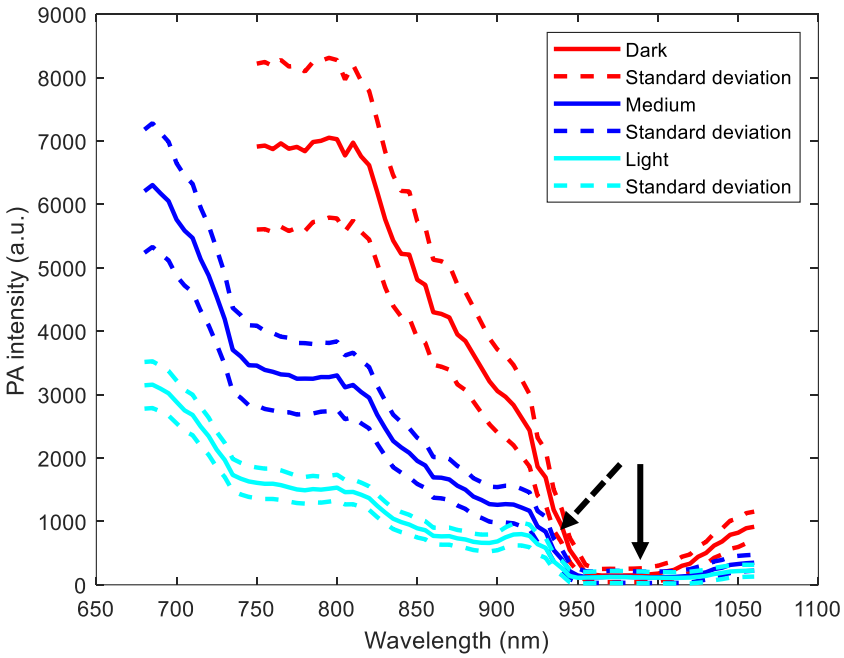

Figure 36: Mean peak PA signal intensity for the three skin-mimicking layers over the wavelength range of 680 nm to 1060 nm. The graphs are an average of the skin signals from the 41 selected transducers. The continuous arrow points towards a dip in the graphs, most likely caused by the water peak. The discontinuous arrow points towards a wavelength region in which the fat peak can be detected in the signal of the light phantom and to a lesser extent in the one of the medium phantom. The data of the dark skin tone phantom in the region between 680 nm and 745 nm is left out due to inaccurate because of saturation of the PA signals.

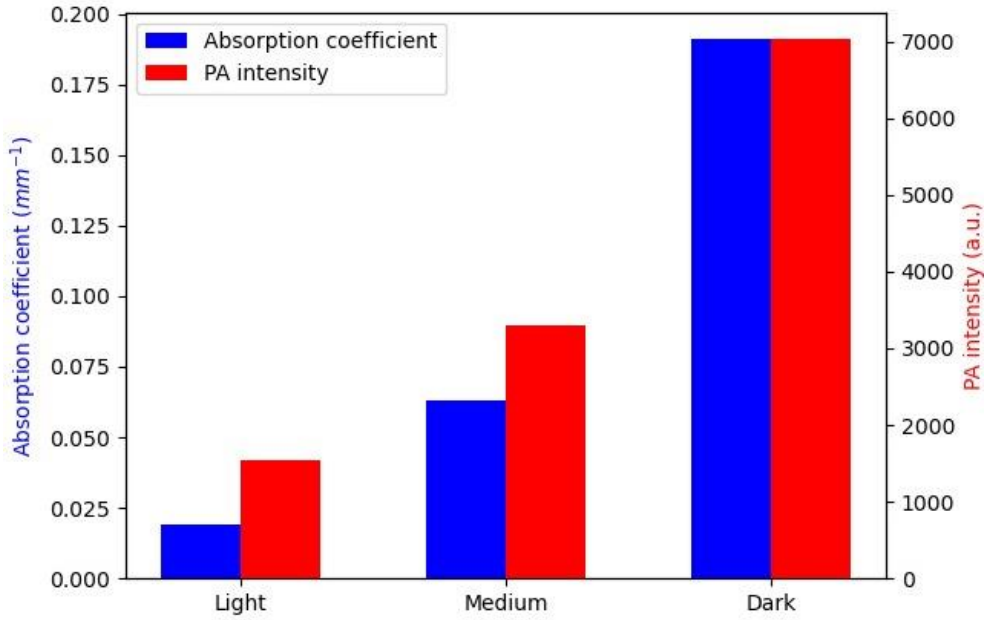

Figure 37: Absorption coefficients and measured peak PA intensity for the three skin-mimicking layers for 800 nm.

6.5. Discussion

This part of the project has the objective of assessing changes in the image quality of a PAT system, specifically the PAM3 system, due to the influence of skin tone by performing a phantom study. In this phantom study, the data from three phantoms mimicking three different skin tones (light, medium, and dark) have been analysed. The mimicked skin tones of the phantoms can be characterised by their related melanosome volume fraction (M_f). For the skin-mimicking layers of the three phantoms, these M_f-values are 3% (light), 9%, and 27% respectively. The analysed data consisted of the time signals from a wavelength sweep and six reconstructed scans for the wavelengths 755, 797, 833, 870, 920 and 1060 nm. The parameters that have been investigated are the imaging depth, the SBR of various targets, the occurrence of artefacts and the PA spectra of the skin. The results and insights gained will be discussed in this section according to the following tasks:

1) Visualization of skin-mimicking layer, imaging targets and possible artefacts

The volumetric MIPs made of the reconstructions show that the signal from the skin becomes more dominant from light to dark phantom. In addition, the imaging targets become less visible both due to the lower signals of the imaging targets themselves as well as due to the increase in background signals. While the contrast between light and medium phantom is in accordance with the expectations, the contrast between the medium and dark phantom for the unprocessed data is not. The difference between the phantoms is minimal and it even seems like the signal from the skin for the medium phantom is higher for 870 nm than for the dark phantom (See Figure 27). Nonetheless, there is a clear difference in the visibility of the imaging targets in the MIPs of the processed data between medium and dark phantom. This seems to suggest that only the values for the skin-mimicking layer in the reconstructions are not in line with the expectations.

One of the novelties of this phantom study is that it is the first one in which a hemispherical PAT system is used to investigate the influence of skin tone on PAI. Because of the different illumination and detection geometry, it was hypothesised that certain effects such as the occurrence of clutter artefacts will be absent in the scans made with this system. In linear and curved arrays, the clutter artefact is of major influence on the imaging performance. And it was found that for darker skin tones, this artefact is more present, which causes a decrease in the image quality [12,14]. Since with a hemispherical PAT system, objects are imaged from different angles, it was hypothesised that the clutter artefact would occur less or would even be absent. Scattered waves, which would cause clutter

in 2D PAI [13,14,16], might not be reconstructed as an object in 3D PAT. The volumetric MIPs of the processed reconstruction show that the visibility of the imaging targets decreases due to enhanced background signals. These 3D noise signals are in appearance similar to the clutter artefact in 2D PAI systems. These clutter-like signals are especially present towards the base of the hemisphere. This is also the part of the phantom with the most defects in the physical phantom and where the fluence is the highest on the surface. It could therefore be that these clutter-like signals are caused or enhanced by these factors.

2) SBR

The results for the SBR over depth for target 1 for the different phantoms show that there is a steeper decrease in SBR for the dark phantom than for the light phantom. It can be seen in the graphs that the SBR values can become negative (See Figure 29). This means that the signal from the imaging targets is lower than the signal from the background. In theory, this could mean that there is a negative contrast, which might cause the imaging targets to still be distinguishable from the background. However, it is more likely that there are some brighter spots in the background. These spots can cause the overall signal of the background to become slightly higher than the signal of the imaging targets. Consequently, the SBR can be negative without the imaging targets being more visible due to a negative contrast. Due to time constraints, the negative SBR values were not further investigated. The SBR values for target 1 show that 797, 833 and 870 nm will give similar visibilities of the imaging targets. However, the SBR of 755 nm is for all phantoms lower. This can be due to the shape of the absorption spectra of the skin-mimicking layer. At 755 nm, the skin-mimicking layer absorbs more light in comparison to the other wavelengths (See Figure 6 page 43). The deviation of the SBR values for 1060 nm might be explained by a second peak in the absorption spectrum of the base material around 1050 nm (See Figure 15 page 54).

The bar charts with the SBR at depth 10-12 mm show that for the different wavelengths, the SBR values for the dark phantom seem to be similar to slightly higher than those of the medium phantom. This is in contrast to the expectations that a darker skin tone will lead to more noisy signals and thus to a lower SBR. In the medium phantom, more air bubbles are present in the phantom material (See Chapter 5 Section 5.4.2 page 56). These air bubbles are likely causing a local increase in the signal values due to the high acoustic impedance difference between the air and the phantom material. The signal values of these air bubbles can cause a slight increase in the value of the background signal for all imaging targets regardless of wavelength. As a result, the SBR can be lower than expected. The increase in the SBR for the middle and dark phantom could be explained by the fact that the fluence on the imaging targets increases for increasing wavelengths due to a decrease in absorption by the skin-mimicking layer. The values for the light skin tone will be more stable, as the difference in absorption by the skin-mimicking layer for a light skin tone is smaller.

The imaging targets are filled with BMFs that have a specific absorption spectrum, with similar values for the absorption coefficients for 797 nm and around 980 nm where all curves roughly cross each other (See Figure 24). In the situation that the absorption spectra can be directly linked to the SBR values, it would be expected that between phantoms the same pattern in the SBR values for the four imaging targets can be found. Because the four imaging targets in a phantom are affected in the same way by the skin-mimicking layer. However, in the bar charts (Figure 30), it can be seen that the pattern between wavelengths differs for the three phantoms. It can therefore be said that the shape of the spectra of the different BMFs cannot be correlated well to the SBR values of the imaging targets. For the light phantom, there is a clear difference between all imaging targets, with the SBR values for target 2 being the highest and for target 4 the lowest. From 755 nm to 1060 nm, the SBR values for target 1 slowly become smaller than those for target 4. However, this still is not in correspondence with the spectra of the BMFs. For the light phantom, there is a difference visible in the SBR values for the different targets. For the medium and dark phantom, the variations are minimal. It was attempted to minimise shadowing effects of the targets on each other. However, it cannot be discounted that some

shadowing still takes place. This can influence the fluence at each imaging target and therefore the PA intensity and thus the SBR.

3) Imaging depth

The results of the imaging depth show a clear decrease in imaging depth between the light and medium phantom. The decrease in imaging depth between the medium and dark phantom is minimal. For some wavelengths and targets, the imaging depth is even higher for the light phantom than for the medium phantom. However, as mentioned above, the medium phantom has more air bubbles in the phantom material, which can influence the SBR for the imaging targets and can therefore confound the effect of the mimicked skin tone on the imaging depth. It can also be seen in the results that the imaging depth for the medium and dark phantom increases between 755 and 797 nm. For wavelengths larger than 800 nm, the decrease in absorption by nigrosin lessens, which is also visible in the results for the imaging depth. For 979, 833, and 870 nm, the imaging depth is similar. For both 920 and 1060 nm, the imaging depth is lower than expected due to the fat peaks in the absorption spectrum of the base material.

The imaging depth for different wavelengths does not seem to be related to the absorption spectra of the imaging targets. If this were the case, the pattern in the imaging depth for a specific target would follow the shape of the corresponding absorption spectrum. However, there is a difference in the imaging depth between imaging targets for the medium and dark phantom. The imaging depth in the medium phantom for target 1 is for instance significantly lower than for target 4. It is not clear why this might be the case.

It should be mentioned that even though the signals might decrease in intensity, by eye they might still be visible at depths at which the SBR crosses the cut of value of 6 dB. This is because visually it is possible to distinguish the imaging target from the background based on morphology as well. And with knowledge of lower depths, it is possible to determine where the signal should be located at deeper layers, which aids in locating the imaging targets.

It is important to note as well that while the imaging depth of 5.1 cm is defined as the maximum imaging depth that can be reached for these phantoms, it is not equal to the maximum imaging depth of the system. It is simply that the analysis of the imaging depth is bounded by the length of the imaging targets. If the phantom had been bigger and the imaging targets longer, the imaging depth over an even larger depth could have been assessed. This might have allowed the assessment of the actual maximum imaging depth of the system for these phantoms.

4) Skin-mimicking layer signal wavelength sweep

For the signal of the skin based on the data of the wavelength sweep, there is a relatively large variation in the PA signal intensities (around 15%). This is due to the differences in signal intensities measured by the different transducers. The geometry and size of the phantoms were chosen to ensure a homogeneous illumination on the surface of the phantom for a full scan with 101 bowl rotations. However, since the fluence distribution for the phantom geometry and size was not determined, there may be still inhomogeneities in the fluence distribution. Moreover, since the imaging bowl is in a static position for the wavelength sweep, there will be more inhomogeneities compared to a scan with a rotating imaging bowl. These inhomogeneities in the fluence will result in variations in PA intensities for different transducers.

The inconsistency between the ratios of the absorption coefficients of the three skin-mimicking layers and the PA intensities measured is striking. However, the influence of the fluence on the PA signal intensities should not be disregarded. While at the surface of the phantom, the fluence might be similar, along the thickness of the layer there is fluence decay due to light attenuation and effects of backscattering of light. As a result, the relation between the absorption coefficients of the layers and the peak PA intensities measured is non-linear. The area under the selected peak was calculated as an alternative metric to assess the signal from the signal. By calculating the area under the peak, not only

the peak height but also the peak width is taken into consideration in the assessment. However, these results did not show any significant changes in the ratio of the signals for the three skin-mimicking layers (See Appendix I Figure 63 and 64).

The signals measured from the skin-mimicking layer are relatively high. The signals from the dark skin-mimicking layer measured by a significant proportion of the selected transducers are clipped. To the best of our knowledge, this event is unprecedented [91]. The absorption coefficients of the skin-mimicking layer are lower than can be expected from epidermal layers because of the compensation for the increased thickness. It was therefore hypothesised that the signals received from these layers would also be lower than in vivo. A possible explanation for the high signal values could be related to the US transducers, which have a centre frequency of 1 MHz and a fractional bandwidth of 123% [76,85,86]. A thin layer of 100 µm results in a pressure signal with a broader frequency bandwidth compared to a much thicker layer of 1 mm. Thus, for the epidermal layer, more of the absorbed energy is converted into higher frequency components, which cannot be detected by the transducer. This will result in lower PA signal intensities measured for the epidermal layer as opposed to the mimicked skin layer. However, to verify this hypothesis, physical experiments with a phantom with a 100 µm layer would have to be performed and/or digital experiments with simulations.

5) Skin-mimicking layer signal reconstructed scans

There are some major uncertainties about the reliability of the values found for the skin-mimicking layer from the reconstructed data. The values found for the skin-mimicking layer signals based on the reconstructions do not correlate to those values found for the signals in the wavelength sweep data. The raw data for the reconstructions was analysed to verify that the performed measurements were executed correctly. The RF data for the reconstructions showed no unexpected deviations that could explain the findings in the reconstructed data. It is therefore hypothesised that during the reconstruction process, some of the information in the RF data is wrongly processed. This could lead to structures being reconstructed wrongly. Due to the uncertainties, it was decided to not compensate for the laser output energy and simply show the unprocessed results.

The unprocessed results show unexpectedly that the medium phantom has higher values for the skin signal than the dark phantom for 755, 797, 833 and 870 nm. This is unrealistic, as this is in contrast to the raw data, the data from the wavelength sweep, and the absorption spectra for the skin-mimicking materials (See Chapter 4 Section 4.5.1. page 42). Moreover, for both the medium and dark phantom, the values for the skin signal between 755 and 870 nm are relatively stable with only a minimal decrease. For the light phantom, the signals match the expectation better. There is a decrease in the signal, with a peak at 920 nm due to the fat peak. However, the decrease in the signal is less than expected between 797, 833 and 870 nm when comparing it to the data from the wavelength sweep or the absorption spectra of the materials. For the dark phantom, the decline in skin signal is very low in general. However, when assessing the data points for the three phantoms at 1060 nm, the value for the skin signal doubles between the phantoms, which is the same pattern that can be found for the wavelength sweep data.

It could be that the signal for the skin-mimicking layer for the phantoms with a medium and dark mimicking skin layer is too high or too steep for the reconstruction process to handle. If there is a sudden high peak in the signal, a higher spatial resolution might be needed in the optical and acoustic computations to resolve the high focal intensity maxima of the skin-mimicking layer signal [92]. If the spatial resolution is too low, only part of the information is reconstructed, which can lead to unexpected results. In this case, it would have resulted in much lower voxel values than should be. This phenomenon might not only have occurred for the medium and dark phantom, but it might even be the case for the light phantom. For 755 and 797 nm, the signal of the skin-mimicking layer might still be too high for the reconstruction process to manage correctly. The results for 1060 nm show that the signal intensities of the skin-mimicking layer for 1060 nm might have been low enough for all three phantoms for the scans to be reconstructed correctly. However, to confirm this, a deeper investigation into the issue is necessary.

Limitations of the study:

In this phantom study, three phantoms that all mimic a different skin tone have been used. The main impediment to using just three phantoms is that any possible non-linear relations between skin tone and the chosen imaging parameters cannot be identified. Nonetheless, the phantom study does give some good indication of the influence of skin tone on imaging performance in PAT. Else et al. and Vogt et al. used three and four phantoms respectively as well. They showed that the overall relation between skin tone and the investigated outcomes can be assessed even with this limited number of skin tones mimicked [17,18]. It would have been informative, however, to have a fourth phantom without nigrosin in the skin-mimicking layer included as well, which could have functioned as a control phantom. The results from this phantom could have been used as a baseline to compare the results of the other phantoms, as was done by Vogt et al and Else et al. [17,18].

In this phantom study, four different oxygen saturations have been mimicked, which include saturations mimicking arterial and venous blood. In theory, this should have made it possible to investigate with a single scan the effect of skin tone on different blood saturations. However, in practice, this was not possible since the results for different wavelengths could not be easily related to the absorption spectra of the respective imaging targets. Nonetheless, if it were to become possible to link the imaging targets absorption properties to certain outcome measures in a different phantom, it could save time and effort during experimentations with the PAM3 as it does not allow real-time imaging.

A major concern in these phantom experiments is the irregularities in the surface of the phantoms and the air bubbles present inside the phantom material. These irregularities and air bubbles can result in signals in the phantom regions that are in the current analysis method considered as the background. Since they can result in significant increases in the “background” signal this can affect the analysis of the SBR and hence the imaging depth. Especially in the medium phantom, there were some issues (See Chapter 5 Section 5.4.2. page 56), which might have caused the unexpected results that the SBR values and therefore also the imaging depths for the medium phantom are lower than for the dark phantom.

The size of the phantom for this study was chosen with the reasoning that a diameter of 6 cm would be large enough to assess the imaging depth. This was based on a previous study with the PAM3 of Dantuma et al. in which an imaging depth as large as 4.8 cm was found [76]. However, insufficient consideration was probably given to the fact that the effect of the optical properties of breast tissue itself, excluding the large blood vessels, can have a significant impact on the imaging depth in vivo. While the base material to some extent does mimic (fatty) breast tissue to some extent, there are smaller blood vessels in the breast tissue, which also absorb light and decrease the imaging depth. Since the absorption by the base material is most likely lower than for actual breast tissue, the phantom should have been larger. This would have allowed the imaging targets to be longer. Consequently, the maximum imaging depth that can be reached with these phantoms could have been assessed better, especially for the light phantom.

Because of the fat peaks at 920 and 1050 nm, the results for 920 and 1060 nm cannot be used properly to investigate the influence of skin tone on PAT with these phantoms. However, it was chosen to assess these wavelengths instead of for instance 680 and 720 nm due to the clipping of the skin signal in the raw data. It was uncertain if these clipped data points might cause some problems in the reconstructions. In hindsight, considering that the reconstructions already showed some issues in the reconstruction of the skin layers anyhow, it might have been less of an issue than thought. This would have allowed the investigation of two more reconstructed scans of which the results would not have been confounded by the optical properties of the base material. Moreover, the results of 755 nm show that for increasing skin tone larger wavelengths, 797 nm and onwards, might be more advantageous to use. If the data of 680 and 720 nm were investigated, this could have been investigated better.

It was assumed that in the reconstructions only the values for the skin-mimicking layer were affected as the volumetric MIPs did not show unexpected results for the imaging targets. This allows comparison of the results between phantoms for the SBR and imaging depth. However, if the signals of the imaging targets are also affected to some extent and if this is phantom dependent it greatly

impacts the study. In the results, no clear sign of the imaging targets being affected can be found. However, simulations should be done for validation purposes.

The last limitation of the study is that there is an inhomogeneous fluence distribution on the surface of the phantom. This can be observed in the volumetric MIPs of the unprocessed reconstructions. In the MIPs of the medium and dark phantom, a bright band can be seen about halfway on the surface. Beforehand, it was hypothesised that the shape and size of the phantom would result in a homogeneous fluence distribution based on Dantuma et al [76,79]. In practice, however, this seems to not be the case. Consequently, some parts of the imaging targets will receive more light therefore increasing the PA signal intensity. These parts of the imaging targets will be better visible. But the noise will also be increased for these parts of the phantom. This can cause some confounding of the results for the phantoms. However, since the phantoms have the same size and geometry and are therefore affected in the same way, comparisons of the results between phantoms can still be done with some reliability. However, the phantom should not have been much larger, as from 6 cm noise and interference signals can start to dominate [76].

6.6. Conclusion

This phantom study aimed to assess the influence of skin tone on the image quality of the PAM3 system. To the best of our knowledge, this is the first physical phantom study to investigate the influence of skin tone in a hemispherical PAT system. Other studies have either used a linear array or a circular array [17,18]. Consequently, the phantoms that were used had a geometry that fit the geometry of the imaging systems. Three hemispherical-shaped phantoms with different skin-mimicking layers have been scanned. A wavelength sweep and the reconstructions of six full scans have been analysed. Since the acoustic and optical properties of the phantoms and their composition are known, the results can be compared directly. Consequently, despite that only three phantoms have been investigated, it is possible to get a fairly reliable impression of how the mimicked skin tone influences the imaging depth and SBR for these phantoms. The signal from the skin-mimicking layers clearly increases with nigrosin concentration as well as the amount of noise in the scans. This noise has the appearance of a 3D variation of the clutter artefact. While between 755, 797, 833, and 870 nm there is little difference in the SBR for the light phantom, the medium and dark phantoms have a slightly higher SBR for the latter three wavelengths compared to 755 nm. And while there is still a decrease in imaging depth from light to dark phantom, for the medium and dark skin tone, the imaging depth is lower for 755 nm than for 797, 833 and 870 nm. This would suggest that the use of longer wavelengths would be more advantageous for darker skin tones as the SBR is slightly increased and the decrease in imaging depth between light and dark skin tones is smaller. While this is an interesting finding, it should be better investigated by analysing some more scans made with shorter wavelengths.

Chapter 7

7. Influence of skin tone on photoacoustic breast imaging: volunteer case study

7.1. Introduction

For more than two decades, researchers have been investigating photoacoustic (PA) imaging for medical purposes. During that period, various imaging systems have been developed [84]. Up until a few years ago, the influence of the skin tone of human subjects on the images obtained with photoacoustic imaging (PAI) was assumed to be of minor consequence [4]. However, the results of studies from the last five years demonstrate clear evidence of unintended skin tone bias in PAI. These studies show among other things a decrease in image quality, imaging depth, and oximetry performance [12,14,15,17,18,20].

The influence of skin tone on PAI has been studied in volunteers by Fernandes et al, Li et al., and Mantri et al. [12,14,15]. The results are consistent with those obtained from phantom studies and simulations. While these volunteer studies have yielded valuable insights, there is a major shortcoming. All three studies featured a 2D PA system with a linear array imaging geometry [12,14,15]. It is uncertain if these results can be generalised to photoacoustic tomography (PAT) systems. It is possible that for 3D imaging systems, some imaging parameters are influenced to a lesser or greater by skin tone than for a 2D system. It is therefore imperative that the influence of skin tone on PAI is also investigated for PAT systems. Furthermore, the imaging site in the reported studies was the forearm and hand of volunteers. It can be beneficial to investigate the impact of skin tone on other anatomical regions to understand the susceptibility of certain PAI applications to unintended biases related to skin tone.

The volunteer case study of this project aims to investigate the influence of skin tone on a hemispherical PAT breast imaging system, specifically the Twente Photoacoustic Mammoscope (PAM) 3 system, in an in vivo setting. Not only will the study give an indication of how PAT is affected by skin tone, but also of what the implications are for PA breast imaging. While a phantom study has also been conducted, the in vivo experiments are imperative to show the performance of the PAM3 in a clinically relevant setting. This chapter of the thesis will explore the conducted retrospective volunteer case report. The parameters that were investigated are the imaging depth, the signal-to-background ratio (SBR) of the blood vessels, and the PA spectra of the skin layer. The SBR of the blood vessels provides an impression of the detectability of the blood vessels.

Related sub-research questions:

- *What changes can be found in the image performance of the PAM3 system between 3D photoacoustic scans made of the breasts of volunteers with different skin tones?*

7.2. Methods

The methods for the volunteer case study are described in this section. The first part of this section pertains to the data that was used and the characteristics of the volunteers. The second section delves

into the data analysis for the signal and PA spectra of the skin, and the imaging depth. All volunteers were scanned with the PAM3. All scans were reconstructed with an iterative least-squares fit model-based reconstruction with a time-of-flight speed-of-sound correction. The radiofrequency (RF) data and reconstructed scans were analysed using MATLAB (Release 2024a, MathWorks). The data analysis approach is described in section 7.2.2.

7.2.1. Data acquisition

Data from the healthy breasts of three volunteers was available for analysis. The skin tone of the volunteers was classified using a questionnaire to determine the Fitzpatrick skin phototypes (FSP), which range from I (light) to VI (black) [10]. For each breast, a wavelength sweep and five full scans had been made. The wavelength sweep was performed from 680 nm to 1060 nm in steps of 5 nm. During the wavelength sweep a single scan is made for each wavelength and the imaging bowl remains in the starting position. The five full scans were made with the standard wavelengths used for a conventional examination with the PAM3 (720, 755, 797, 833, and 870 nm). For a full scan, 101 scans are made per wavelength and the imaging bowl rotates in between scans to cover 360° in 100 steps. These 101 scans are reconstructed into a volumetric dataset. The relevant characteristics of the three volunteers can be found in Table 10. During the measurements, the breasts of the volunteers were supported with an optically and acoustically transparent breast cup [76] with an appropriate size.

Table 10: Characteristics of the volunteers.

	Volunteer 1	Volunteer 2	Volunteer 3
Breast (L/R)	Right	Left	Left
Breast cup size	5	6	8
Skin tone (FSP)	II	III almost IV	V
Skin marks	x	x	Birthmark superior of the nipple

7.2.2. Data analysis

Signal from the skin

The signal from the skin layer is determined from both the RF data from the wavelength sweep and the reconstructed data of the five full scans. For the analysis, a similar methodology was applied as in Chapter 6 (Section 6.3.3. page 67). Thus, the raw time signals of the wavelength sweep of 41 out of the 512 transducers were analysed. The position of the 41 transducers in the imaging bowl and the rationale behind the selection can be found in Chapter 6 Section 6.3.3. page 67. The skin layer is the first tissue component that can produce a detectable PA signal. An estimation of the distance between the selected transducers and the different breast cups was used to determine in which range of the time signals the signal of the skin should be located. The first peak of significance in the time signals, within the determined time range, was assumed to be the signal produced by the skin layer. For each selected transducer, the amplitude of this peak was determined for all measured wavelengths and a compensation for the wavelength-dependent laser output energy was applied. To determine the signal from the skin from the reconstructed data, it was attempted to isolate voxels corresponding to the skin layer. The average voxel value of these selected voxels was determined for all five scans. Likewise, as in the analysis of the wavelength sweep data, a compensation for the variation in laser output energy was applied.

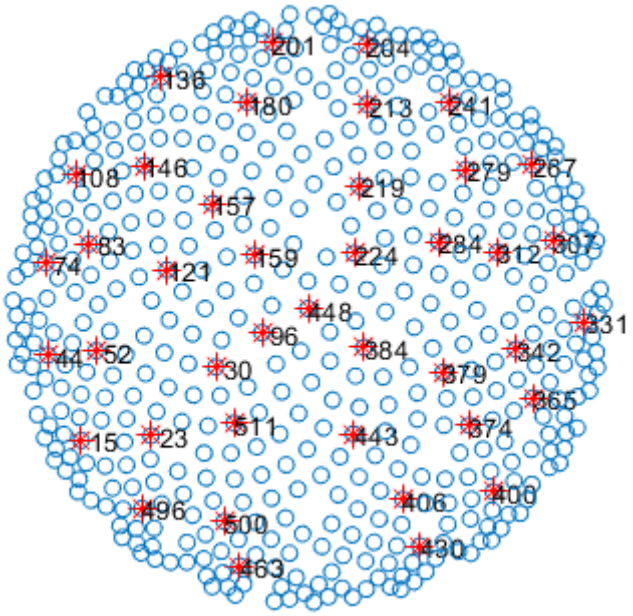

Figure 38: Position of the transducers in a cross-sectional projection. Since it is a projection, the distance between the 512 transducer positions in the image is not representative of the actual distance between the transducers.

Imaging depth and signal-to-background ratio

A Hessian filter followed by a threshold was applied to the reconstructions to isolate the blood vessels in the reconstructions. For each wavelength, a measure of reached imaging depth was extracted by following the blood vessels in the image and locating the maximum depth at which a blood vessel could still be identified in the reconstruction. The SBR for the blood vessels was determined for different depth layers [90]. The depth layers were defined from the imaging cup radially inwards to account for the decrease in the fluence and thus the decrease in signal amplitude (See Figure 39). Each depth layer encompasses about 2.5 mm of breast tissue. For each depth layer, the average value of the voxels corresponding to a blood vessel was calculated as well as the average value of the voxels corresponding to the background. The background was defined as all voxels not corresponding to a blood vessel.

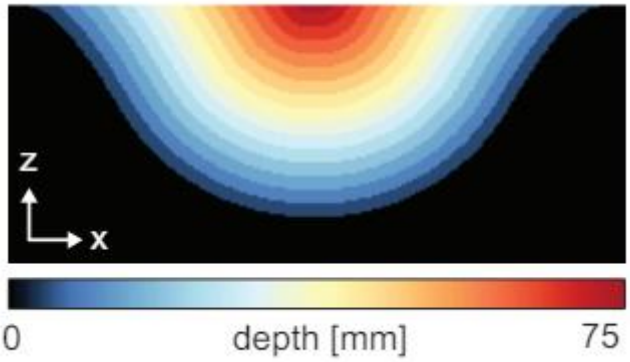

Figure 39: Image adapted from Dantuma 2021: A schematic overview of how the depth layers are defined.

7.3. Results

To assess the changes in the imaging performance of the PAM3 system for different skin tones, the imaging depth, SBR of the blood vessels, and signal of the skin were assessed. The results are described in this section. First, the pre-processed data from the reconstructions of all three volunteers were visualised to obtain an initial impression of the data and to assess if there were any irregularities in the scans. Thereafter, a filter to enhance the signals from the blood vessels was applied and the SBR and

imaging depth were analysed. To investigate the change in the signals from the skin, the reconstructions and the raw time signals from the wavelength sweep were assessed.

7.3.1. Volumetric maximum intensity projections

In Figures 40 and 41, a bottom and side view of the volumetric maximum intensity projections (MIP) of one of the reconstructed scans of each volunteer (hereafter they will be referred to as FSP II, FSP III-IV, and FSP VI) can be seen. The MIPs in Figure 40 are from before the Hessian filter is applied to isolate the blood vessels, and the MIPs in Figure 41 are from after using the filter. The higher the PA intensity the brighter the colour of the structure is.

It can be appreciated from the unfiltered volumetric MIPs (Figure 40) that the signal from the skin increases with skin tone. For FSP III-IV and FSP VI, there is an area in the MIPs at the surface of the breast that could correspond to the nipple region. These areas have a round shape and are located close to the centre of the imaging bowl. While for FSP III-IV the area has a similar intensity as the rest of the upper layer, for FSP VI the area has a higher intensity.

From the unfiltered MIPs it can also be appreciated that the visibility of the blood vessels seems to decrease with increasing skin tone. Especially for FSP VI, the signal from the skin layer dominates in the MIP and only a few blood vessels are visible. After isolating the blood vessels and removing the skin, it can be seen that for PFS III-IV and FSP VI more blood vessels have become visible (See Figure 41). It can be appreciated that the signal intensities of the newly visible blood vessels are fairly lower than those of the blood vessels that were already visible in the unfiltered MIPs. It can also be seen that the MIPs contain more noise-like signals for increasing skin tone. This already shows that the contrast between blood vessels and background is higher for lighter skin tones.

For FSP VI, an artefact appears in the unfiltered MIPs with a square shape (Figure 40). This artefact is not visible for the other two volunteers. However, it cannot be ruled out that this artefact may also be present in the other MIPs but is simply less visible to the naked eye. Such an artefact has been also found in other scans made with the PAM3 of both volunteers and patients [80,90].

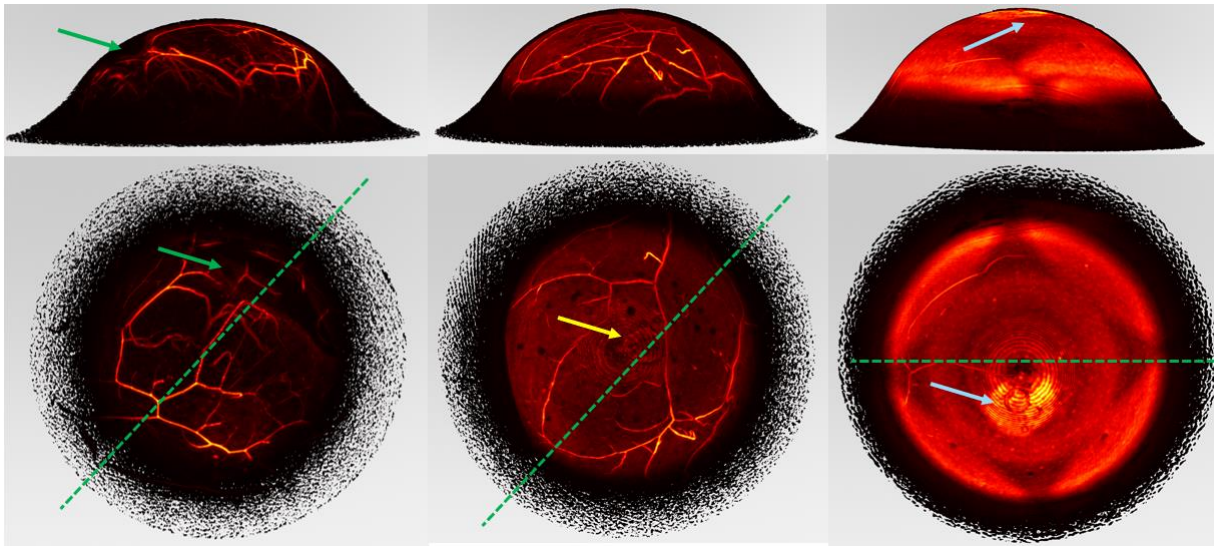

Figure 40: Bottom and side views of volumetric MIPs of an unprocessed reconstruction at 720 nm for FSP II and at 870 nm for FSP III-IV and FSP VI (from left to right: FSP II, FSP III-IV, and FSP VI). The green dotted lines in the bottom views show the orientation of the side view of the MIPs shown in the upper images. The green arrows point towards a region in the MIPs of FSP II at which there seems to be a fold in the breast tissue. The yellow arrow (for FSP III-IV) and light blue arrows (for FSP VI) point to a region in the MIPs that might correspond to the nipple.

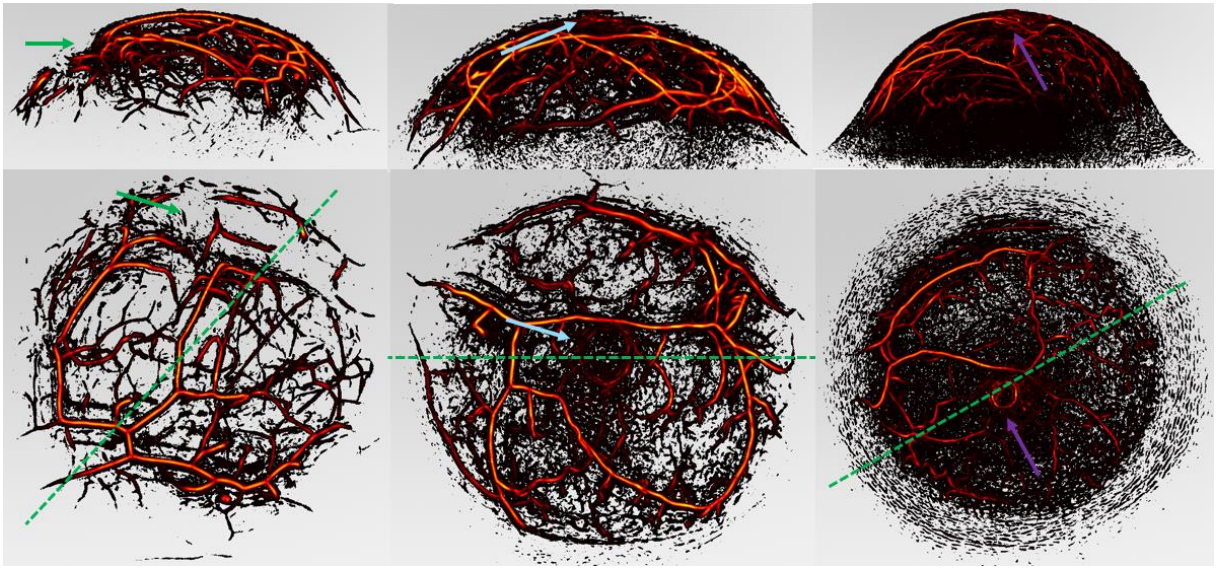

Figure 41: Bottom and side views of volumetric MIPs of a reconstruction after filtering for the vessels at 720 nm for FSP II and at 870 nm for FSP III-IV and FSP VI (from left to right: FSP II, FSP III-IV, and FSP VI). The green dotted lines in the bottom views showcase the orientation of the side view of the MIPs shown in the upper images. The green arrows point towards a region in the MIPs of FSP II at which there seems to be a fold in the breast tissue. The light blue arrows (for FSP III-IV) and purple arrows (for FSP VI) point to a region in the MIPs that might correspond to the nipple.

7.3.2. Imaging depth for different wavelengths

A measure of imaging depth has been determined for the five wavelengths 720, 755, 797, 833 and 870 nm from the reconstructed data. As mentioned, per wavelength this measure is determined as the maximum depth at which a blood vessel is identified. Henceforth, this measure of imaging depth will be referred to simply as imaging depth. In the MIPs for these five wavelengths, differences between wavelengths can already be observed (See Figures 42 to 44). For FSP II, some blood vessels become less visible with increasing wavelength. And while the images seem to contain less noise for FSP III-IV, some blood vessels also become less apparent. For FSP VI, however, the amount of noise in the images decreases while the number of visible blood vessels increases. The observations made from these MIPs are consistent with the quantitative results for the imaging depth (See Figure 45). For FSP II and FSP III-IV, the imaging depth overall decreases. However, the imaging depth for 797 nm deviates from this trend as for these wavelengths a larger imaging depth was found. The imaging depth for FSP VI increases with increasing wavelength. While the imaging depth for 797 nm is higher than would be expected based on the trend, the deviation from the other data points is not as significant as for the other volunteers. A graph with the normalised imaging depth for all volunteers can be found in Appendix J Figure 65. Overall, the imaging depth that can be reached is the highest for FSP II and the lowest for FSP VI. This is in agreement with the expectation that for a darker skin tone, more light is absorbed and thus the penetration depth decreases. For each wavelength, the imaging depth was verified by inspecting if the found location visually corresponded to a blood vessel (See Appendix J Figure 66 to 68).

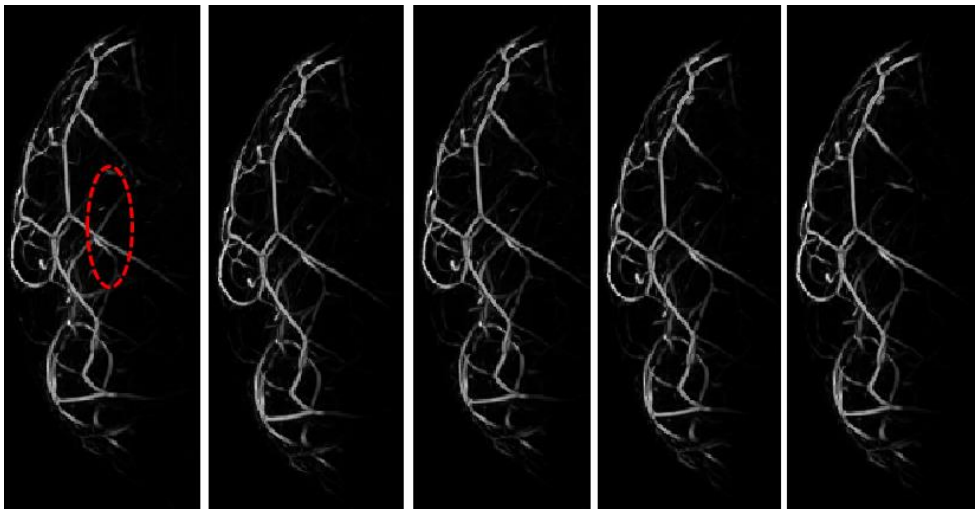

Figure 42: MIPs for FSP II for the five wavelengths (from left to right: 720, 755, 797, 833, and 870 nm). The red arrow points to a blood vessel that becomes less visible with increasing wavelength.

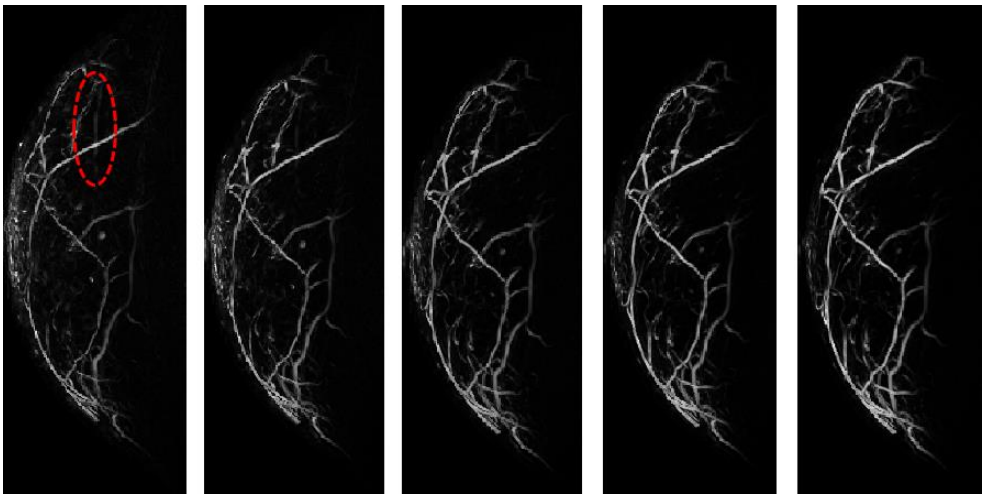

Figure 43: MIPs for FSP III-IV for the five wavelengths (from left to right: 720, 755, 797, 833, and 870 nm). The red arrow points to a blood vessel that becomes less visible with increasing wavelength.

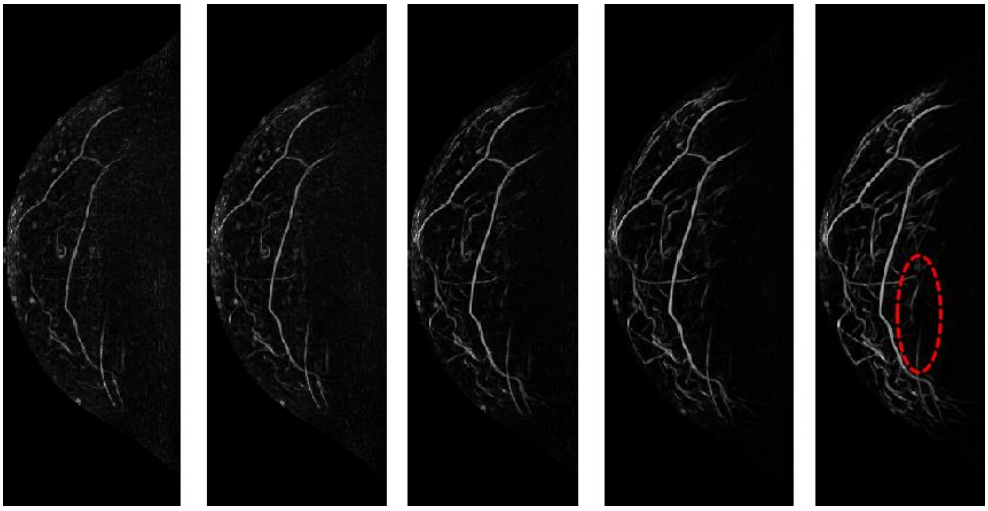

Figure 44: MIPs for FSP VI for the five wavelengths (from left to right: 720, 755, 797, 833, and 870 nm). The red arrow points to a blood vessel that becomes more visible with increasing wavelength.

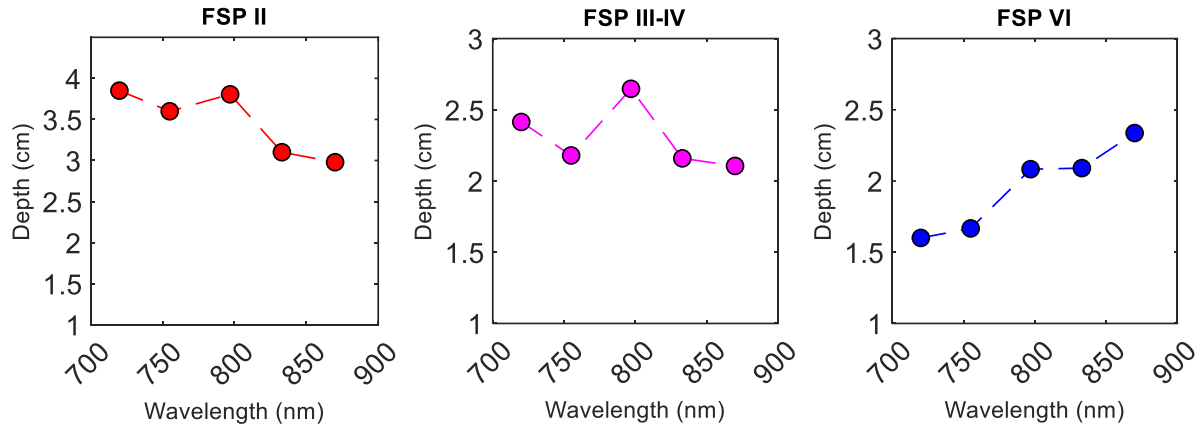

Figure 45: A measure of the imaging depth for the five wavelengths visualised in a graph separately for each volunteer. The dashed lines are simply to guide the eye.

7.3.3. Signal-to-background ratio blood vessels

The SBR has been calculated for each volunteer for different depth layers. The last depth layer that is analysed, is the layer in which the maximum imaging depth is reached. For FSP II, the SBR decreases with increasing imaging depth (See Figure 46). Between the different wavelengths, there is little variation in the values for the SBR, except for 720 nm. For this wavelength, the SBR appears to be slightly higher. For the other two volunteers, the SBR shows a different trend (See Figure 46). After the first depth layer, the SBR increases and remains relatively stable in comparison to the SBR for FSP II. There are some slight variations, but there is no clear increase or decrease. For FSP III-IV there seems to be a trend that for longer wavelengths, the SBR decreases.

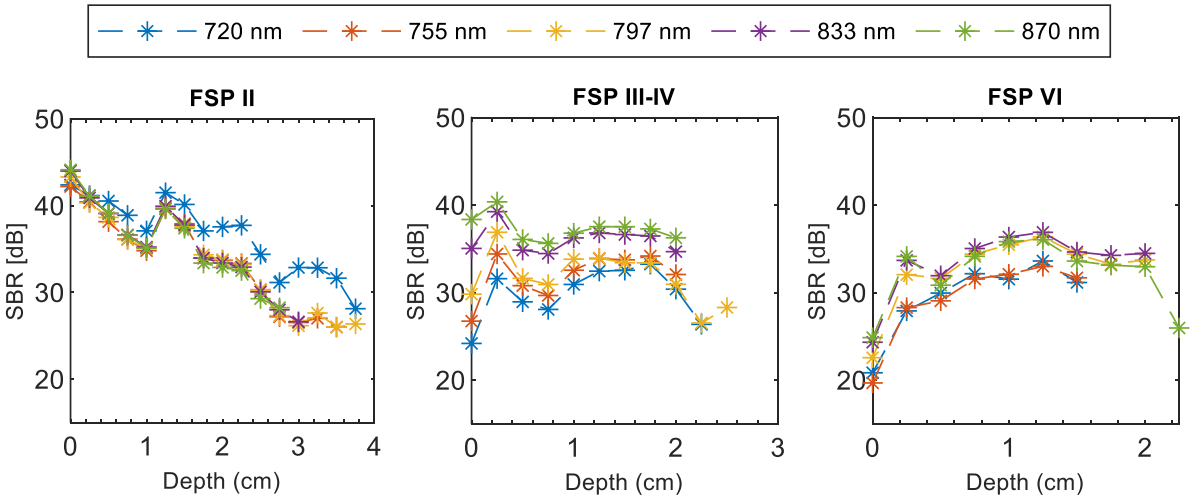

Figure 46: SBR for the three volunteers for different depth layers. Be aware that while the first data point is at "depth" 0 cm, this means that this is the SBR for the blood vessels present within the depth layer 0-2.5 mm. The dotted lines are simply to guide the eye.

7.3.4. Signal from the skin

Visual inspection of the MIPs of the skin layer for the different wavelengths already shows for FSP III-IV and FSP VI that the signal from the skin decreases with increasing wavelength (See Figures 48 and 49). For FSP III-IV, the decrease in signal intensity from the skin appears to be accompanied by an increase in signal intensity from a large superficial blood vessel. For FSP II, the changes are less apparent.

However, there is a region with a higher intensity at 720 nm compared to the rest of the scan. The intensity of this region does decrease with wavelength (See Figure 47). This could be a region with an elevated melanin content compared to the rest of the skin, for instance, the nipple. The graphs in Figure 50 show the normalised average voxel values of this skin layer for the different wavelengths for all volunteers. In Appendix J Figure 69, the raw average values for each volunteer can be found. The signal intensity of the skin increases with skin tone, which aligns with the theory that a higher concentration of melanin will result in a higher absorption of light and thus a higher PA signal. For FSP III-IV, the decrease in signal intensity for increasing wavelength is significant and this is in agreement with the observations from the MIPs. The decrease in signal intensity for FSP VI is less substantial, which can also be observed in the MIPs. However, for FSP II, the relation between skin signal intensity and wavelength shows an opposite trend: first, there is a decrease until 797 nm, after which it increases again.

The analysis of the time signals provides more detailed information about how the PA signal intensity of the skin changes with wavelength. The signal intensity values differ significantly between transducers as a result of the geometry of the breast cup. Furthermore, between volunteers, the signal intensities also differ due to differences in breast cup size. It is therefore that the data is normalised, and the mean and standard deviation of the normalised data are shown (See Figure 51). For all volunteers, a decrease in the PA signal was found for the wavelength range of 680 to about 900 nm. Around 975 nm, a peak can be detected in all three graphs. This peak most likely corresponds with the signal from water [76] This was confirmed through analysis of changes in the PA signal amplitude for a peak occurring at a time coordinate corresponding to a location inside the imaging bowl but outside of the breast (See Appendix J Figure 70 to 72). This water peak dominates the normalised signal intensity for FSP II for the wavelength range 900-1060 nm. Another feature in the data of FSP II is the peak at 760 nm. This could be the influence of haemoglobin, as haemoglobin has a peak around 760 nm as well. If the skin and a blood vessel are close to each other, these signals might have merged.

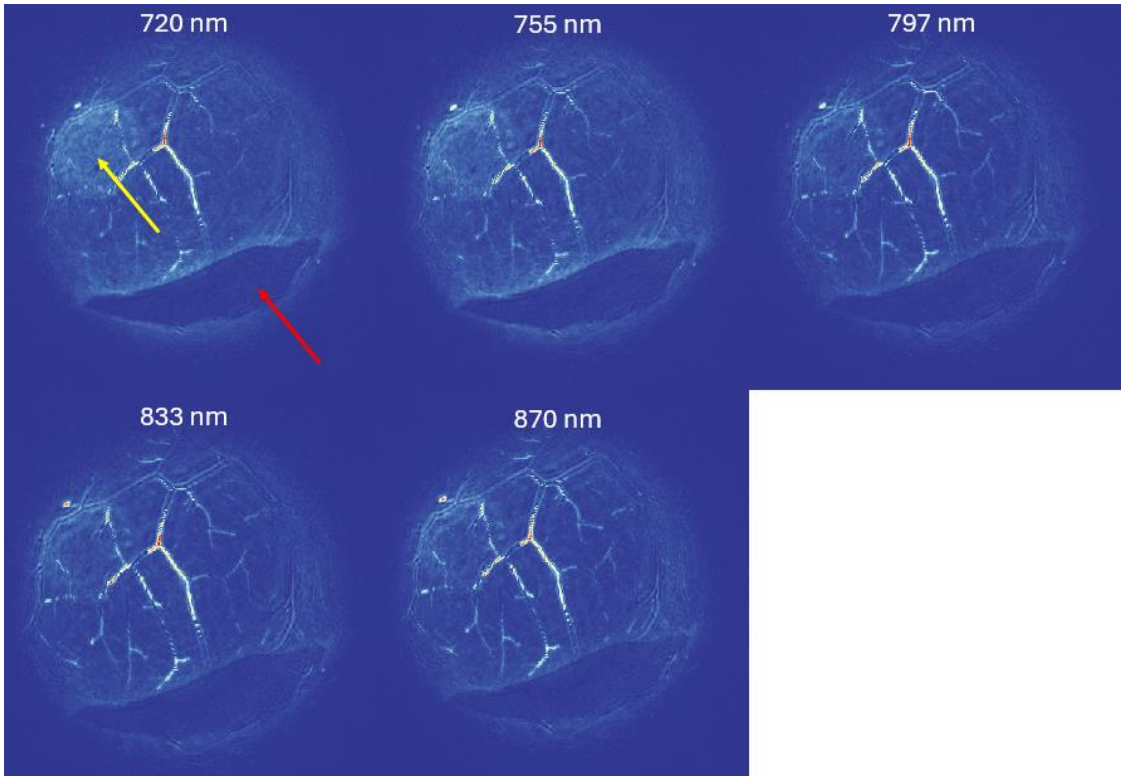

Figure 47: MIP for just the layer in which the epidermis should be present for FSP II for the different wavelengths. The yellow arrow points toward a region where the intensity decreases with increasing wavelength. The red arrow points towards the region where there is most likely a fold in the breast.

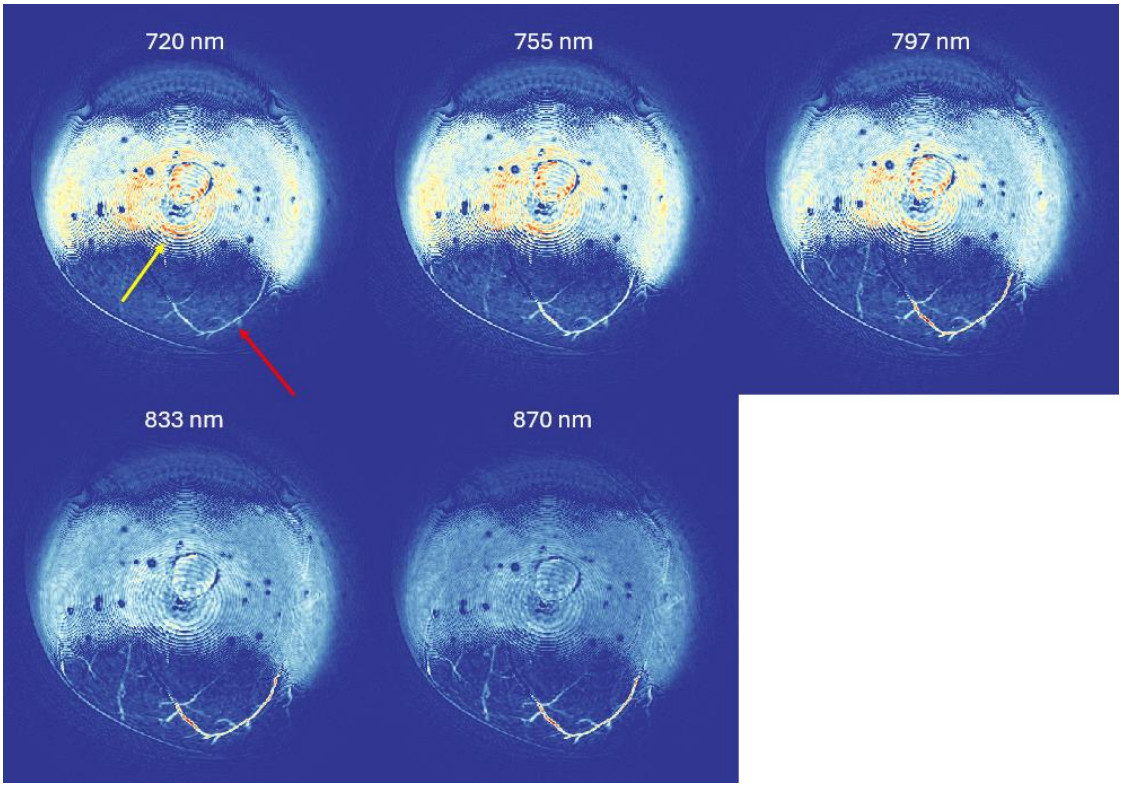

Figure 48: MIP for just the layer in which the epidermis should be present for FSP III-IV for the different wavelengths. The yellow arrow points toward a region where the intensity decreases with increasing wavelength. The red arrow points toward a blood vessel where the intensity increases with increasing wavelength.

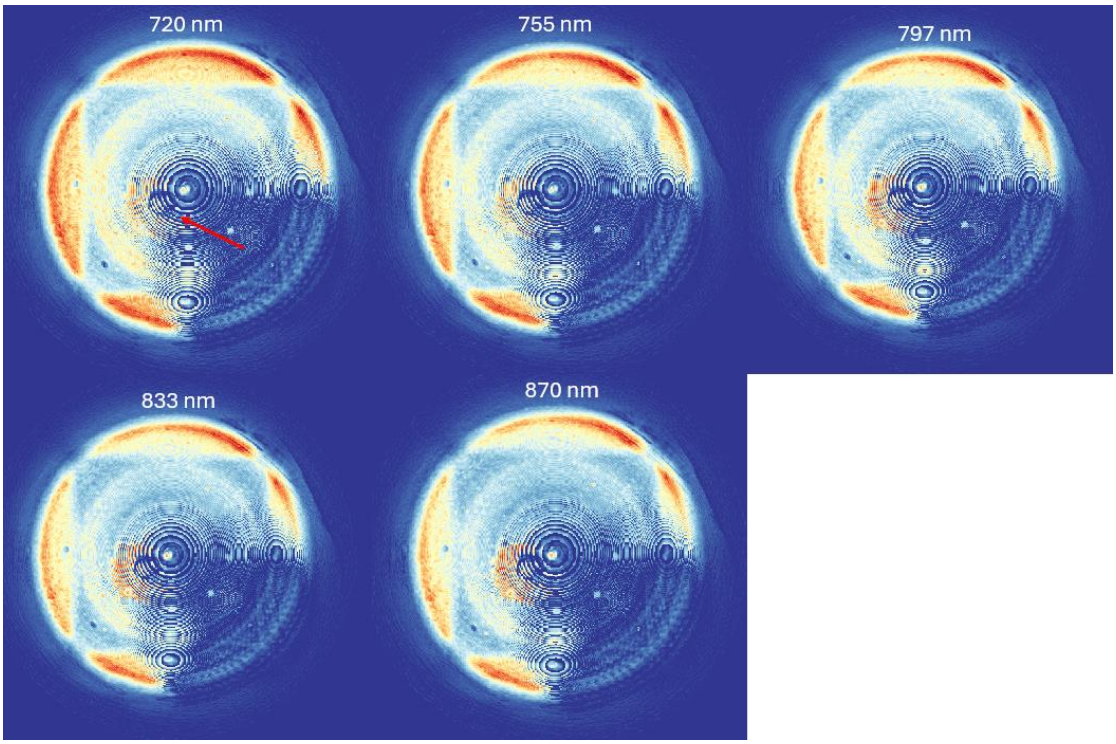

Figure 49: MIP for just the layer in which the epidermis should be present for FSP VI for the different wavelengths. The red arrow points towards a region where the intensity first seems to increase after which it decreases again.

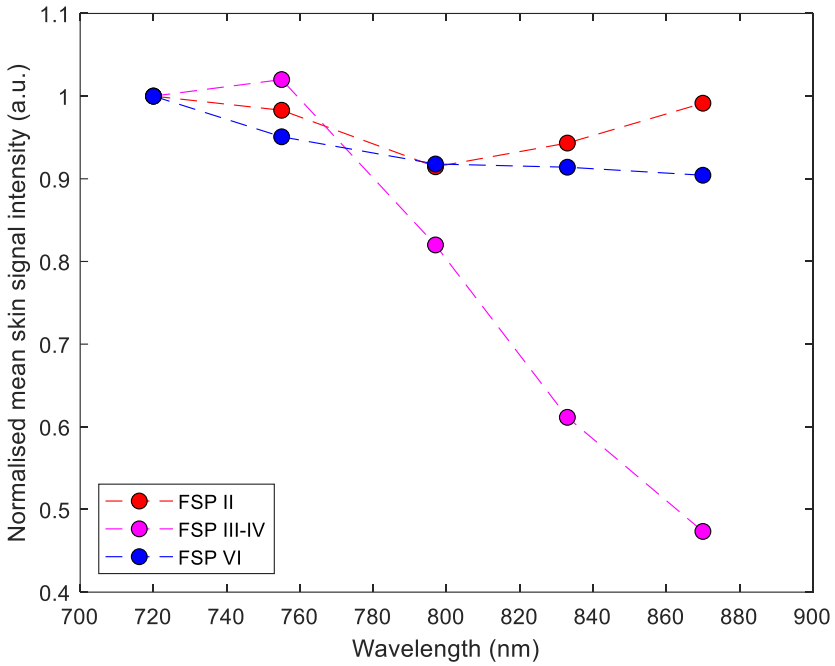

Figure 50: Normalised average skin signal intensity for the five wavelengths for each volunteer. The dotted lines are simply to guide the eye.

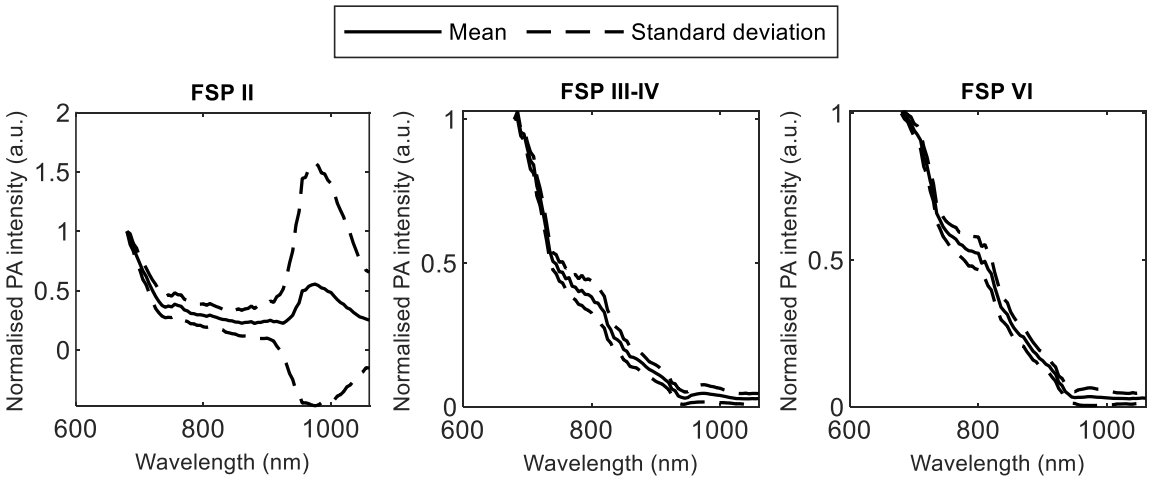

Figure 51: The average normalised peak PA signal intensity of the skin for 680 nm to 1060 nm for the 41 transducers for the light skin tone.

7.4. Discussion

This part of the project aims to investigate, in vivo, the influence of skin tone on the image quality of PAT, with a special focus on breast imaging with the PAM3 system. In this retrospective case study, data from a healthy breast from three volunteers has been analysed. The skin tone of the three volunteers was characterised by the FSP: II (light), III-IV (medium), and VI (dark). The data consisted of the time signals from a wavelength sweep and five reconstructed scans for the wavelengths 720, 755, 797, 833 and 870 nm. The parameters that have been investigated are the imaging depth, the SBR of the blood vessels, the occurrence of artefacts and the PA spectra of the skin. The different volunteers all had different breast sizes and therefore different breast supporting cups were used during the measurements. For FSP II a medium-sized breast cup (cup size 5) was used, for FSP III-IV a cup of one size larger and for FSP VI the largest breast cup (cup size 8). Dantuma et al. showed that different cup

sizes can lead to differences in the fluence distribution on the surface of the cup [79,80]. Differences in fluence result in differences in PA signals. Further, the composition of breast tissue could vary between the volunteers. Consequently, it is difficult to directly compare the results from the three volunteers with each other. However, valuable insights have been gained, and these and the obtained results are discussed in this section according to the following tasks:

1) Visualization of skin, blood vessels and possible artefacts

The volumetric MIPs made of the reconstructed data before filtering for the blood vessels show that the signal of the skin becomes more dominant with increasing skin tone (See Figure 40). This causes a detriment in the visualisation of the blood vessels. While some blood vessels are still visible in the MIP for FSP VI, the difference with the other MIPs is evident. These results are in correspondence with the results found in volunteer studies in which a linear or curved transducer array was used [12,14]. In addition to the increase in signal from the skin in the MIP, there is also a square-shaped shadow imprinted on the reconstruction. This is a reconstruction artefact due to the reconstruction grid being a square grid [91]. For darker skin tones, this will be more visible. This artefact can be reduced by rotating the reconstruction grid during the reconstruction for future image reconstructions of the same data sets [91]. For the present case, the presence of the artefact did not present substantial interference to qualitative and quantitative analyses, and for the conclusions arrived at.

With the linear and curved arrays imaging geometries, a clutter artefact is present for higher melanin content. This artefact is a major cause of the decrease in imaging quality in 2D PAI cases [12,14]. As discussed in Chapter 6 Section 6.5 page 77, it is hypothesised that for a hemispherical geometry, the clutter artefact will occur less or will even be absent. In the data analysed in this volunteer study, the volumetric MIPs of the processed scans show no clear signs of clutter artefacts. However, there is an increase in the background noise present in the scans (See Figure 41). This background noise might originate from smaller or deeper blood vessels of which the signals are too weak to be either fully reconstructed or detected by the filter as vessels. Nonetheless, it should be mentioned the absence of clear signs of the clutter artefact does not mean that a 3D variant of the clutter artefact is not present. As far as blood vessels are concerned, while the skin does decrease the visibility of blood vessels and background noise is increased, signals of the blood vessels can still be isolated using the Hessian filter. Since PAT tomography makes it possible to follow the path of a blood vessel, it is easier to distinguish between blood vessels and noise or 3D clutter artefacts. In summary, while the total effect in the reconstruction might not lead to a visible 3D clutter artefact, the noise in the scan appears to be increased. Thus, the image quality still decreases.

2) Imaging depth

The absorption by blood increases with increasing wavelength [76], but the scattering of the background decreases with increasing wavelength [38]. Both the blood in the vessels of interest, i.e. the imaging targets, and the smaller blood vessels in the “background” tissue absorb more light with increasing wavelength. However, due to the decrease in the optical scattering of the background, it was hypothesised that the imaging depth would slightly increase with increasing wavelength as the light will penetrate deeper. While for FSP VI the results are in agreement with this hypothesis, for FSP II and FSP III-IV the results deviate. For these volunteers, the imaging depth decreases with increasing wavelength (See Figure 45).

For FSP II and FSP III-IV, the imaging depth for 797 nm is significantly higher than expected when compared to the imaging depth found for 755 nm and 820 nm (See Figure 45). This cannot be explained by the differences in laser output energy, as the output energy for 797 nm is not higher than for 755 nm [93]. Furthermore, in the absorption spectra of blood, there is also no significant drop in or spike in the absorption coefficient, which could explain this occurrence (See Figure 24 Chapter 6 Section 6.3.1 page 66). Moreover, it is also something that is not observed in the results for FSP VI (See Figure 45).

Breast contents, such as the relative presence of fat and glandular tissue, define the scattering and absorption properties of light and influence light penetration. Further, the amount and distribution

of blood vessels, which are the imaging targets, are not the same in all breasts. With the further knowledge that breast sizes are also different, which changes the fluence on the breast surface, absolute values of imaging depth should be treated with caution. Even the comparison and interpretation of the trends for the imaging depth for the volunteers is challenging due to the unknown breast compositions. For a reliable comparison, the cup sizes would have had to be the same or the population size would have had to be larger to assess the effects of the various confounding factors. However, the values do give an impression of how the imaging depth can change with skin tone.

3) SBR

As mentioned above, caution has to be taken in the interpretation and comparison of the results. For longer wavelengths, the SBR is in general slightly higher than for shorter wavelengths (See Figure 46). This could be explained by the shape of the absorption spectrum of blood. In the range of 700 to 900 nm, the absorption coefficient in general slightly increases with wavelength (See Figure 24 Chapter 6 Section 6.3.1 page 66). This slight increase can result in a slightly higher PA signal intensity for the blood vessels for that wavelength region. Similar observations were also found in the results of Fernandes et al. who imaged the arms of different volunteers with different skin tones [14].

The decrease in SBR with depth for FSP II is in agreement with the expectations that contrast resolution decreases with depth as the fluence decreases. However, for FSP III-IV and FSP VI, the SBR does not show this relation, as the SBR is relatively constant over depth (See Figure 46). It would imply that the intensity of the PA signals from the blood vessels and that of the background decreases at a similar rate. Blood vessels that are not detected by the filter can contribute significantly to the background signal. For increasing depth, the decrease in PA signal intensity for the background will then follow the same pattern as the PA signal intensities for the detected blood vessels. If for FSP II all major blood vessels are detected, it could be that the undetected blood vessels have a less significant impact on the background. This could explain why for FSP II, the results are different. Nonetheless, likely, other unknown factors are also of influence here, such as breast size. It is therefore important to stress that it is not possible to draw hard conclusions from these results since it is incorrect to compare the results from the volunteers directly. It should be mentioned that the physical focus of the transducers in the imaging bowl is towards the centre of the breast. As a result, both noise and actual signals will have a higher measured PA amplitude. Consequently, if the increase in signal amplitude due to the focussing increases compensates for the decrease in fluence the net effect will also result in an SBR that will remain relatively stable with depth.

In the graphs for the SBR over depth for FSP III-IV and FSP VI, it can be seen that the SBR of the first depth layer is lower compared to that for the other layers (See Figure 46). It should also be mentioned that the total thickness of the skin at the site of the breast can be between 0.6 and 2.7 mm [38], or even as thick as 4.8 mm [51]. While it is not known what the thickness of the skin of the three volunteers was, it might be possible that the skin was slightly thicker for FSP III-IV and FSP VI than for FSP II. If the first depth layer mostly contains the skin, fewer blood vessels will be detected. Furthermore, if the skin itself also has a high signal, this contributes to the background signal. Consequently, the SBR might be lower for the first depth layer compared to the next layer. The volunteer with FSP II might have a thinner skin as well. As a result, the signal from the blood vessels might have been more apparent in that first depth layer, resulting in a higher SBR.

4) Skin signal wavelength sweep

The signals from the skin based on the wavelength sweep data show a clear decrease in signal intensity for increasing wavelength (See Figure 51), which is in line with the decrease in signal intensity of the skin layers in the reconstructions (which can be observed in the MIPs in Figure 47 to 49). The curves are not as smooth as would be expected from just melanin or just the epidermis. The various irregularities and the peak around 970 nm show that some other absorbing tissue components have also contributed to the PA signals in the time signals. Considering that the epidermal layer is around 80 µm [51] and the axial resolution of the PAM3 system is more than 400 µm [76], traces of signals

produced by absorbing tissue constituents close to the epidermis may be present in the signal of the melanosomes.

The water peak around 970 nm is visible for all volunteers (See Figure 51), which is likely because the amount of water relative to the amount of melanin is high. As a result, the water signal will dominate around 970 nm, for which the signal of melanin is relatively low. For a light skin tone, the amount of melanin is low resulting in low signal amplitudes from the epidermal layer compared to the amplitude of the water signal. Consequently, the water peak can dominate the signal from the skin for the 900-1060 nm range for FSP II.

Some assumptions were made for the position of the signal of the skin: the skin will produce the first significant PA signal found in the time signal, and the location of the signal of the skin will not change over time due to motion. The breast cups are made from polyvinyl chloride (PVC) and are supposed to be optically and acoustically transparent. However, there is still a possibility that the cup will produce a small detectable acoustic signal. This signal might be difficult to distinguish from the signal from the skin in the case of a light skin tone when the signal of the skin itself is also small. However, it was theorised that if the wrong signal was picked, this would be visible in the results. Regarding the fixed location of the breast, it was assumed that there would be minimal to no movement of the skin layer because of the breast cup. Consequently, for a specific transducer, the signal of the skin was assumed to have the same shape and location for all measurements performed during the wavelength sweep. Therefore, selecting the same position in the time signal of a specific transducer for the different wavelengths should be an adequate method to determine the change in the PA signal amplitude of a specific point in the time signals.

5) Skin signal reconstructed data

The results for the skin signal from the reconstructed data are less straightforward than the results from the wavelength sweep. As this method is based on voxel values, there is even more effect of other tissue components as for the wavelength sweep data. Each voxel is a combination of different signals and crosstalk between signals can occur. Isolating the voxels corresponding with just the skin layer based on depth relative to the imaging cup is challenging. There is a risk of including voxels from other structures. This can already be seen in the MIPs. When inspecting the MIPs, they seem to suggest that there are large blood vessels present in the skin layer, which in general is not the case (See Figure 47 to 49). These erroneous signals will also contribute to the results causing unexpected deviations. For instance, the decrease in the average signal intensity for FSP VI is less than expected and for FSP II there is no decrease at all.

For some volunteers, the skin of the breast was not in direct contact with the breast cup, such as for FSP II. The selection of the voxel layers was performed with the use of a depth map based on the breast cups. Deviations in the position of the skin with respect to the breast cup were not taken into consideration. As a result, not all voxels corresponding to the skin layer were used in the calculation for the mean skin signal amplitude and some voxels that were used did not correspond to the skin. This will have led to an underestimation of the signal of the skin. However, since between scans the position of the skin is assumed to not change, the trend of the results would not have differed only the values.

The average signal intensities are compensated for the variations in the laser output energies. It can be argued that it is not appropriate to apply this compensation to data obtained from the reconstructions since the reconstructions are a result of various operations performed on the raw data. The correct way to compensate for the laser output energy differences is to take it into consideration during the reconstruction algorithm.

Limitations of the study:

An important limitation of this study is the small population size, as only three volunteers were included. Unfortunately, due to the time constraint, it was not possible to include new volunteers. While the skin tones of the three volunteers can be classified as three different skin tones according to the FSP, the sample size is n = 1. Furthermore, the cup size of the volunteers was not the same. Dantuma et al. showed that different cup sizes result in different fluence distributions on the surface [76,79]. Not

only is the breast size of the volunteers different, but the breast composition is also most likely quite different as well. Factors that can differ for instance are the number of blood vessels and their distribution, the amount of glandular tissue and the ratio of glandular tissue to fatty tissue. Since the intensity of PA signals is dependent on the fluence distribution, differences in fluence can itself cause differences in the scans between volunteers regardless of skin tone. As a result, it is not possible to draw conclusions from the obtained results.

Moreover, since the data was collected before the start of the project, the SkinColorCatch was not yet available. Consequently, the skin tones of the volunteers were only classified with the FSP and not with a more objective metric such as the ITA, like Fernandes et al. did [14]. It is therefore more difficult to compare the results of the volunteer study with the results of the phantom study of Chapter 6. While direct comparison would never have been possible, it would have been easier to find links between the two studies.

Another limitation of the study is that only the PA spectrum of the skin could be determined as opposed to the PA spectrum of other tissue constituents [94]. Due to the specific working mechanism of the system itself it is difficult to trace specific points in the time signals back to specific structures in the scanned object. This is especially the case for in vivo data due to the uncertainty about the position and depths of certain structures at the time of the scan. In addition, since the reconstructions consist of a combination of 101 data collections, the intensities in a single time signal can be relatively low. While in the reconstruction the structure can become visible due to the combination of all signals, in a single time trace the signal can be difficult to identify. This can also be seen in Dantuma et al. [76].

7.5. Conclusion

The main purpose of this case study is to showcase the influence of skin tone on the image performance of the PAM3 system in imaging the female breast. To our knowledge, this study is the first in which the influence of skin tone on PAI is investigated with human data for a hemispherical system. The studies that have already been published regarding this research topic used either a linear or a curved array transducer [12,14]. The healthy breasts of three volunteers have been scanned and for each breast, the raw data from a wavelength sweep and the reconstructions of five full scans were analysed. Due to the limited number of volunteers included, the unknown differences between the breast compositions, and the differences in breast size, no hard conclusions can be drawn. However, the study does give a decent impression of the influence of skin tone on PAT with a hemispherical system. A fairly reliable impression can be obtained of the skin signal and a good impression can be obtained of how skin tone changes the imaging depth and SBR for the blood vessels. The imaging depth decreases with melanin content. While the imaging depth also decreases with increasing wavelength for FSP II and FSP III-IV, the imaging depth increases for FSP VI. While the SBR decreases with depth for FSP II, the SBR stays relatively constant for the other two volunteers. However, their data shows that longer wavelengths result in higher SBRs. The signal intensities of the skin from the reconstructed data show clearly that the signal from the skin increases with melanin content. The data from the wavelength sweep shows a decrease in the signal intensity for increasing wavelength as expected from the absorption spectrum of melanin. More volunteers will have to be included to perform a more thorough investigation of the problem studied here. Something that would in particular be interesting to see, is if the new data would also advocate for the use of scans made with wavelengths at the end of the 680-900 nm range.

Chapter 8

8. General discussion

The aim of this project was to investigate the influence of skin tone on imaging the breast with a 3D photoacoustic computed tomography (PAT) system with a focus on the Twente Photoacoustic Mammoscope (PAM) 3 system. To investigate this, a phantom experiment has been performed as well as a volunteer case report in which data from volunteers has been analysed retrospectively. For the phantom study, three phantoms with a 1 mm thick skin-mimicking layer have been developed. To investigate different skin tones, a copolymer-in-oil (CiO) based skin-mimicking material has been developed with which different melanosome volume fractions (M_f) can be mimicked by adjusting the concentration of alcohol-soluble nigrosin. For the volunteer case study, the data of three volunteers with skin tones characterised as Fitzpatrick skin phototype (FSP) II, III-IV and VI has been analysed. To assess the imaging performance from the available data, a measure of the imaging depth, signal-to-background ratio (SBR) and signal from the skin or skin-mimicking layer have been investigated. The presence of imaging artefacts has also been evaluated. The main results and insights have already been discussed in the separate chapters. However, some general points of discussion and recommendations will be discussed here.

1) Comparison phantom study and volunteer case study:

The noise present in the volumetric maximum intensity projections (MIPs) of the processed scans of the medium and dark phantom has the appearance of a 3D variation of the clutter artefact seen in linear and curved arrays. Some spherical and ellipsoidal structures lower the contrast between the clutter-like signals and the imaging targets. However, for the volunteer study, the noise in the processed reconstructions was less similar to the clutter artefact. It could be that the irregularities in the phantoms themself have caused or enhanced the clutter-like signals. Furthermore, in the unprocessed reconstructions, no significant clutter-like regions were visible. It might be that the filter, which enhanced the imaging targets, has also enhanced certain noise signals in the regions of these irregularities in the phantoms. Consequently, they could appear as clutter artefacts. To be more certain about the origin of the noise in the phantom and to explore if it could indeed be a 3D alternative to the clutter artefact, more experimentation is necessary.

There appears to be a deviation around 800 nm in the shape of the curve for the PA spectrum for the skin based on the wavelength sweep for both the volunteers and the phantoms. The absorption spectrum of both the epidermis and the skin-mimicking layers lack a peak around 800 nm. On the other hand, the absorption spectrum of water shows a very subtle dip around 800 nm [95]. It could be speculated that this slight decrease in absorption by the water in the imaging bowl can cause an increase in the fluence on the surface of the phantom and the breast. Consequently, this could lead to a higher photoacoustic (PA) signal. Moreover, the volunteer case study shows that for all three volunteers, the imaging depth for 797 nm is higher than expected. This occurrence might also be explained by a higher fluence due to the decreased absorption by water. Furthermore, the water in the tissue itself might also absorb less light, increasing the fluence deeper in the breast. Conversely, a greater imaging depth at 797 nm was not observed in the phantom results. A possible explanation for this might be that the phantom materials are oil-based.

Based on the results of both the phantom study and volunteer case study, it might be interesting to explore the added value of using wavelengths in the second half of the 680-900 nm range for darker skin tones. The five wavelengths, which are currently typically used for the volunteer and patient measurements, are centred around 797 nm. However, the phantom study shows that the SBR and imaging depth are higher for the medium and dark phantom for 797, 833 and 870 nm compared to 755 nm. Moreover, while there is still a difference in imaging depth between light, medium and dark phantom, the difference is smaller for the aforementioned three wavelengths than for 755 nm. In the volunteer case study, the results suggest that for FSP VI longer wavelengths result in higher SBR, a more constant SBR over depth and a higher imaging depth. In summary, both studies provide ground to believe that a possible approach to mitigate the impact of darker skin tones on PAI performance would be to use longer wavelengths. This can be attributed to the lower optical absorption by melanin for longer wavelengths, resulting in a higher fluence in the breast.

2) Practical implications:

Due to an increase in the number of breast cancer cases, the burden breast cancer care has on the health care system rises [1]. In the medical imaging field, research towards efficient and effective diagnostic imaging modalities is therefore a major concern. Photoacoustic imaging (PAI) has the ability to provide morphological as well as functional information about the imaged tissue. It is therefore regarded as a promising imaging modality for breast imaging for different indications [8,9]. However, for the translation of the PAM3 to the clinic, a good understanding of how skin tone might influence its imaging performance is crucial to avoid racial bias.

Both the phantom study and volunteer case study show that skin tone does influence the imaging performance of the PAM3 system. An increase in skin tone will result in a decrease in both the imaging depth and the SBR for different depths. The decrease in SBR is also due to an increase in background noise, which obscures the presence of the imaging targets or blood vessels. In practice, this could mean that for darker skin tones deeper lying tumours or smaller superficial tumours are more difficult to detect. This has a major impact on the practical application of the PAM3 as currently there is an unintended racial bias in the system.

With the PAM3, a wide range of wavelengths (680-1060 nm) can be used to scan the breast. And while this decrease in imaging performance could be seen for various wavelengths, for longer wavelengths the imaging performance seems to decrease less. This has to be investigated further to verify if this is indeed the case. However, the implications for the PAM3 in its current state would then be that it is best to image the breast with longer wavelengths to minimise the unintended racial bias. In practice, this could mean either that the general imaging protocol has to be altered to obtain scans with the best possible image quality for the whole population, or that for different skin tones different imaging protocols have to be developed.

3) Recommendations phantom study:

An important limitation of the phantom used for the phantom study is the presence of irregularities in the skin-mimicking layer and air bubbles in the material itself. To improve the results, it is necessary to improve the phantoms themselves and thus the fabrication process. Due to time constraints, there was limited time to perform iterations on the fabrication process. Therefore, some refinements are necessary to make sure the fabrication process becomes easier, more reliable, and more reproducible. It would be recommended to experiment with different methods to pour the base material into the mould without the production of air bubbles. These air bubbles could greatly influence the reconstructions and minimalizing their presence is of the essence. One method would be to put the mould into the vacuum oven while it is at a medium temperature to degas the base material again. The temperature of the oven should be set to a temperature at which the base material is liquid, and the skin-mimicking material is not. Otherwise, there is a risk of damaging the skin-mimicking layer.

It was attempted to characterise the skin tone of the phantoms with the individual typology angle (ITA°) using a colorimeter. While the ITA° values of the phantoms corresponded well with the desired skin tones, the melanin index values were not reliable. In order to be able to link phantom

experiments with volunteer experiments, being able to characterise the skin tone of the phantoms correctly with the same metrics as used in vivo is important. Therefore, it is recommended to further investigate the relation between skin-mimicking materials with different nigrosine concentrations and ITA° and/or melanin index values.

For a future iteration of the phantoms, it would be recommended to investigate if there is a method with which the skin-mimicking material or a variation of the material can be moulded into a thinner skin-mimicking layer. Due to time constraints, it was decided to create a layer of 1 mm as the material was difficult to mould into thinner layers in a controlled manner. However, in the data of both the wavelength sweep and the reconstructions, it can be seen that the signals for the skin-mimicking layers are much higher than those found for the skin in the volunteers. In itself this does not have to be a problem if the imaging system can manage such high values and if the reconstruction method still works correctly. However, the data from the phantom study strongly suggest that the PAM3 and the reconstruction method cannot properly deal with these high signals. To make sure that as much information can be obtained from the measured data it would be necessary to avoid these issues. While making the layers even thicker might be a possible solution, new issues might be introduced. To determine beforehand which maximum layer thickness can be used for the phantom to still obtain correct data, it might be prudent to use simulations. Once the thickness is determined some revisions in the skin-mimicking material might be necessary. Perhaps that CiO with a different ratio of constituents might make it more liquid, which would allow smaller a layer thickness to be created. A possible risk can be that the layer will become more fragile.

Regarding the possibility that the reconstruction method cannot properly manage high or steep signals, it would be recommended to perform some digital experiments to investigate if the voxel values for the imaging targets in the reconstructions are valid. Based on the results for the SBR and imaging depth for the different phantoms and wavelengths, it was assumed that the signals of the imaging targets were not or minimally affected. However, this should be confirmed to ensure that certain conclusions can be drawn.

Another recommendation to the phantom would be to slightly increase the size of the phantom. Currently, the diameter of the hemisphere is 6 cm. However, due to how the imaging targets are placed, not the full 6 cm in depth can be used. Increasing the size would allow the targets to be placed in a similar configuration and with the same orientation. However, the imaging depth can be assessed for deeper layers. Another option would be to change the angle with which the imaging targets are placed in the phantom. The steeper the angle, the more of the phantom is in the imaged volume.

4) Recommendations volunteer case study:

Unfortunately, due to time constraints, it was not possible to perform new volunteer measurements. Not only is the number of cases too low to have statistically significant results, but the variation in the breast size and the variations in breast composition also make it impossible to compare the results since these factors influence the fluence on the breast. To draw conclusions about the influence of skin tone on the imaging performance of the PAM3 in vivo, new measurements with a larger population would have to be performed (a possible protocol for these measurements can be found in Appendix K). It would be recommended to have a population with many different skin tones as well as breast sizes. This would allow the stratification of the population into more homogeneous classes, which makes it easier to draw conclusions.

Not only is it recommended to increase the study population, but it is also recommended to increase the number of full scans made of the breast. Currently, full scans are made with five wavelengths. It is possible to increase this number to at least eight full scans while staying under the limit for the exposure of the breast to the laser. With more wavelengths, more information about the imaging depth and signal-to-background ratio can be obtained as well as about the effect of scanning with shorter or longer wavelengths.

Because the volunteer case study is retrospectively analysed, it is more difficult to link the results from the volunteers to the results of the phantom experiments. For a better comparison, the

classification of the skin tone of the volunteers must be performed with the same metric as was done for the phantoms. This means that the individual typology angle (ITA°) has to be determined for all volunteers. A benefit of using the ITA° is that it is a quantitative and objective method for skin characterisation. However, to be able to properly link the ITA° to M_f values more skin-mimicking samples with a wide range of different concentrations of nigrosin would have to be made and the ITA° value would have to be measured.

5) General recommendation:

While phantom and volunteer studies are highly informative, the investigation of skin tone on imaging performance in PAT would be even more comprehensible with the addition of digital phantom experiments [20]. In digital phantom experiments, the conditions and the optical and acoustic properties of the phantom and its components can be precisely defined and set to desired values. Furthermore, compared to physical phantoms, it is easy to increase the complexity and realism of digital phantoms or develop a large number of phantoms to mimic a variety of skin tones and anatomies [20]. There are various ways in which digital phantom experiments can be of great value besides physical phantom and in vivo measurements. The results of the digital experiments can for instance be used to investigate the difference between expected and obtained results from physical measurements. Moreover, the digital experiment can aid in the development of physical phantoms. As previously mentioned, digital experiments might aid in determining which layer thickness should be reached to obtain good data from phantoms with a skin-mimicking layer. Performing digital phantom experiments, not just to investigate the effect of skin tone on PAT but also to support the physical experiments, is therefore highly recommended.

During the phantom study, an issue with the measurement of the signal from the skin-mimicking layer was encountered as well as an issue with the reconstruction of this layer. While the absorption coefficients of the skin-mimicking layers were significantly lower than those of the epidermis, the signals were much higher. For the dark phantom, this resulted in the clipping of some of the raw signals. These high values for the skin-mimicking layer might also be the cause of the problems in the reconstructions. It is hypothesised that the issues might be caused by the thickness of the skin-mimicking layer, which was 1 mm. However, should this indeed be the case, it is worthwhile to investigate if similar effects occur with in vivo data. It is very likely that in the breast there are blood vessels with diameters in the range of 1 mm. If the PAM3 system is more sensitive to the signals from these vessels, the intensity of these vessels in the reconstructions might not match the expectations based on the absorption coefficients or the depth of the vessels. This might have a considerable impact on quantitative PAI since for this type of imaging being able to rely on the correctness of the measured data is crucial. Moreover, for objective and quantitative measurements, the PA signal intensities should depend on the optical absorption properties of the tissue and not on the dimensions of the structures of interest.

Chapter 9

9. General conclusion

As mentioned above, the motivation for studying the influence of skin pigmentation on the imaging performance of photoacoustic tomography imaging with the Twente Photoacoustic Mammoscope (PAM) 3, is the importance of avoiding unintended racial bias in medical imaging of the breast. The investigation was divided into a physical phantom study and a volunteer study.

Before the phantom study could be performed, different phantoms capable of mimicking different skin tones first had to be developed. The development of a stable skin-mimicking material with tuneable optical properties suitable for photoacoustic imaging (PAI) was more difficult than expected. The criteria that the material should be mouldable into a thin layer in a controlled and reproducible manner proved to be a major obstacle in the development process. The developed skin-mimicking material based on copolymer-in-oil and alcohol-soluble nigrosine mimics the optical absorption of the skin fairly well. However, the efforts to achieve a thickness similar to the epidermis within the available time were unsuccessful. The decision was made to adopt the approach in which there is compensation for the larger thickness of the skin-mimicking layer in the absorption properties. This facilitates the possibility of still mimicking the effect of the skin on the fluence deeper in the physical phantom.

A major hurdle in the development of the physical phantom was the fact that the phantom had to match the geometry of the PAM3. A hemispherical configuration for a phantom was the most straightforward approach. However, creating a thin layer of the developed skin-mimicking material on a curved surface with a reproducible method proved to be challenging. An aluminium mould was custom-made to fabricate physical phantoms with a skin-mimicking layer thickness of 1 mm for the phantom experiment. Four imaging targets in the phantom can be used to investigate different metrics. While some iterations of the phantoms will be necessary to obtain better quality phantoms, the developed phantoms and the obtained insights provide a solid foundation upon which to build. Not only can the acquired knowledge be used to improve the skin-mimicking phantom, but it can also be useful for the development of other phantoms for the PAM3.

The parameters that were assessed during the phantom study to investigate the influence of skin pigmentation on image quality are the imaging depth, the signal-to-background ratio (SBR) of various targets, the occurrence of artefacts and the PA spectra of the skin. And these parameters showed clearly how skin tone can influence the imaging performance of the PAM3. There was a decrease in imaging depth and SBR for the phantoms that mimicked a medium and dark skin tone. However, for longer wavelengths, the imaging performance was less affected by the mimicked skin tone.

Similar results were found in the retrospective volunteer case study in which the scans of three volunteers with three different skin tones were evaluated. This volunteer case report is the first in-depth study of the effect of skin tone on in vivo imaging with a hemispherical photoacoustic tomography (PAT) system. However, the study population is too small and too heterogeneous to assert robust claims. To strengthen the study, more volunteers would have to be included with a wide range of skin tones, with for each skin tone enough volunteers, and different breast sizes. The skin tone of these volunteers will have to be determined quantitatively using the individual typology angle. Due to the setup of the current study, this was not possible.

Based solely on the results of this study, the imaging depth and the SBR, and therewith the imaging performance of the PAM3, appear to be significantly compromised by skin tone. Further investigation is necessary, but it can be imagined that for the PAM3 to be suitable for clinical applications, improvements have to be made. The advantage of not having to use contrast agents to image the whole beast with the PAM3 does not outweigh the major issue of only being suitable for a select part of the female population. To make PAI accessible to a more diverse population and make it possible to translate the technique to clinical practice, significant energy and time investment will be required for the development of compensation methods for counteracting the effect of skin tone. While using longer wavelengths might be a more straightforward and faster solution, for some applications scanning with shorter wavelengths is more practical or simply necessary due to the optical properties of the tissue of interest. A possible compensation method can be based on a skin-tone-specific fluence compensation during the reconstruction. This fluence compensation can also benefit research towards improving the extraction of blood oxygen saturation for quantitative PAI.

To conclude this thesis, this study showed just how relevant the investigation of an inadvertent technical “racial” bias in optical imaging modalities such as PAI is. While in 2019, the effect of skin tone on PAT of the breast with the PAM3 was still thought to be marginal [4], in this study it was clearly shown that skin tone does impact the imaging performance of a hemispherical PAT system. For the future, this means that a compensation method has to be developed to counteract this effect and make photoacoustic breast imaging possible for women regardless of skin colour. Only then can PAT of the breast start to compete with other medical imaging modalities for breast imaging.

Reference list

1. Arnold M, Morgan E, Rumgay H, Mafra A, Singh D, Laversanne M, et al. Current and future burden of breast cancer: Global statistics for 2020 and 2040. Breast. 2022 Dec 1;66:15–23.
2. Zalev J, Richards LM, Clingman BA, Harris J, Cantu E, Menezes GLG, et al. Opto-acoustic imaging of relative blood oxygen saturation and total hemoglobin for breast cancer diagnosis. J Biomed Opt. 2019 Dec 17;24(12):1.
3. Zhou Y, Yao J, Wang L V. Tutorial on photoacoustic tomography. J Biomed Opt. 2016 Apr 1;21(6):61007.
4. Manohar S, Dantuma M. Current and future trends in photoacoustic breast imaging. Photoacoustics. 2019 Dec 1;16.
5. Oraevsky AA, Su R, Nguyen H, Moore J, Lou Y, Bhadra S, et al. Full-view 3D imaging system for functional and anatomical screening of the breast. 2018 Apr 11;248.
6. Lou Y, Oraevsky A, Anastasio MA. Application of signal detection theory to assess optoacoustic imaging systems. Photons Plus Ultrasound: Imaging and Sensing 2016. 2016 Mar 15;9708:97083Z.
7. Kratkiewicz K, Pattyn A, Alijabbari N, Mehrmohammadi M. Ultrasound and Photoacoustic Imaging of Breast Cancer: Clinical Systems, Challenges, and Future Outlook. J Clin Med. 2022 Mar 1;11(5).
8. Lin L, Wang L V. The emerging role of photoacoustic imaging in clinical oncology. Nat Rev Clin Oncol. 2022 Jun 1;19(6):365–84.
9. Han S, Lee H, Kim C, Kim J. Review on Multispectral Photoacoustic Analysis of Cancer: Thyroid and Breast. Metabolites. 2022 May 1;12(5).
10. Gupta V, Sharma VK. Skin typing: Fitzpatrick grading and others. Clin Dermatol. 2019 Sep 1;37(5):430–6.
11. Li N, Yang XX, Yang R ya, Yi F. Study of the characteristics of facial skin tone status in 1092 young Chinese females according to the ITA°. J Cosmet Dermatol. 2022 May 1;21(5):2073–81.
12. Mantri Y, Jokerst J V. Impact of skin tone on photoacoustic oximetry and tools to minimize bias. Biomedical Optics Express. 2022 Feb 2;13(2):875.
13. Fernandes GSP, Uliana JH, Bachmann L, Carneiro AAO, Lediju Bell MA, Pavan TZ. Impact of skin pigmentation on photoacoustic imaging using linear array transducer: a pilot in vivo study. IEEE International Ultrasonics Symposium, IUS. 2022;2022-Octob.
14. Fernandes GSP, Uliana JH, Bachmann L, Carneiro AAO, Lediju Bell MA, Pavan TZ. Mitigating skin tone bias in linear array in vivo photoacoustic imaging with short-lag spatial coherence beamforming. Photoacoustics. 2023 Oct 1;33:100555.
15. Li X, Dinish US, Aguirre J, Bi R, Dev K, Attia ABE, et al. Optoacoustic mesoscopy analysis and quantitative estimation of specific imaging metrics in Fitzpatrick skin phototypes II to V. Journal of Biophotonics. 2019 Sep 1;12(9).

16. Schwab HM, Beckmann MF, Schmitz G. Photoacoustic clutter reduction by inversion of a linear scatter model using plane wave ultrasound measurements. Biomedical Optics Express. 2016 Apr 1;7(4):1468.

17. Else TR, Hacker L, Gröhl J, Bunce E V, Tao R, Bohndiek SE. The effects of skin tone on photoacoustic imaging and oximetry. Journal of Biomedical Optics. 2023 Dec 1;29(S1).

18. Vogt WC, Wear KA, Pfefer TJ. Phantoms for evaluating the impact of skin pigmentation on photoacoustic imaging and oximetry performance. Biomedical Optics Express. 2023;14(11):5735–48.

19. Mota JP, Carvalho JLC, Barja PR. Identificação dos fototipos de pele através de medidas fotoacústicas in vivo. Revista Brasileira de Engenharia Biomedica. 2012;28(3):288–93.

20. Park S, Villa U, Oraevsky A, Anastasio M. Numerical investigation of impact of skin phototype on three-dimensional optoacoustic tomography of the breast. In: ProcSPIE. 2023. p. PC123790E.

21. Park S, Villa U, Oraevsky A, Anastasio M. Numerical investigation of impact of skin phototype on three-dimensional optoacoustic tomography of the breast. In: ProcSPIE. 2023. p. PC123790E.

22. Moore KL, Dalley AF, Agur AMR. Thorax. In: Moore KL, Dalley AF, Agur AMR, editors. Clinically oriented anatomy. 7th ed. Philadelphia: Wolters Kluwer Health; 2014.

23. Jones EE. Fertilization, pregnancy, and lactation. In: Boron WF, Boulpaep EL, editors. Medical Physiology. 2 Updated. Philadelphia: Elsevier Health Sciences Division; 2012.

24. American College of Surgeons. Your breasts [Internet]. [cited 2023 Jan 2]. Available from: https://www.facs.org/for-patients/home-skills-for-patients/breast-cancer-surgery/breast-cancer-types/your-breasts/

25. Mulligan A, O'Malley F. The breast. In: Rubin E, Reisner H, editors. Essentials of Rubin's pathology. 6th ed. Philadelphia: Wolters Kluwer, Lippincott Williams & Wilkins; 2014.

26. Nationaal Borstkanker Overleg Nederland. Borstkanker. 2020.

27. Schoustra SM. A photoacoustic 3D tomographic breast imager [PhD thesis]. Universiteit Twente; 2022.

28. American College of Radiology. Reporting system. In: Breast Imaging Reporting & Data System Atlas [Internet]. 2013. Available from: https://www.acr.org/-/media/ACR/Files/RADS/BI-RADS/Mammography-Reporting.pdf

29. About Cancer. Breast cancer imaging [Internet]. [cited 2023 Mar 29]. Available from: https://www.aboutcancer.com/breast_cancer_imaging.htm

30. Singh D, Singh AK. Role of image thermography in early breast cancer detection- Past, present and future. Computer Methods and Programs in Biomedicine. 2020;183.

31. Wang Y, Li S, Wang Y, Yan Q, Wang X, Shen Y, et al. Compact fiber-free parallel-plane multi-wavelength diffuse optical tomography system for breast imaging. Optics Express. 2022;30(5):6469–86.

32. Zhu Q, Poplack S. A review of optical breast imaging: Multi-modality systems for breast cancer diagnosis. European Journal of Radiology. 2020;129.

33. Covington MF. Contrast-Enhanced Mammography Implementation, Performance, and Use for Supplemental Breast Cancer Screening. Radiologic Clinics of North America. 2021;59(1):113–28.

34. Pei Y, Zhang Y, Hu S, Wang Z, Li Y, He C, et al. Breast Transmission Ultrasound Tomography Based on Capacitive Micromachined Ultrasonic Transducer Linear Arrays. IEEE Sensors Journal. 2022;22(2):1209–17.

35. O'Connell AM, Karellas A, Vedantham S, Kawakyu-O'Connor DT. Newer Technologies in Breast Cancer Imaging: Dedicated Cone-Beam Breast Computed Tomography. Seminars in Ultrasound, CT and MRI. 2018;39(1):106–13.

36. Rao AP, Bokde N, Sinha S. Photoacoustic imaging for management of breast cancer: A literature review and future perspectives. Applied Sciences (Switzerland). 2020;10(3).

37. Yim W, Zhou J, Sasi L, Zhao J, Yeung J, Cheng Y, et al. 3D-Bioprinted Phantom with Human Skin Phototypes for Biomedical Optics. Advanced Materials. 2023 Jan 19;35(3).

38. Dantuma M, van Dommelen R, Manohar S. Semi-anthropomorphic photoacoustic breast phantom. Biomedical Optics Express. 2019;10(11):5921–39.

39. Nikitichev DI, Murawski K, Harris G, Perkins G, Mosse S, Maneas E, et al. 3D printed kidney phantoms for an LED-based photoacoustic and ultrasound imaging system. In: ProcSPIE. 2019. p. 1087868.

40. Fonseca M, Zeqiri B, Beard P, Cox B. Characterisation of a PVCP based tissue-mimicking phantom for quantitative photoacoustic imaging. Optics InfoBase Conference Papers. 2014 Jul 21;

41. Hacker L, Ivory AM, Joseph J, Gröhl J, Zeqiri B, Rajagopal S, et al. A Stable Phantom Material for Optical and Acoustic Imaging. JoVE. 2023;(196):e65475.

42. Garrett J, Fear E. A New Breast Phantom With a Durable Skin Layer for Microwave Breast Imaging. IEEE Transactions on Antennas and Propagation. 2015;63(4):1693–700.

43. Chen AI, Balter ML, Chen MI, Gross D, Alam SK, Maguire TJ, et al. Multilayered tissue mimicking skin and vessel phantoms with tunable mechanical, optical, and acoustic properties. Medical Physics. 2016 Jun 1;43(6):3117–31.

44. Morsink CF, Dam-Vervloet AJ, Krommendijk ME, Kaya M, Cuartas-Vélez C, Knop T, et al. Design and characterization of color printed polyurethane films as biomedical phantom layers. Biomedical Optics Express. 2023 Sep 1;14(9):4485.

45. Saager RB, Kondru C, Au K, Sry K, Ayers F, Durkin AJ. Multilayer silicone phantoms for the evaluation of quantitative optical techniques in skin imaging. Design and Performance Validation of Phantoms Used in Conjunction with Optical Measurement of Tissue II. 2010 Feb 11;7567:756706.

46. Afshari A, Saager RB, Burgos D, Vogt WC, Wang J, Mendoza G, et al. Evaluation of the robustness of cerebral oximetry to variations in skin pigmentation using a tissue-simulating phantom. Biomedical Optics Express. 2022 May 1;13(5):2909.

47. Hacker L, Wabnitz H, Pifferi A, Pfefer TJ, Pogue BW, Bohndiek SE. Criteria for the design of tissue-mimicking phantoms for the standardization of biophotonic instrumentation. Nature Biomedical Engineering. 2022 May 1;6(5):541–58.

48. Agache P, Lihoreau T, Mac-Mary S, Fanian F, Humbert P. The Human Skin: An Overview BT - Agache's Measuring the Skin: Non-invasive Investigations, Physiology, Normal Constants. In: Humbert P, Fanian F, Maibach HI, Agache P, editors. Cham: Springer International Publishing; 2017. p. 1–4.

49. Cao N, Li Y, Zhang R, Liu S, Xiong Y, Cao H. Theoretical analysis of photoacoustic effects in a multilayered skin tissue model. AIP Adv. 2023 Mar 3;13(3):035007.

50. Monnier J, Tognetti L, Miyamoto M, Suppa M, Cinotti E, Fontaine M, et al. In vivo characterization of healthy human skin with a novel, non-invasive imaging technique: line-field confocal optical coherence tomography. Journal of the European Academy of Dermatology and Venereology. 2020 Dec 1;34(12):2914–21.

51. Oltulu P, Ince B, Kokbudak N, Findik S, Kilinc F. Measurement of Epidermis, Dermis, and Total Skin Thicknesses from Six Different Body Regions with a New Ethical Histometric Technique. Turkish Journal of Plastic Surgery. 2018;26(2).

52. Adhikari M, Ali A, Kaushik N, Choi E. Perspective in Pigmentation Disorders. In: Comprehensive Clinical Plasma Medicine: Cold Physical Plasma for Medical Application. 2018. p. 363–400.

53. Duteil L, Roussel K, Bahadoran P. Skin Color and Pigmentation BT - Agache's Measuring the Skin: Non-invasive Investigations, Physiology, Normal Constants. In: Humbert P, Fanian F, Maibach HI, Agache P, editors. Cham: Springer International Publishing; 2017. p. 35–48.

54. El Hajji Y, El Rhaleb EH. Melanin effect on light beam intensity distribution in skin as a function of wavelength and depth from 200 to 1000 nm using Monte Carlo simulation. J Quant Spectrosc Radiat Transf. 2023 Jan 1;295.

55. Ly BCK, Dyer EB, Feig JL, Chien AL, Del Bino S. Research Techniques Made Simple: Cutaneous Colorimetry: A Reliable Technique for Objective Skin Color Measurement. Journal of Investigative Dermatology. 2020 Jan 1;140(1):3-12.e1.

56. Dadzie OE, Sturm RA, Fajuyigbe D, Petit A, Jablonski NG. The Eumelanin Human Skin Colour Scale: a proof-of-concept study. British Journal of Dermatology. 2022 Jul 1;187(1):99–104.

57. Vasudevan S, Vogt WC, Weininger S, Pfefer J. Melanometry for objective evaluation of skin pigmentation in pulse oximetry studies: a critical analysis. In: ProcSPIE. 2023. p. PC123700D.

58. Kasraee B. The measurement of skin color. In: Humbert P, Fanian F, Maibach HI, Agache P, editors. Agache's Measuring the Skin: Non-invasive Investigations, Physiology, Normal Constants. 2nd ed. Springer International Publishing; 2017. p. 49–54.

59. Baquié M, Kasraee B. Discrimination Between Cutaneous Pigmentation and Erythema: Comparison of the Skin Colorimeters Dermacatch and Mexameter BT. In: Humbert P, Fanian F, Maibach HI, Agache P, editors. Agache's Measuring the Skin: Non-invasive Investigations, Physiology, Normal Constants. 2nd ed. Cham: Springer International Publishing; 2017. p. 55–66.

60. Belmonte E. Know your skin type and color according to the Fitzpatrick Scale [Internet]. 2019 [cited 2023 Mar 29]. Available from: https://www.abellaskincare.com/blogs/abella-tips/know-your-skin-type-and-color-according-to-the-fitzpatrick-scale

61. Del Bino S, Ito S, Sok J, Nakanishi Y, Bastien P, Wakamatsu K, et al. Chemical analysis of constitutive pigmentation of human epidermis reveals constant eumelanin to pheomelanin ratio. Pigment Cell Melanoma Res. 2015 Nov 1;28(6):707–17.

62. Xia J, Yao J, Wang L V. Photoacoustic tomography: principles and advances. Electromagnetic waves (Cambridge, Mass). 2014;147:1.

63. Wang L V. Tutorial on Photoacoustic Microscopy and Computed Tomography. IEEE Journal of Selected Topics in Quantum Electronics. 2008;14(1):171–9.

64. Setchfield K, Gorman A, Simpson AHRW, Somekh MG, Wright AJ. Relevance and utility of the in-vivo and ex-vivo optical properties of the skin reported in the literature: a review [Invited]. Biomedical Optics Express. 2023;14(7):3555–83.

65. Zonios G, Dimou A. Light scattering spectroscopy of human skin in vivo. Optics Express, Vol 17, Issue 3, pp 1256-1267. 2009 Feb 2;17(3):1256–67.

66. Morsink CF. Setting the Tone A Phantom Study on the Effect of Skin Pigmentation on Transcutaneous Bilirubin Measurements. Universiteit Twente; 2022.

67. Jacques SL. Skin optics [Internet]. 1998. Available from: https://omlc.org/news/jan98/skinoptics.html

68. Jacques SL. Optical properties of biological tissues: a review. Physics in Medicine & Biology. 2013 May 10;58(11):R37.

69. Foschum F, Bergmann F, Kienle A. Precise determination of the optical properties of turbid media using an optimized integrating sphere and advanced Monte Carlo simulations. Part 1: theory. Applied Optics. 2020;59(10):3203–15.

70. Bergmann F, Foschum F, Zuber R, Kienle A. Precise determination of the optical properties of turbid media using an optimized integrating sphere and advanced Monte Carlo simulations. Part 2: experiments. Applied Optics. 2020;59(10):3216–26.

71. Prahl S. Everything I think you should know about Inverse Adding-Doubling. 2011.

72. Xia W, Piras D, van Hespen JCG, Steenbergen W, Manohar S. A new acoustic lens material for large area detectors in photoacoustic breast tomography. Photoacoustics. 2013 May 1;1(2):9–18.

73. van Dommelen R. A semi-anthropomorphic photoacoustic breast phantom [Master thesis]. Universiteit Twente; 2018.

74. Hacker L, Joseph J, Ivory AM, Saed MO, Zeqiri B, Rajagopal S, et al. A Copolymer-in-Oil Tissue-Mimicking Material With Tuneable Acoustic and Optical Characteristics for Photoacoustic Imaging Phantoms. IEEE transactions on medical imaging. 2021 Dec 1;40(12):3593–603.

75. Grillo FW, Cabrelli LC, Sampaio DRT, Carneiro AAO, Pavan TZ. Glycerol in oil-based phantom with improved performance for photoacoustic imaging. IEEE International Ultrasonics Symposium, IUS. 2017 Oct 31;

76. Dantuma M, Lucka F, Kruitwagen SC, Javaherian A, Alink L, van Meerdervoort RPP, et al. Fully three-dimensional sound speed-corrected multi-wavelength photoacoustic breast tomography. 2023 Aug 13 [cited 2024 Jan 4]; Available from: https://arxiv.org/abs/2308.06754v1

77. Vogt WC, Jia C, Wear KA, Garra BS, Joshua Pfefer T. Biologically relevant photoacoustic imaging phantoms with tunable optical and acoustic properties. Journal of Biomedical Optics. 2016 Feb 17;21(10):101405.

78. Maneas E, Xia W, Ogunlade O, Fonseca M, Nikitichev DI, David AL, et al. Gel wax-based tissue-mimicking phantoms for multispectral photoacoustic imaging. Biomedical Optics Express. 2018 Mar 1;9(3):1151.

79. Dantuma M, Kruitwagen SC, Weggemans MJ, Op't Root TJPM, Manohar S. Suite of 3D test objects for performance assessment of hybrid photoacoustic-ultrasound breast imaging systems. Journal of Biomedical Optics. 2021 Dec 9;27(07).

80. Dantuma M. A hybrid multispectral photoacoustic-ultrasound breast imager from the lab towards the clinic [PhD thesis]. Universiteit Twente; 2021.

81. Schoustra SM, op 't Root TJPM, Pompe van Meerdervoort RP, Alink L, Steenbergen W, Manohar S. Pendant breast immobilization and positioning in photoacoustic tomographic imaging. Photoacoustics. 2021 Mar 1;21:100238.

82. Cuartas-Vélez C, Middelkamp HHT, van der Meer AD, van den Berg A, Bosschaart N. Tracking the dynamics of thrombus formation in a blood vessel-on-chip with visible-light optical coherence tomography. Biomedical Optics Express. 2023;14(11):5642–55.

83. Else TR, Hacker L, Bohndiek SE. Evaluating the impact of melanin on spectral colouring in photoacoustic imaging. In: ProcSPIE. 2021. p. 116424M.

84. Riksen JJM, Nikolaev A V, Soest G van. Photoacoustic imaging on its way toward clinical utility: a tutorial review focusing on practical application in medicine. Journal of Biomedical Optics. 2023 Jun 1;28(12):121205.

85. PAMMOTH. Photoacoustic Mammoscopy for evaluating screening-detected lesions in the breast: Progress [Internet]. [cited 2023 Mar 30]. Available from: https://www.pammoth-2020.eu/workplan.html

86. PAMMOTH. Photoacoustic Mammoscopy for evaluating screening-detected lesions in the breast: Objectives [Internet]. [cited 2023 Mar 30]. Available from: https://www.pammoth-2020.eu/objectives.html

87. Fonseca MB, An L, Cox BT. Sulfates as chromophores for multiwavelength photoacoustic imaging phantoms. Journal of Biomedical Optics. 2017 Dec 1;22(12):125007.

88. Kirchner T, Frenz M. Multiple illumination learned spectral decoloring for quantitative optoacoustic oximetry imaging. Journal of Biomedical Optics. 2021 Aug 4;26(8).

89. Prahl S. Tabulated Molar Extinction Coefficient for Hemoglobin in Water [Internet]. [cited 2024 Feb 23]. Available from: https://omlc.org/spectra/hemoglobin/summary.html

90. Bulthuis RFG, Dantuma M, Kruitwagen SC, van Gameren FDP, Lucka F, Javaherian A, et al. Insights from healthy human studies with a photoacoustic tomography system for breast imaging. 2021.

91. Lucka F. Private communication about photoacoustic reconstructions for the PAM3 13th of June. Centrum voor Wiskunde en Informatica; 2024.

92. Lucka F. Private communication about photoacoustic reconstructions for the PAM3 25th of June. Centrum voor Wiskunde en Informatica; 2024.

93. PA Imaging. IMDD ANNEX A. 2020.

94. Else T. How does skin colour affect photoacoustic imaging in vivo? [Thesis chapter]. Cambridge university; 2024.

95. Konugolu Venkata Sekar S, Dalla Mora A, Bargigia I, Martinenghi E, Lindner C, Farzam P, et al. Broadband (600-1350 nm) Time Resolved Diffuse Optical Spectrometer for Clinical Use. IEEE Journal of Selected Topics in Quantum Electronics. 2015 Jan 1;22:1.

96. Mbonyiryivuze A, Nuru ZY, Ngom BD, Mwakikunga B, Dhlamini SM, Park E, et al. Morphological and Chemical Composition Characterization of Commercial Sepia Melanin. American Journal of Nanomaterials. 2015 Jul 8;3(1):22–7.

97. Krommendijk ME. A study on the influence of neonatal skin pigmentation on transcutaneous bilirubin measurements [Internship thesis]. Universiteit Twente; 2021.

98. Caratenuto A, Li S, Wan Y, Zheng Y. Optical Epidermal Mimicry from Ultraviolet to Infrared Wavelengths. ACS Applied Bio Materials. 2022 Nov 21;5(11):5231–9.

99. Krommendijk ME. Design of an ultrasound brain phantom for testing of an ultrasound imaging needle for ventricle drainage [Bachelor thesis]. University of Twente; 2020.

100. Ivory AM, Shah A, Rajagopal S, Zeqiri B. Development and investigation of the acoustic properties of tissue-mimicking materials for photoacoustic imaging techniques. IEEE International Ultrasonics Symposium, IUS. 2019 Oct 1;2019-October:1489–92.

101. Cabrelli LC, Grillo FW, Sampaio DRT, Carneiro AAO, Pavan TZ. Acoustic and Elastic Properties of Glycerol in Oil-Based Gel Phantoms. Ultrasound in Medicine and Biology. 2017 Sep 1;43(9):2086–94.

102. Oiseth S, Jones L, Maza E. Breast Cancer Screening [Internet]. 2023 [cited 2024 Apr 22]. Available from: https://www.lecturio.com/concepts/breast-cancer-screening/

Appendices

Appendix A: Additional requirement tables phantom materials

Melanin-mimicking substance

For an initial idea of which absorber should be used to mimic melanin, various papers in which researchers have attempted to create skin phantoms have been assessed. Six possible absorbers were chosen for further evaluation based on various criteria (See Table 11): synthetic melanin, natural melanin, water-soluble nigrosin, alcohol-soluble nigrosin, polydopamine (PDA) and coffee. In the paper of Yim et al. PDA has shown to be a very versatile and promising substance to mimic not just melanin but also melanosomes. It has a similar absorption spectrum as melanin and the PDA particle size, and its clustering can be adjusted [37]. The other 5 substances scored lower than PDA in the decision matrix. However, this is mainly because these substances cannot be used or have not been used yet to mimic melanosomes. While derivations from or equivalent forms of melanin are optically supposedly very similar to melanin, they are also relatively expensive. Nigrosin is a more affordable substance that on paper also has a similar optical absorption spectrum as melanin. There are two nigrosin variations: water-soluble (WS) and alcohol-soluble (AS). According to the paper of Afshari et al., the water-soluble version has a more similar spectrum as melanin than the alcohol-soluble one [46]. While coffee is the most affordable substance, it is difficult to achieve high enough absorption values with it for the darkest skin tones [46].

Table 11: Multiple-criteria decision-making matrix for melanin-mimicking material.

Requirement (R) / wish (W)	**Weight**	**Synthetic melanin (M0418)**	**Natural melanin (Sepia melanin)**	**Nigrosin (water-soluble)**	**Nigrosin (alcohol-soluble)**	**Polydopamine**	**Coffee**
R: particles in the range of 100-500 nm. W: three different sizes (100, 300, 500 nm).	1	0	1 [96]	0	0	3 [37]	-1
R: No clustering W: Sensible and controlled clustering	1	0	0	0	0	3 [37]	0
R: homogeneous distribution of the particle sizes (all around one distinct size). W: Sensible mix of 2-3 different sizes.	1	0	0	0	0	3 [37]	0
R: similar to the absorption of melanin in the range of 600-900 nm. W: equal to the absorption of melanin in the range of 600-900 nm.	4	2 [46,97]	2 [46,97]	2 [46]	1 [46]	3 [37,98]	1 [46,97]
Requirement: Scattering within the given range for the wavelength range of 600-900 nm.	3	1 [97]	1 [97]	1 [46]	0	1 [37]	0

Wish: Scattering within the given range for the wavelength range of 600-900 nm AND minimal differences between the skin tones.							
R: Compatible with PVCP	4	1	1	0	0	0	1
R: Compatible with copolymer-in-oil	4	-1 (Perhaps when using glycerol) [75]	-1 (Perhaps when using glycerol) [75]	-1 (Perhaps when using glycerol) [75]	2 (Perhaps better when using glycerol) [74,75]	-1 (Perhaps when using glycerol) [75]	1 (Dissolving in methanol necessary) [97]
R: Compatible with native gel wax	4	-1 (Perhaps when using glycerol, based on likeness to CiO) [75]	-1 (Perhaps when using glycerol, based on likeness to CiO) [75]	-1 (Perhaps when using glycerol, based on likeness to CiO) [75]	2 (Perhaps better when using glycerol, based on likeness to CiO) [74,75]	-1 (Perhaps when using glycerol, based on likeness to CiO) [75]	1 (Dissolving in methanol necessary, based on likeness to CiO) [97]
R: Compatible with PDMS	4	1	1	0	0	1	1
Total score		11	12	3	20	20	19

Explanation of the scores:
-2 → Does not meet the requirement at all
-1 → Does not meet the requirement but could be acceptable in certain conditions (condition is given between brackets).
0 → Neutral or N/A
1 → Meets the requirement
2 → Meets the requirement and further possibilities can be explored
3 → Meets the requirement fully and also meets the wish(es)

Base material for skin-mimicking material

Based on extensive research towards materials used for skin-mimicking phantoms and their potential in PAI four materials were picked to be compared more extensively based on predefined criteria (See Table 14-18). The four materials that were picked are polydimethylsiloxane (PDMS), polyvinylchloride plastisol (PVCP), copolymer-in-oil (CiO) and native gel wax (NGW). The decision matrix showed that PVCP scored the highest with NGW as the second-best material (See Table 12). CiO scored the lowest number of points. The optical and acoustic properties of PVCP can be tuned well, which is a major advantage. While oil-based materials are considered very promising materials for PA phantoms [41,47] they are not yet used for organ-sized tissue-mimicking PA phantoms. A disadvantage of oil-based materials is the limited achievable speed of sound [41,47,78]. While the achievable speed of sound is high enough to mimic fat and glandular breast tissue, it is much lower than the speed of sound of the skin [73]. Since the layer of the skin is supposed to be very thin, it can be argued that the discrepancy in the speed of sound between the material and real skin is of less importance for this project.

The choice of the materials for this phantom and the skin-mimicking layer was made with careful consideration. After much deliberation, it was chosen to investigate both CiO and NGW further. While PVCP has on paper excellent properties, its difficult fabrication method makes it a less practical material for such an explorative study. The oil-based materials have the advantage that they can be reused easily by reheating the solid material. Moreover, CiO is considered a potential standard material for PA imaging phantoms. Despite the lack of papers in which CiO has been used as the material for (semi)anthropomorphic phantoms its potential makes it interesting to be one of the first to make an attempt.

Base material for phantom

Different factors have been taken into consideration in the choice for the material for the base material, in other words, the breast-mimicking material: compatible with the skin-layer mimicking material, producible in large volumes, tuneable to achieve the optical and acoustic properties of (fatty) breast tissue. The material for the base part of the phantom should be compatible with the material for the skin-mimicking layer. The two parts should adhere well to each other to ensure the integrity of the phantoms. However, there should not be any mixing between the materials during the fabrication of the phantoms. Furthermore, there should be minimal loss of signal due to the possible differences in optical or acoustic properties. As the influence of the different skin-mimicking layers is studied, the other parts of the phantoms should be identical. This means that it should be possible to produce the material for the base part of the phantom in large volumes to avoid differences in properties.

In previous studies, M. Dantuma and R. van Dommelen have investigated materials with which to make breast phantoms. PVCP was chosen because of its good optical and acoustic tunability. However, it was mentioned that producing the material in bulk could be difficult due to overheating and burning of the material during polymerisation. As a result, creating a large solid phantom was difficult [38]. M. Dantuma has also made a large phantom by fabricating it layer by layer, which was visible in the result [79]. This material is therefore less ideal if the goal is to have multiple phantoms that are almost identical. Since the material for the skin-mimicking layer is most likely going to be NGW or CiO, using CiO for the rest of the phantom should be feasible. It is easy to make in bulk and similar optical and acoustic properties as breast tissue can be achieved according to the literature [74].

Table 12: Multiple-criteria decision-making matrix for (skin) phantom material.

Requirement (R) / wish (W)	**Weight**	**PVCP**	**PDMS**	**Copolymer-in-oil**	**Native gel wax**
Shape R: 3D shape	5	1 [79]	1 [73]	1 [75]	2 [39,99]
Size R: PAM cup size 1 W: PAM cup size 4-5	4	3 [73]	3	0	2 [99]
Layers R: Epidermal and “average” breast tissue. W1: Epidermis (+ dermis), fatty tissue, glandular tissue, blood vessels. W2: blood flow	5	1 [73]	1 [73]	0	0
Thickness skin R: the thickness should be around 1 mm. W: the thickness is between 50 and 100	4	2 [97]	3 [97]	0	0

µm (ideally around 54.3 µm).					
Speed of sound R: Tuneable to around 1540 m/s W: Tuneable SOS → skin 1600 m/s, glandular tissue 1520 m/s, fat tissue 1440 m/s [73,100]	4	2 [73]	-1 (If PDMS is only used for the epidermis and the acoustic properties of the skin are of less importance) [73]	-1 (Only for fat and glandular tissue it could be acceptable) [47,74]	-1 (If it is only used for the skin layer as for such a thin layer the speed of sound is of less importance) [99]
Acoustic attenuation R: Tuneable attenuation → skin 1 dB/cm/MHz, breast tissue 2 dB/cm/MHz W: skin 1.5 dB/cm/MHz, gland. tissue 2.3 dB/cm/MHz, fatty tissue 1.4 dB/cm/MHz [73,74,77]	4	2 [73]	-1 (See above) [73]	1 [47]	1 [99]
R: Tuneable to average absorption properties of fat and fibroglandular tissue. W: Tuneable to have corresponding absorption properties for the different layers.	4	3 [73]	1 [73]	3 [47]	2 [78]
R: Tuneable to average scattering properties of fat and fibroglandular tissue. W: Tuneable to have corresponding scattering properties for the different layers.	3	3 [73]	1 [73]	3 [47]	2 [78]
R: No air between the layers W: No visible transition at all.	4	2 [79]	0	0	0
R: no disconnection of the layers during the measurement. W: The phantom should consist of a base part on which the epidermis-mimicking layer can be fixated.	4	1 [79]	0	0	0

R: Stability for 4 weeks. W: Stability for at least a year.	3	2 [97]	2 [97]	2 [47]	2 [99]
R: Reproducible	5	2 [97]	0	-1 (Depends on the precise materials used) [74]	-1 (If a commercial product is used there may be differences between batches)
R: Easy fabrication W: Reusable	3	1 [97]	1 [73,97]	3 [75,101]	3 [39,78,99]
Total score		98	42	36	52

Explanation of the scores:
-2 → Does not meet the requirement at all
-1 → Does not meet the requirement but could be acceptable in certain conditions (condition is given between brackets).
0 → Neutral or N/A
1 → Meets the requirement
2 → Meets the requirement and further possibilities can be explored
3 → Meets the requirement fully and also meets the wish(es)

Table 13: SWOT analysis PVCP.

Strengths: - Good tunability of the optical and acoustic properties - Thin layers are possible - Long stability of the phantom for future measurements	Weaknesses: - Fabrication can be difficult for large-volume phantoms - Custom-made PVCP is more difficult and expensive to prepare
Opportunities: - A lot of literature is available - Acoustic properties can be tuned using additives such as DEHA and BBP - Optical properties can be tuned using TiO2 and absorbing substances - Wide variety of possible absorbing substances.	Threats: - There is a chance of toxic chemicals, depending on the materials used for custom-made PVCP

Table 14: SWOT analysis PDMS.

Strengths: - Thin layers can be achieved - Easy to combine with additives	Weaknesses: - Very low SOS (1300 m/s) - Curing PDMS can be difficult when trying to obtain a homogeneous distribution of additives.
Opportunities: - Optical properties can be tuned using water-insoluble absorbers and TiO2	Threats: - No anthropomorphic PA phantoms made yet with this material

Table 15: SWOT analysis CiO.

Strengths: - Good tunability of acoustic and optical properties - By reheating the material it is possible to remodel or reuse the material provided that the material has not been contaminated with other substances or materials.	Weaknesses: - Low SOS (1400-1500 m/s) - Only oil-based or oil-compatible absorbing substances can be used.
Opportunities: - SOS tuneable using paraffin wax, glycerol, or LDPE - Optical properties can be adjusted using oil-soluble absorbers (such as nigrosin) and TiO_2 - Might be 3D printable	Threats: - Not much literature about this material. - No previous tissue-mimicking phantoms made with this material

Table 16: SWOT analysis NGW.

Strengths: - High stability - Easy fabrication - By reheating the material it is possible to remodel or reuse the material provided that the material has not been contaminated with other substances or materials.	Weaknesses: - Limited SOS (around 1440 m/s), which is not tuneable - Only oil-based or oil-compatible absorbing substances can be used
Opportunities: - Paraffin wax can be used to tune the acoustic properties - Might be 3D printable - Oil-based absorbers and TiO2 can be used to tune optical properties	Threats: - Not much literature about this material

Appendix B: Protocol skin-mimicking material fabrication

Materials

- High molecular weight SEBS
- LDPE
- Mineral oil light
- 99.9% Ethanol
- Alcohol-soluble nigrosin
- Glass beaker
- Mechanical stirrer
- Oil bath
- Vacuum oven

Methods

1. Preheat the vacuum oven to 150 °C.
2. Weigh off all the materials depending on the desired concentration of nigrosin and the desired amount of material.
    a. X % w/v nigrosin (X grams per 100 ml mineral oil)
    b. 12 % w/w High molecular weight SEBS
    c. 5 % w/w LDPE
    d. 83 % w/w mineral oil (directly in the glass beaker)
3. Add 9.1 % v/v ethanol to the nigrosin (based on the volume of mineral oil) and mix well until all the nigrosin is dissolved.
4. Heat the mineral oil.
    a. Turn on the oil bath and heat it to 150 °C.
    b. Place the beaker with mineral oil in the oil bath.
    c. Place the mechanical stirrer in the beaker and turn it on at a medium rotation speed (the stirrer will be on for the rest of the steps).
    d. Heat the mineral oil for at least 30 minutes.
5. Slowly add the nigrosin solution to the mineral oil using a pipet of a maximum of 2 mL to dose the amount of nigrosin.
6. Mix the nigrosin through the mineral oil for 15 minutes.
7. Carefully add the SEBS and LDPE in parts to avoid large clumps.
8. Stir for an hour or until all of the material is dissolved and regularly check for aggregates.
    a. The mechanical stirrer can be turned to a higher number of rotations.
    b. If there are aggregates, try to break them with a metal spatula at the start of the stirring process.
    c. If there is material stuck to the glass beaker, carefully remove it with a metal spatula.
9. Put the beaker in the vacuum oven and degas it until no more air bubbles are formed. If the number of bubbles is too high, turn off the vacuum, until the air bubbles are gone. Turn on the vacuum again. This can be repeated as many times as necessary.
10. Pour the mixture into the mould for direct use or container (for storage).

Appendix C: IAD measurements skin-mimicking materials

The optical properties of the skin-mimicking material, i.e. the reduced scattering and absorption coefficients, were determined in our group by measuring the transmission and reflectance of 3 mm thick slabs of the materials. For this, a spectrophotometer with an integrating sphere module (UV-2600i, Shimadzu) was used. The absorption and reduced scattering coefficients were determined using the inverse adding-doubling method (IAD) [71]. In the IAD method, the optical properties of a material are determined by repeatedly estimating them and comparing calculated total transmittance and diffuse reflectance values with the values of the actual measurements. The optical properties are those estimated values that result in the lowest error between the calculated and measured values [71].

There is a clear deviation of the IAD data from the intended curves with melanosome volume fractions (M_f) values of 3%, 9% and 27% (See Figure 52 on the left). It can be seen that for the materials with nigrosin, the corresponding epidermis layers have M_f-values of 4.5%, 11% and 38%. The sum of squares errors (SSE) between the measured values and the theoretical values for M_f-values of 0%, 4.5%, 11%, and 38% in the wavelength range of 600-1100 nm was: 0.104, 0.149, 0.103 and 0.897, respectively. These values are higher than the SSE values found for the measurements by the Institute for Laser Technologies in Medicine and Metrology (ILM). Visually, it can also be appreciated that the correspondence between the curves shows a greater discrepancy compared to the ILM values.

The reduced scattering coefficient of the four different skin-mimicking materials determined with the IAD method can be found in Figure 52 on the right. It can be seen that for the 0.009% w/v sample, the reduced scattering coefficient could not be determined for the complete wavelength range of 680-1060 nm. The reduced scattering coefficients for the other three materials are consistently below the theoretical curves for the epidermis from Afshari et al. and Jacques et al. [46,67]. This is in contrast to the ILM data, which showed higher reduced scattering coefficients.

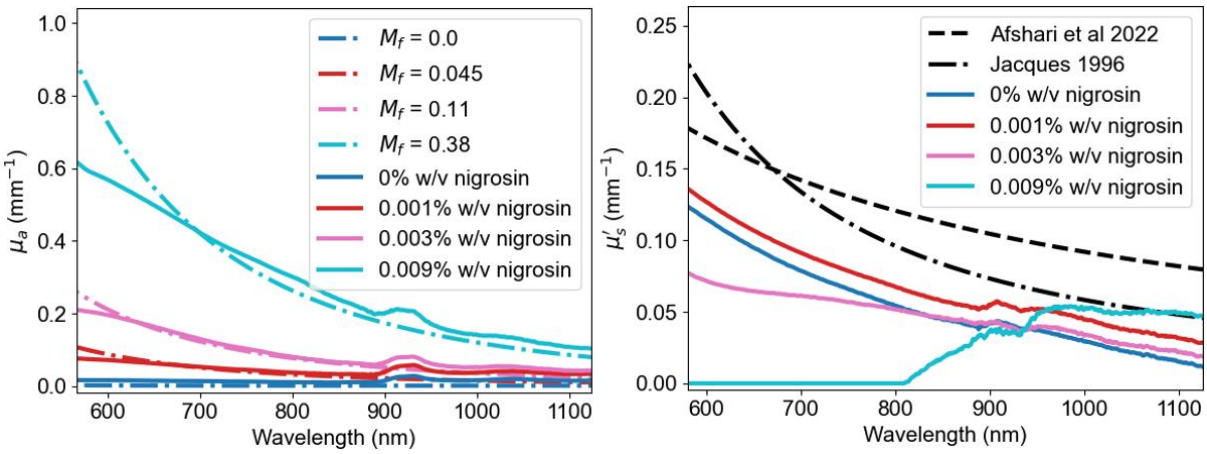

Figure 52: Absorption coefficients (left) and reduced scattering coefficients (right) of the four different skin-mimicking materials determined with the IAD method. The absorption coefficients of the materials are compared to the desired theoretical absorption coefficients of the epidermis with different melanosome fractions (M_f). The reduced scattering coefficients of the materials are compared to the desired theoretical reduced scattering coefficients of the epidermis.

Appendix D: Protocol base material fabrication

Materials

- Native gel wax
- Paraffin
- TiO_2
- 99.9% ethanol
- Glass beaker
- Mechanical stirrer
- Oil bath
- Vacuum oven

Methods

1. Preheat the vacuum oven to 120 °C.
2. Weigh off all the materials depending on the desired amount of base material.
    a. 0.15% w/v TiO_2 (0.15 grams per 100 ml base material)
    b. 8 % w/w Paraffin
    c. 92% w/w Native gel wax
3. Turn on the oil bath and heat it to 120 °C.
4. Place a beaker with NGW in the oil bath.
5. If not all the material fits directly in the beaker, just fill it as much as possible and let the NGW melt.
6. Meanwhile, add 1.6 % v/v ethanol to the TiO_2 and put it in the sonification bath for 1 hour (do not heat the sonification bath).
7. Once the NGW is (partially) melted add paraffin (and the rest of the NG) in parts.
8. If the NGW and paraffin mixture is melted, place the mechanical stirrer in the beaker and turn it on at a medium rotation speed (the stirrer will be on for the rest of the steps).
9. Slowly add the TiO_2 solution to the mineral oil using a pipet of a maximum of 2 mL to dose the amount of TiO_2.
10. Mix the TiO_2 through the mineral oil for 1 hour at medium or high speed.
11. Put the beaker in the vacuum oven and degas it until no more air bubbles are formed. If the number of bubbles is too high, turn off the vacuum, until the air bubbles are gone. Turn on the vacuum again. This can be repeated as many times as necessary.
12. Pour the mixture into the mould for direct use or container (for storage).

Appendix E: IAD measurements base material and new batch skin-mimicking material

Base material

The optical properties of the base material and the new batch of light skin-mimicking material, i.e. the reduced scattering and absorption coefficients, were determined in our group using the inverse adding doubling (IAD) method [71]. The approach for the optical characterisation of the base material and the new batch of skin-mimicking material is the same as in Appendix C for the skin-mimicking materials.

Two separate batches of phantom base material were made, due to limitations in the volume of the available glass beakers. When comparing the determined absorption coefficients for batch 1 with the values found by the Institute for Laser Technologies in Medicine and Metrology (ILM) for the same batch, we can see that they differ (Figures 53 and 54). There is an increasing difference between the absorption coefficients found with the ILM measurements and those found with the IAD measurements. The absorption coefficients for the IAD measurements are lower than those of the ILM measurements until around 650 nm, after which they become higher. A similar pattern can be seen for the reduced scattering coefficients.

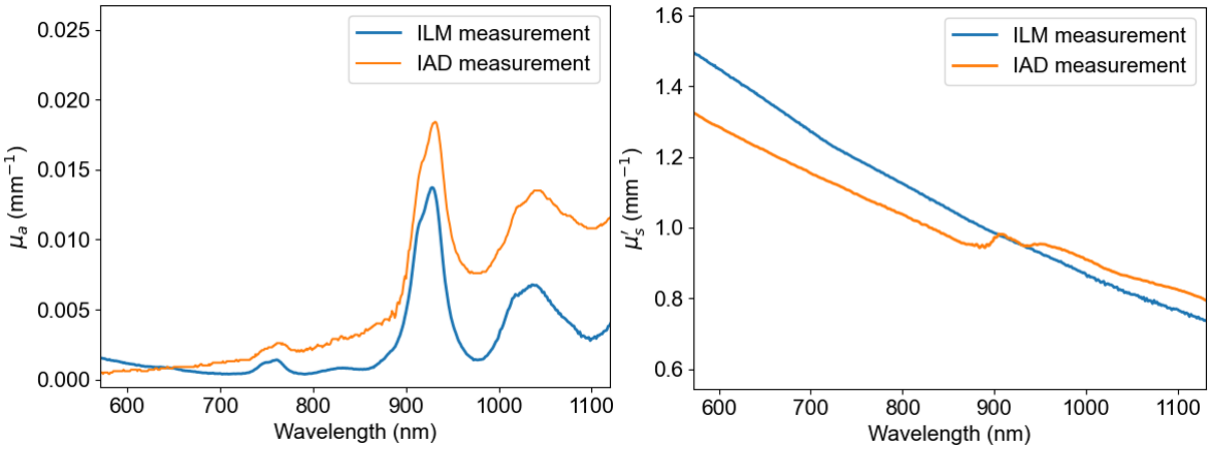

Figure 53: Comparison of the absorption coefficients (left) and reduced scattering coefficients (right) for the base material measured by ILM and with the IAD method.

The optical properties of batch 2 have only been determined with the IAD method. The spectrum for batch 2 seems to have an offset in comparison to the spectrum of batch 1. The values for batch 2 are consistently higher than those for batch 1 with about 0.005 mm^{-1}. A large difference in the scattering properties between the two base material batches can also be found. The reduced scattering coefficients of batch 1 are consistently higher than those of batch 2 with a factor of about 1.5. The inconsistencies in the reduced scattering coefficients between the two batches could be partially explained by the fact that TiO_2 in a low-viscosity substance tends to sink to the bottom as explained in Chapter Section 5.5 page 59. However, this does not fully explain the difference found in the absorption coefficients. Differences in the concentration of TiO_2 should not influence the values found for the absorption coefficients as much as it does [78]. Moreover, the deviation in the absorption coefficients does not seem to be linked directly to the deviation in the reduced scattering coefficients. The deviation in the former seems to be purely based on an offset, whereas the deviation in the latter seems to be based on a ratio. This highlights the uncertainty around the reliability and accuracy of the current approach for the IAD method.

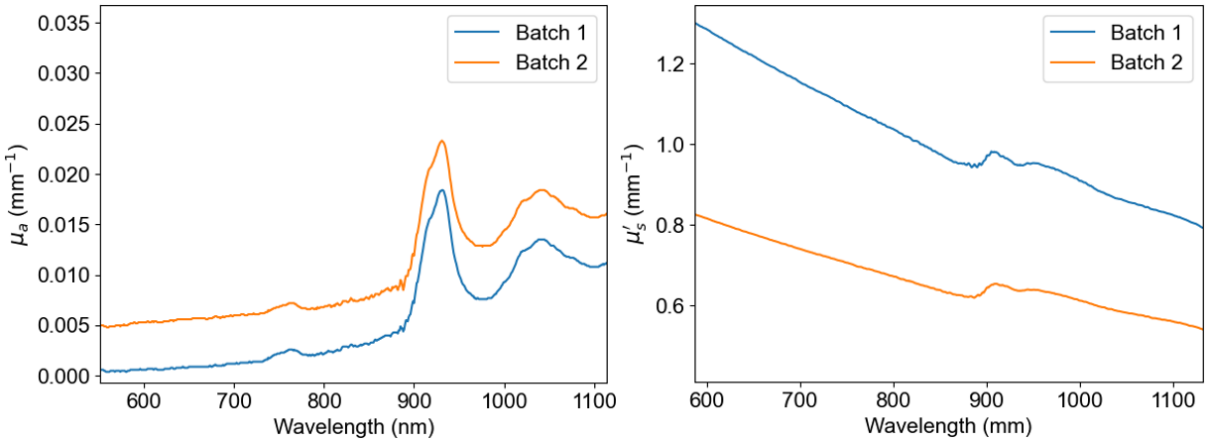

Figure 54: Absorption coefficients (left) and reduced scattering coefficients (right) of the two batches of base material determined with the IAD method.

New batch light skin-mimicking material

Figure 55: A photograph of two samples of light skin-mimicking material. On the left, is a sample of the previous batch of the material and on the right a sample of the newly made batch of material.

The new batch of light skin-mimicking material for the phantom with the light skin tone was made following the same protocol as for the previous batch. However, the optical properties found with the IAD method are significantly different from those found for the previous light skin tone material. The absorption coefficients are consistently higher than for the previously made batch, while the reduced scattering coefficients are consistently lower (See Figure 56). Visually, samples of the two batches have a similar colouring, which is as expected since the same protocol was used to develop the two materials (See Figure 55). On the left is the sample of the first batch of light skin-mimicking material. On the right is the sample of the new batch, which was used to fabricate the phantom with the light skin-mimicking layer. In case the concentration of nigrosin had been higher, it would be expected that only the absorption coefficients would be higher. The scattering properties should be minimally changed by adding nigrosin.

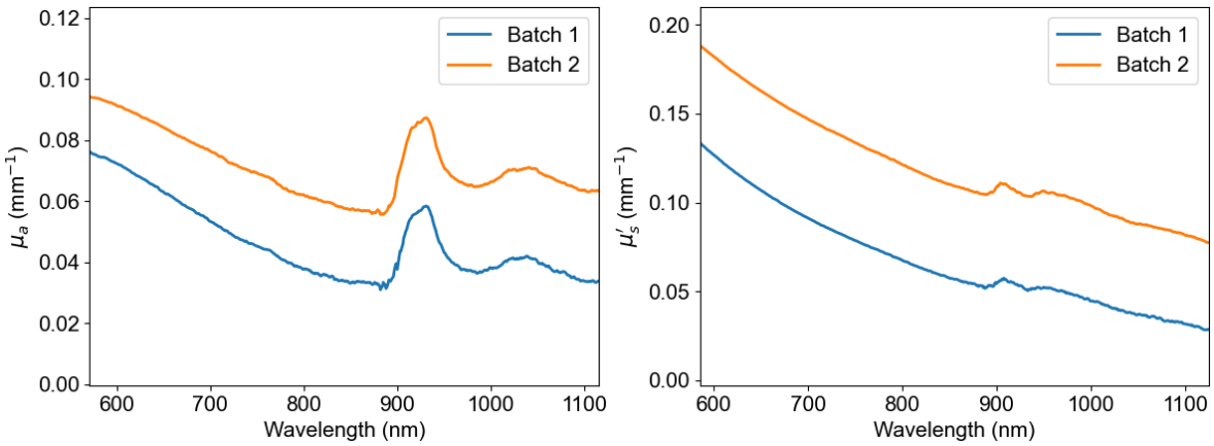

Figure 56: Absorption coefficients (left) and reduced scattering coefficients (right) of the two batches light skin-mimicking material (old and new) determined with the IAD method.

Appendix F: Protocol phantom fabrication

Materials

- Skin mimicking material
- Base material
- Ice chips
- Mould
    - Aluminium bottom part
    - 1st Aluminium top part for the skin mimicking layer
    - 2nd Aluminium top part for the channels
    - 4 Stainless steel rods (3 mm in diameter)
    - 4 Sleeves for fixating the rods
    - 1 Sleeve for the 3D-printed component
    - 2 screws for the air openings in the moulds
    - 6 nylon screws
    - 3 stainless steel pins
    - 1 thread push to connect fitting
- 3D-printed fixation component
- Metal blocks
- Silicon spray
- Vacuum oven
- Oil bath

Methods

1. Determine how far the rods have to be placed in the phantom and place the sleeves at the right location for each rod. Mark the rods with I to IV, corresponding with the holes in the 2nd top part of the mould. The sleeves will prevent the rods from further sliding in the phantom.
2. Preheat the vacuum oven to 150 °C.
3. Heat the oil bath to 150 °C.
4. Heat the skin-mimicking material until it is completely melted.
5. Put 2 pins in the aluminium bottom part.
6. Put the 2 screws for the pressurised air opening in the mould.
7. Heat the bottom part of the mould in the oven for 30 minutes (use the metal blocks for stabilisation).
8. Pour about 50-60 ml of the skin-mimicking material into the mould.
9. Degas the material while it is in the mould until no air bubbles form.
10. Coat the top part of the mould (with the hemisphere) with the silicon spray until it is fully covered.
11. Put it in the oven for another 30 minutes.
12. Remove the moulds from the oven.
13. Put the top part in the bottom part using the pins for alignment and press until the mould is fully closed (use the metal blocks for stabilisation).
14. Put ice chips in the mould to cool the top part of the mould down.
15. Remove excess material.
16. Slowly release the top mould by lifting it straight up using the nylon screws.
17. If happy with the results resume with step 17 otherwise remove the material from the mould and go back to step 6.
18. Heat the oil bath to 120 °C and put the vacuum oven at 120 °C.
19. Heat the base material until it is completely melted.
20. Meanwhile, place the 2nd top part of the mould on the bottom part using the pins for alignment.

21. Place the 3D-printed component in the centre and fixate it with a sleeve.
22. Place the four rods in the corresponding holes in the mould.
23. Degas the base material.
24. Slowly and carefully pour the base material into the mould.
25. Tap on the bottom of the mould to remove air bubbles.
26. After the phantom has completely cooled down and solidified gently remove the top part of the mould.
    a. Remove the sleeve around the 3D-printed component.
    b. Remove the four rods by pulling on them firmly but with care.
    c. Lift the top part with the use of the three nylon screws.
27. Release the whole phantom from the bottom component of the mould.
    a. Remove the screw that closes the hole on the bottom of the bottom component of the mould.
    b. Put the push to connect the fitting in the hole.
    c. Connect a tube to an air supply on one side and the push to connect fitting on the other hand.
    d. Pump air into the mould.
    e. Use gentle manual manipulation to help release the phantom.

Appendix G: Protocol blood mimicking fluids

Protocol obtained from S. Karremans (2023-2024)

Materials

- Nickel(II) sulfate hexahydrate
- Copper(II) Sulfate Pentahydrate
- MilliQ

Methods

All is explained for BMF 2a: strength of 150 g Hb / liter with aimed saturation 80%.

1. Make two stock solutions:
    a. CuSO4: 1M
    b. NiSO4: 2.2 M
2. Measure the μ_a of the stock solutions.
    a. CuSO4: 25.190 cm^{-1} @797 nm
    b. NiSO4: 4.094 cm^{-1} @797 nm
3. Prahl2012 contains HbO2 and Hb tabulated spectra, which form my ground truth haemoglobin spectra.
4. With Prahl2012 values you can calculate the μ_a for a specific BMF.
    a. The example for BMF 2a: @797 nm; $\mu_a = 0.8 * \mu_{a\_HbO2} + 0.2 * \mu_{a\_Hb} = 4.266\ cm^{-1}$
5. The desired absorption values of the separate sulfate solutions are calculated for 797 nm with $\mu_a = (\mu_{a\_CuSO4} + \mu_{a\_NiSO4})/2$.
    a. $\mu_{a\_CuSO4} = 0{,}8 * \mu_{a\_HbO2} * 2 = 6.832\ cm^{-1}$
    b. $\mu_{a\_NiSO4} = 0{,}2 * \mu_{a\_Hb} * 2 = 1.699\ cm^{-1}$
6. The desired molarities of the separate sulfate solutions are given by:
    a. CuSO4: $1M * \mu_{a\_CuSO4\_desired} / \mu_{a\_CuSO4\_stock} = 1 * 6.832/25.190 = 0.271$ M
    b. NiSO4: $2.2M * \mu_{a\_NiSO4\_desired} / \mu_{a\_NiSO4\_stock} = 2.2 * 1.699/4.094 = 0.913$ M
7. The stock solutions need to be diluted (see volumes tab).
    a. $V_{CuSO4\_stock} = 1.5$ mL (arbitrary number of Stock solution volume), this contains 1.5 mmol CuSO4. $V_{CuSO4l} = 1.5$ mmol / 0.271 M = 5.530 mL. So add 5.530 - 1.500 = 4.030 mL milliQ to the 1.5 mL stock solution.
    b. $V_{NiSO4\_stock} = 2.295$ mL (calculated by $V_{CuSO4} * 0.913M / 2.2M$), this contains 2.2*2.295 = 5.049 mmol NiSO4. $V_{NiSO4} = 5.049$ mmol / 0.913 M = 5.530 mL. So add 5.530 – 2.295 = 3.235 mL milliQ to the stock solution.
    c. So, to get a 1:1 mixture in one tube you can add: 1.5 mL stock of CuSO4 + 2.295 mL stock of NiSO4 + 7.265 ml milliQ which results in a volume of 11,061 BMF.

Appendix H: Protocol phantom experiment

Materials

- PAM3 system
- 3 phantoms with a skin-mimicking layer
- 4 blood mimicking fluids (BMFs)
- 5x 1 mL syringes
- 5x 12 cm long needles
- Beaker with milliQ
- 1 container for liquid waste (for the BMFs)
- 1 raised water column set-up

Phantoms

There are three different phantoms, which mimic three different skin tones: light, intermediate and dark. The phantoms have the shape of a hemisphere with a radius of 6 cm attached to a cylinder of the same diameter and a height of 3 cm. The majority of the phantom consists of a base material made from a mixture of paraffin, native gel wax and TiO2. On top of the base material is a 1 mm layer from Copolymer-in-oil doped with alcohol-soluble nigrosin (0.001% w/v, 0.003% w/v, and 0.009% w/v respectively). All phantoms have four wall-less channels running through them at an angle of about 53°, which can be filled with a fluid using a syringe and needle. A 3D-printed component protrudes from the base of the phantom (which is at the cylindrical part). This can be used to fixate and position the phantom during the measurements.

BMF

Four different solutions $NiSO_4$ and $CuSO_4$ are used that function as blood-mimicking fluids. These solutions mimic a blood oxygen saturation of 55%, 70%, 85% and 100%.

Methods

1. The four channels of all phantoms should be marked with a marker from I to IV. The marking should be in the same order for all phantoms. This can be done, well in advance.
2. An overview of the irregularities and blemishes for each quadrant of the phantoms should be made (See Figure 57). This too can be done in advance.
3. Prepare the positioning of the raised water column set-up.
    a. Place the tube of the raised water column on the PAM3.
    b. Align the tube well with the imaging bowl.
    c. Place markings around the tube on the examination table and on the tube itself. These markings will be used to position the set-up correctly each time.
4. Prepare the positioning of the phantoms.
    a. Place the tube of the water column in the correct place.
    b. Screw a phantom on the rod.
    c. Loosely fixate the rod in the lid.
    d. Place the lid on the tube.
    e. Change the height of the phantom by pushing the rod further or pulling it up until the desired height is reached. The hemispherical part of the phantom should be fully under the water line.
    f. Place a marking on the rod at the level of the lid to mark at which location the rod and the lid should be each time a phantom is placed in the imaging bowl.
5. Practise placing and removing the phantom to make sure it goes smoothly when the channels in the phantom are filled with the BMFs.
6. Fill the channels with a needle with the BMF with channel I the lowest saturation and channel IV the highest saturation using a 1 ml syringe. Use hand gloves!!

   a. Put the needle on the syringe.
   b. Fill the syringe with the BMF.
   c. Place the needle carefully in the channel.
   d. Slowly fill the channel with fluid. Do not push the plunger too fast to make sure that air can leave the channel.
   e. After filling the channel close it using the nylon tip.
7. Carefully fixate the phantom in the raised water column set-up.
   a. Place the tube on the imaging table and position it using the markers.
   b. Screw the rod in the 3D-printed component.
   c. Fixate the lid on the rod at the marked location.
   d. Slowly and carefully lower the phantom in the imaging bowl.
8. Use the markings of the channels to rotate the phantom until channel I is pointed straight towards the head of the table and channel III to the feet.
9. Perform the wavelength sweep. Write down any noticeable peculiarities.
   a. Use a wavelength range of 680-1060 nm with steps of 3 nm
   b. Bowl positions: 1
   c. US per position: 180
   d. Averages: 3
   e. Burst length: 3
10. Perform the full scans. Write down any noticeable peculiarities.
   a. Use the wavelengths: 680, 720, 755, 797, 833, 870, 920, 970, 1010, 1060
   b. Bowl positions: 101
   c. US per position: 180
   d. Averages: 3
   e. Burst length: 2
   f. Perform the scan of the first wavelength with 9 US pulses for the US reconstruction. This can be used during the reconstructions to compensate for the SOS differences.
   g. Perform the other scans without US pulses.
11. Gently remove the phantom from the imaging bowl by lifting the lid of the water column set up.
12. Remove the BMFs from the channels and collect them in the waste container.
13. Flush the channels a few times by filling them with Milli-Q and removing the liquid. Collect the fluids in the waste container.
14. Repeat steps 6 to 13 for the other phantoms.

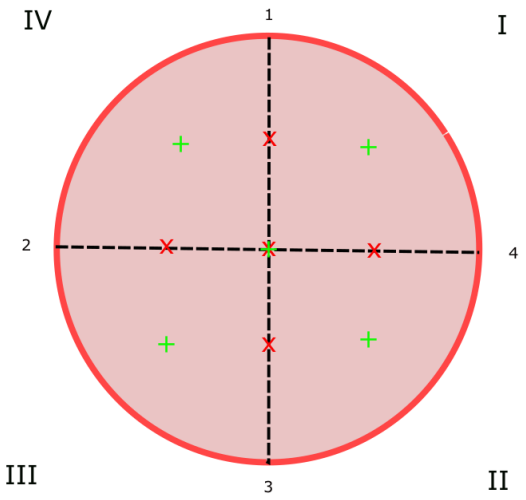

Figure 57: Schematic representation of the top view of the phantom. Four lines divide the surface into four quadrants. The green + signs are the locations for the colorimetric scans and the red x signs are the locations for the ultrasound scans. At the centre of the phantom, both a green and a red sign are located.

Appendix I: Extra figures phantom study

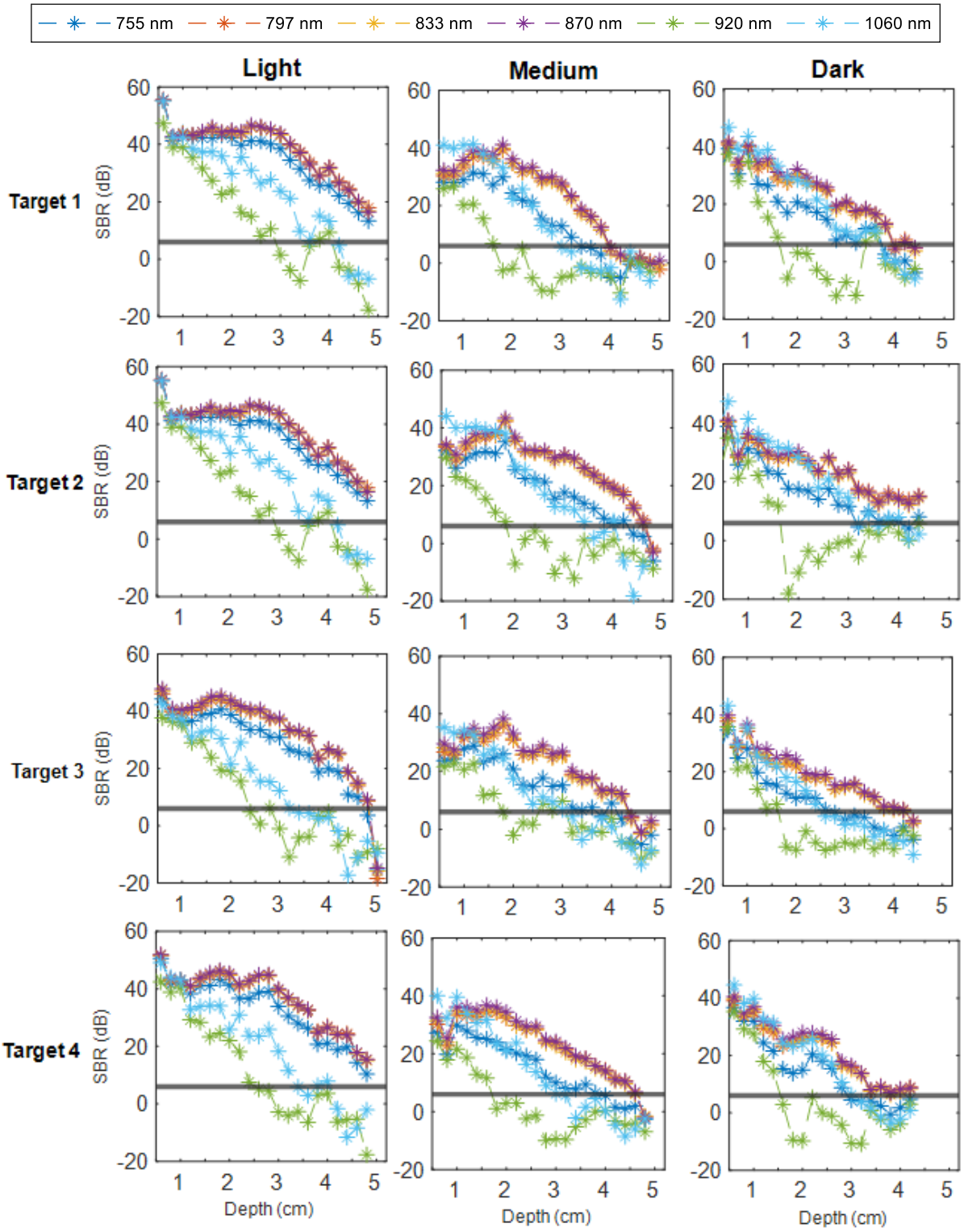

Figure 58: SBR as a function of depth for all six wavelengths for the different targets and the three different phantoms. For targets 1, 2 and 4 the data points for the light phantom stop before they cross the threshold at a depth of 5-5.2 cm. This is the last depth at which the imaging depth could be assessed with the phantom due to the absence of an imaging target in deeper layers.

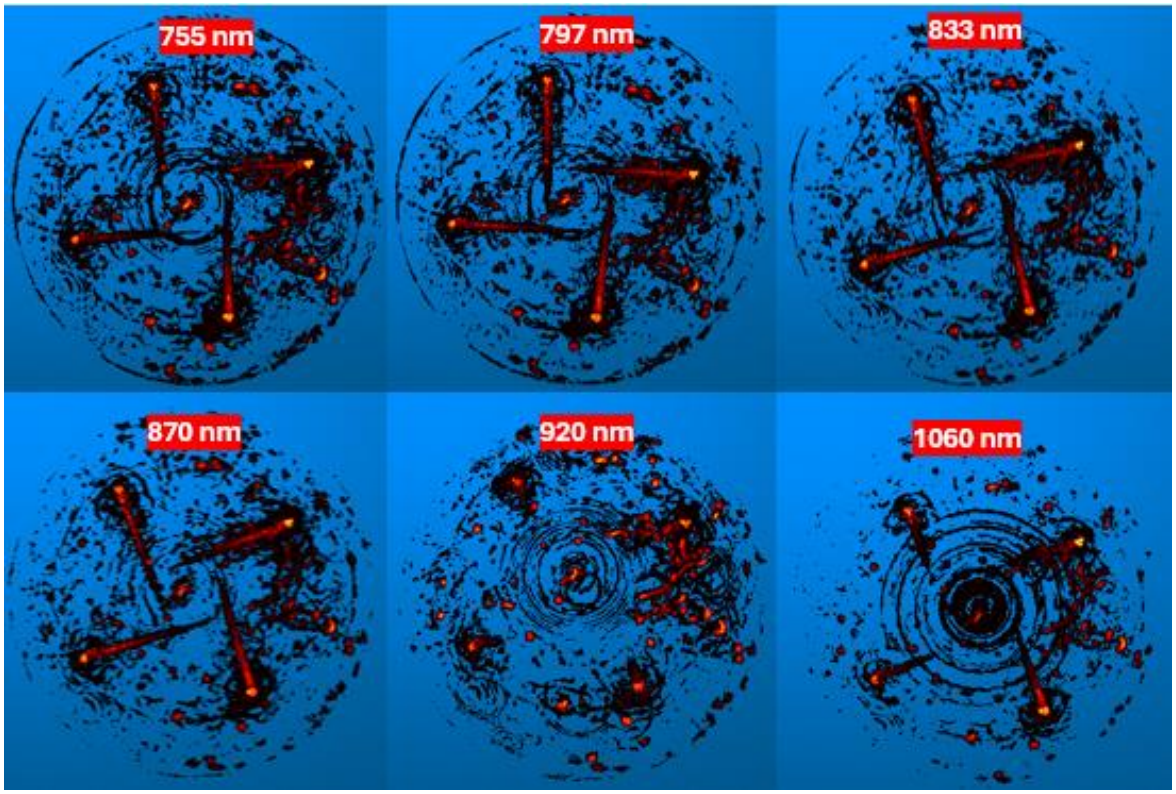

Figure 59: Volumetric MIPs of the processed reconstructions for the light phantom for the six wavelengths.

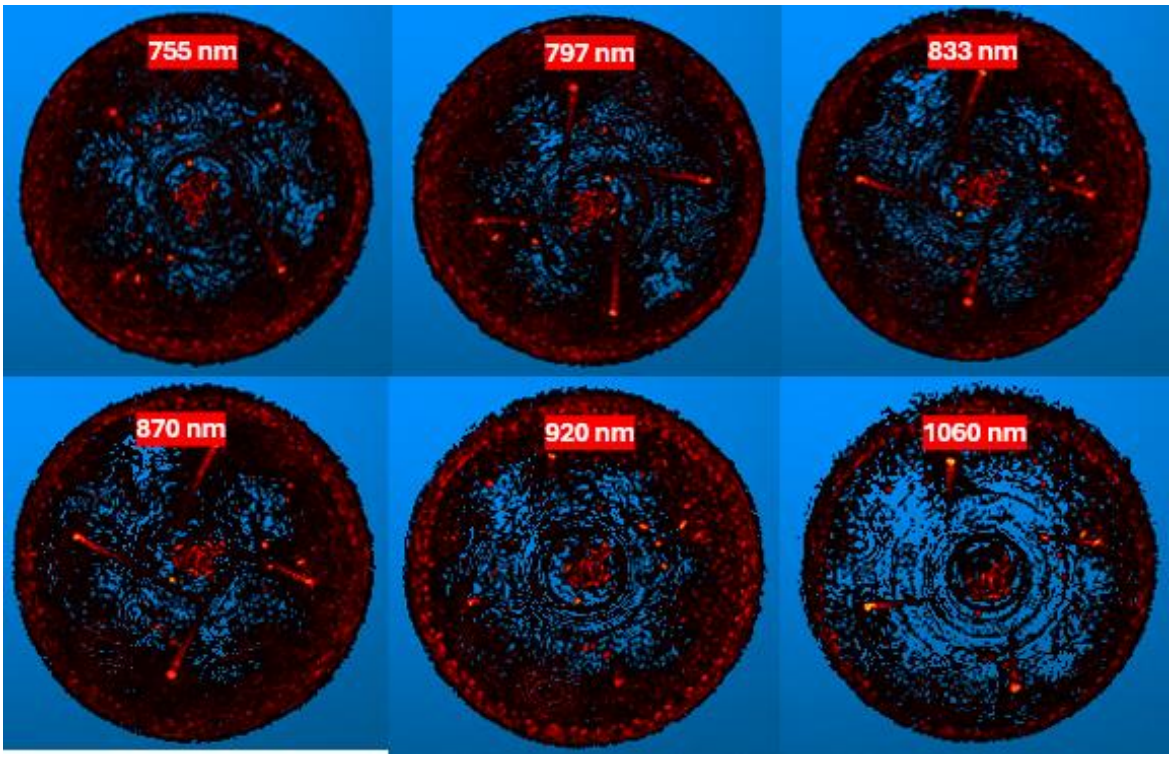

Figure 60: Volumetric MIPs of the processed reconstructions for the medium phantom for the six wavelengths.

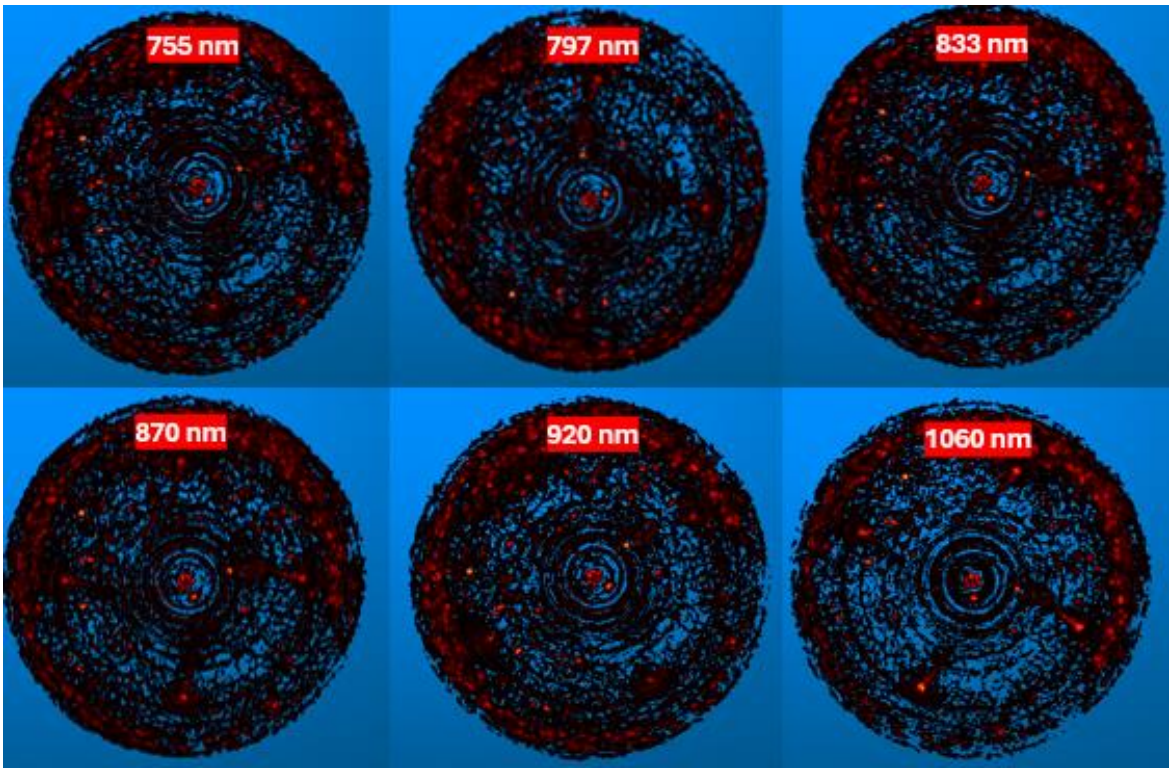

Figure 61: Volumetric MIPs of the processed reconstructions for the dark phantom for the six wavelengths.

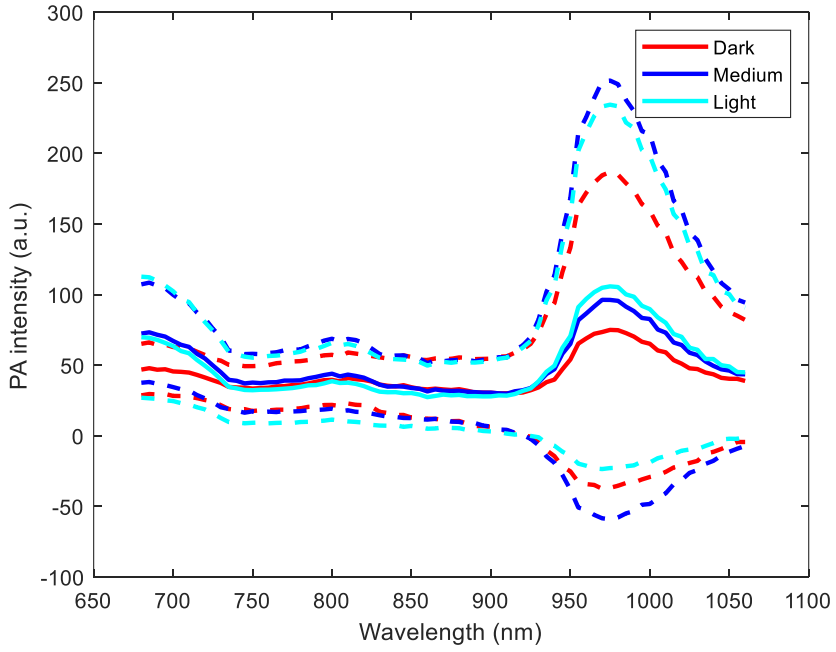

Figure 62: Peak PA intensity of a peak in the signal corresponding to a region in water in the imaging bowl.

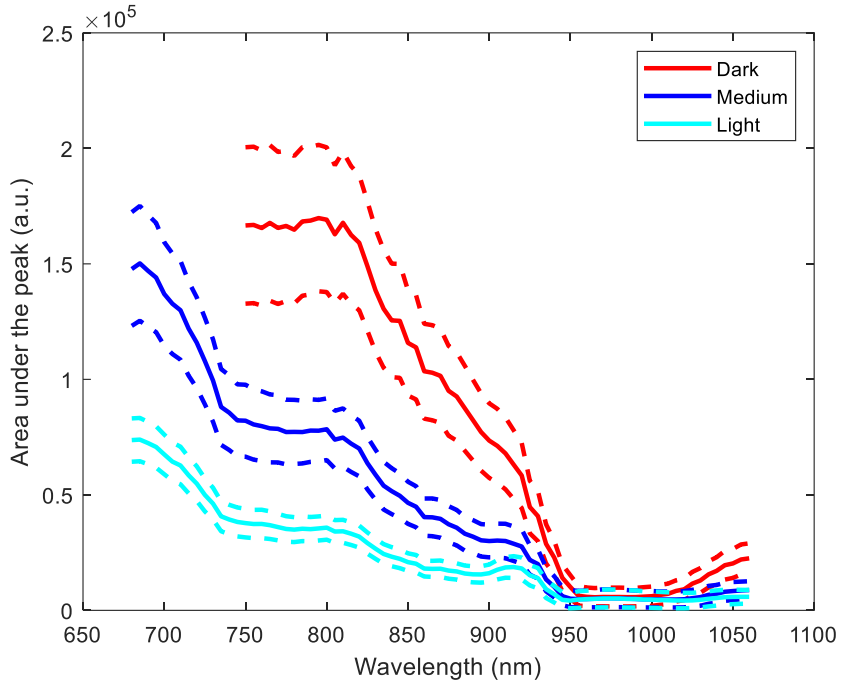

Figure 63: Area under the peak of the skin layer peak for the three skin-mimicking layers over the wavelength range of 680 nm to 1060 nm. The mean (continuous) and standard deviation (dashed) for the area under the peak for the 41 selected transducers are shown. The data of the dark skin tone phantom in the region between 680 nm and 745 nm is left out due to inaccurate because of saturation of the PA signals.

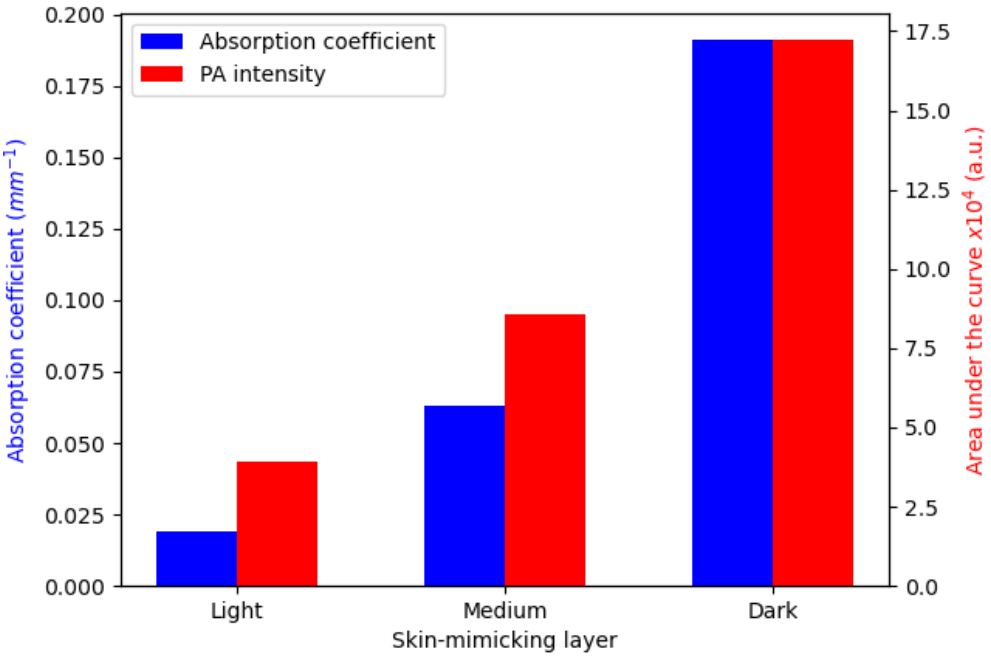

Figure 64: Absorption coefficients and calculated area under the peak for the skin layer peak for the three skin-mimicking layers for 800 nm.

Appendix J: Extra figures volunteer case report

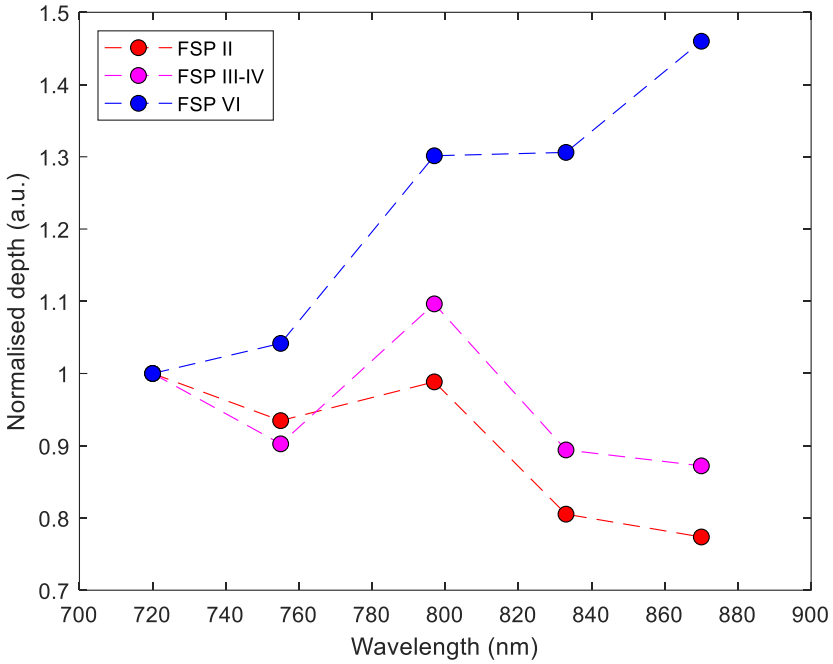

Figure 65: Imaging depth for the five wavelengths normalised at 720 nm for all three volunteers shown in one graph. Be aware that or 720 nm, the data point for all three volunteers has a value of 1 as the normalisation is done at 720 nm. The dotted lines are simply to guide the eye.

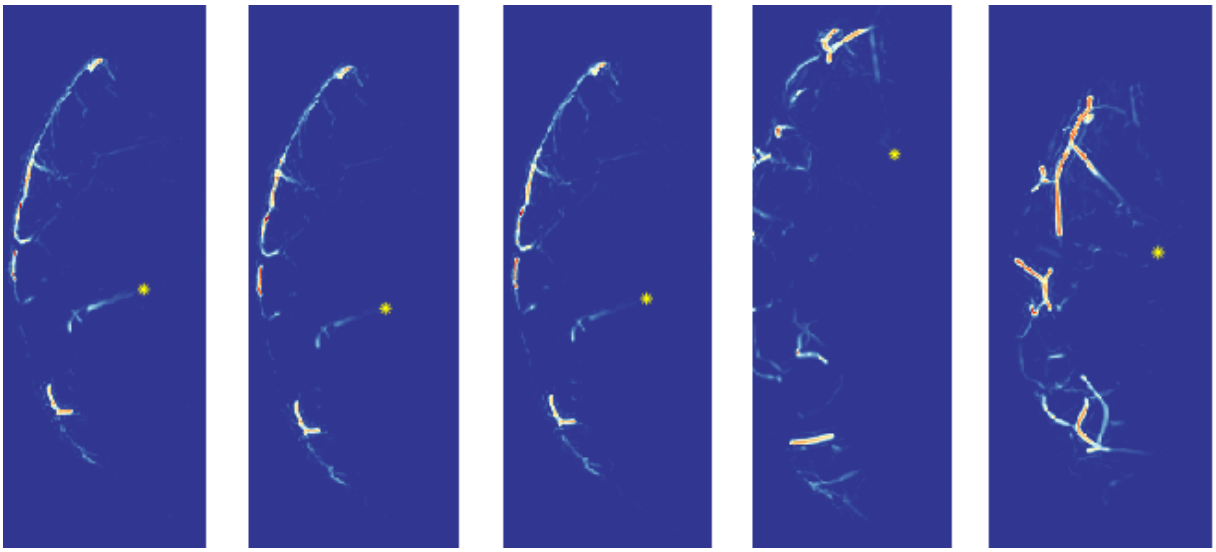

Figure 66: MIPs of a slice of 1 mm around the position at which the maximum imaging depth was found for FSP II (the maximum depth at which a blood vessel could be identified) for the 5 wavelengths from left to right 720, 755, 797, 833, and 870 nm.

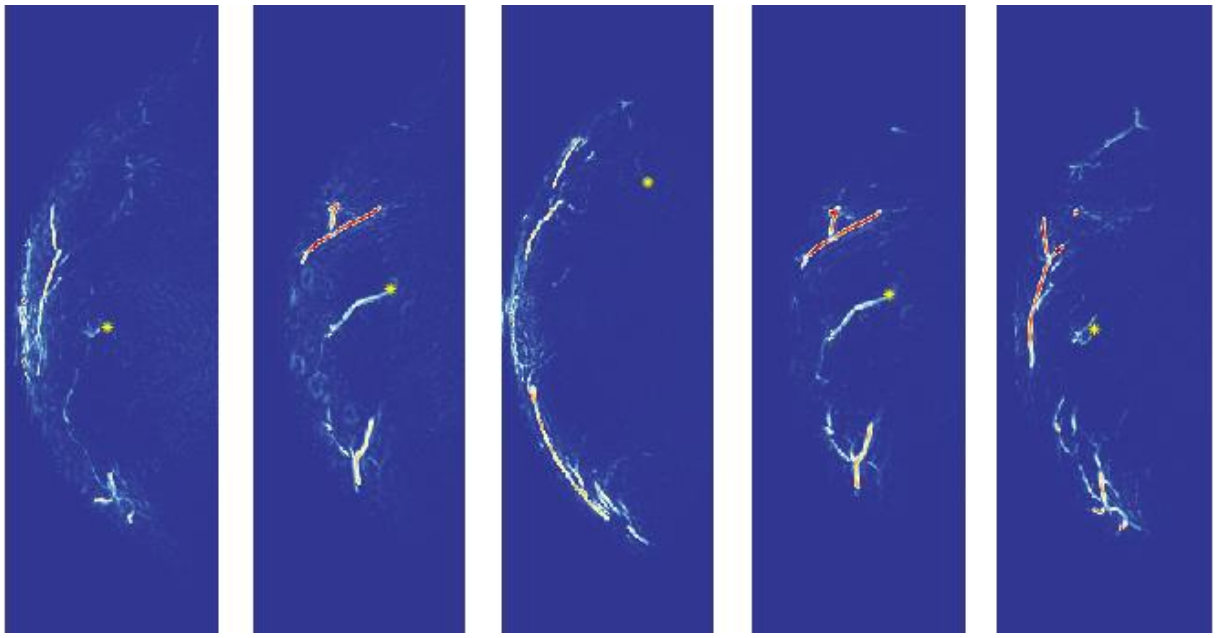

Figure 67: MIPs of a slice of 1 mm around the position at which the maximum imaging depth was found for FSP III-IV (the maximum depth at which a blood vessel could be identified) for the 5 wavelengths from left to right 720, 755, 797, 833, and 870 nm.

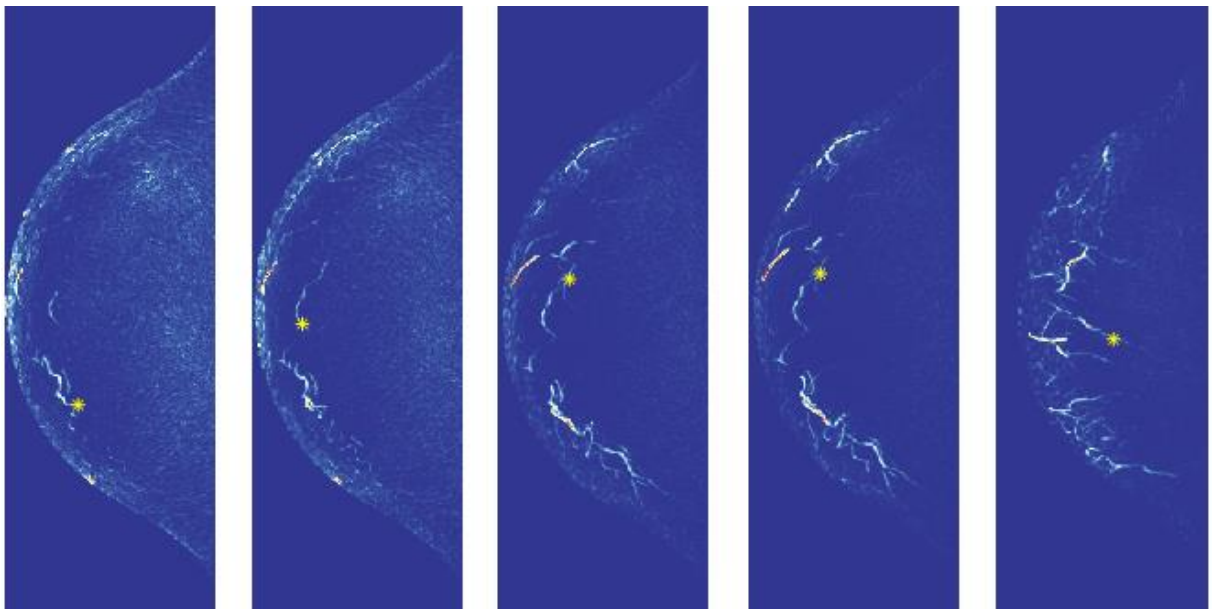

Figure 68: MIPs of a slice of 1 mm around the position at which the maximum imaging depth was found for FSP VI (the maximum depth at which a blood vessel could be identified) for the 5 wavelengths from left to right 720, 755, 797, 833, and 870 nm.

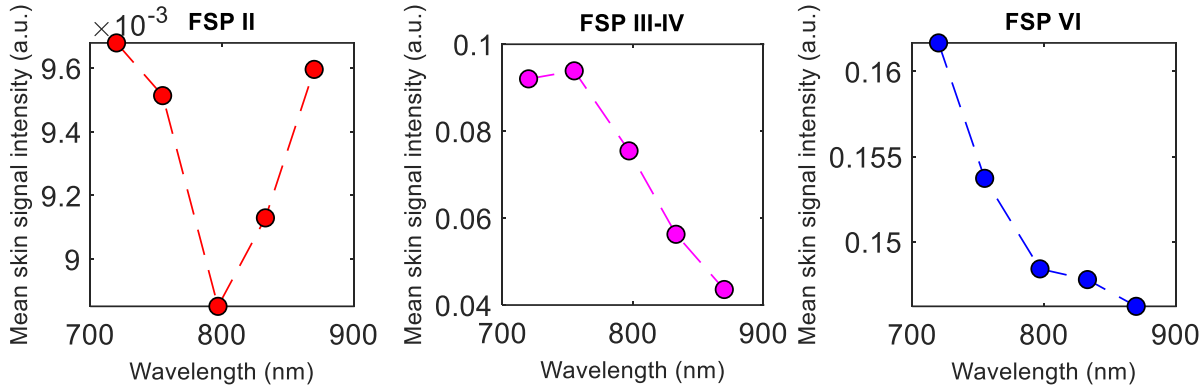

Figure 69: Average skin signal intensity for the five wavelengths. Data is shown for each volunteer separately. Note the Y-axes for the cases have different intensities measured, with the highest signals measured for FSP VI and the lowest for FSP II. The dotted lines are simply to guide the eye.

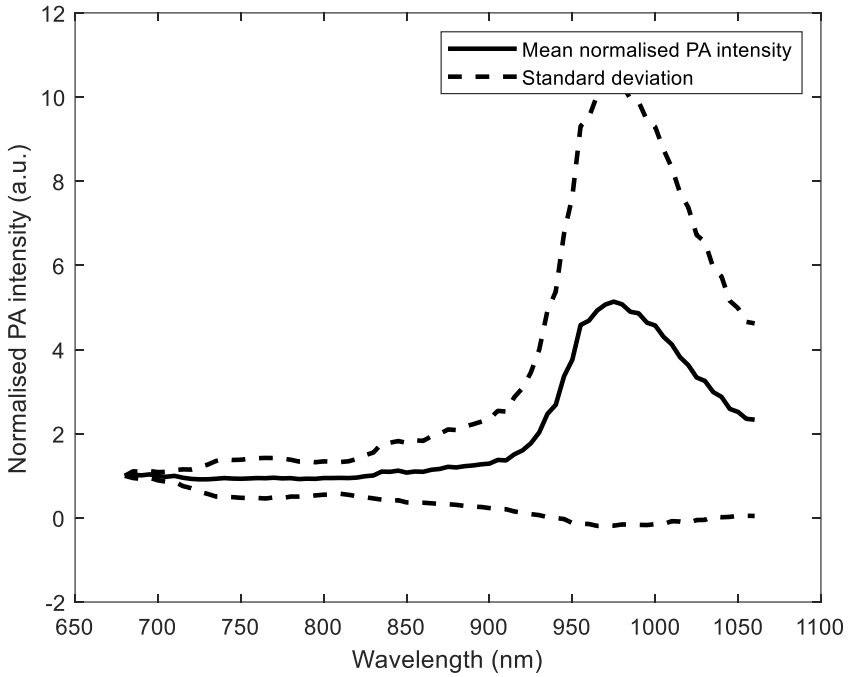

Figure 70: Peak PA intensity of a peak in the signal corresponding to a region in water in the imaging bowl for FSP II.

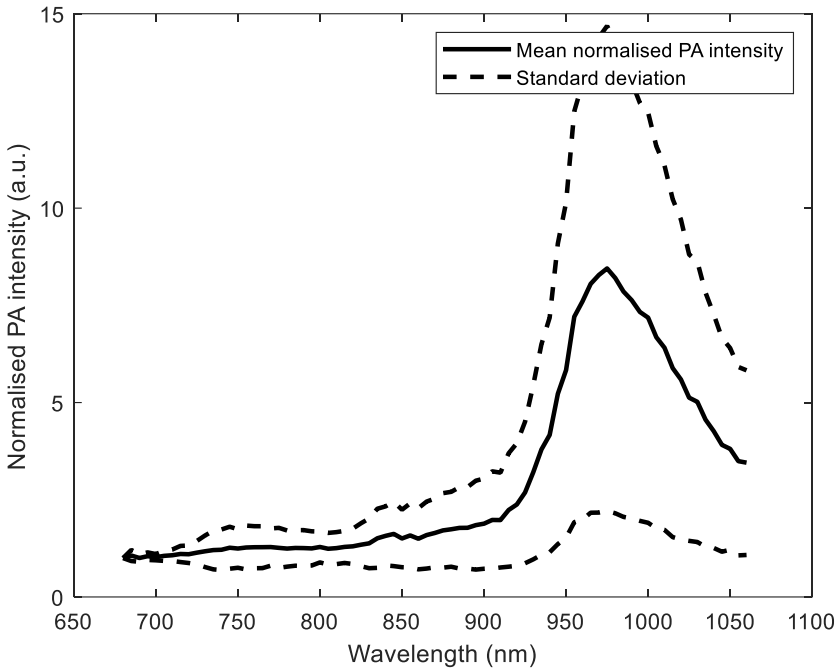

Figure 71: Peak PA intensity of a peak in the signal corresponding to a region in water in the imaging bowl for FSP III-IV.

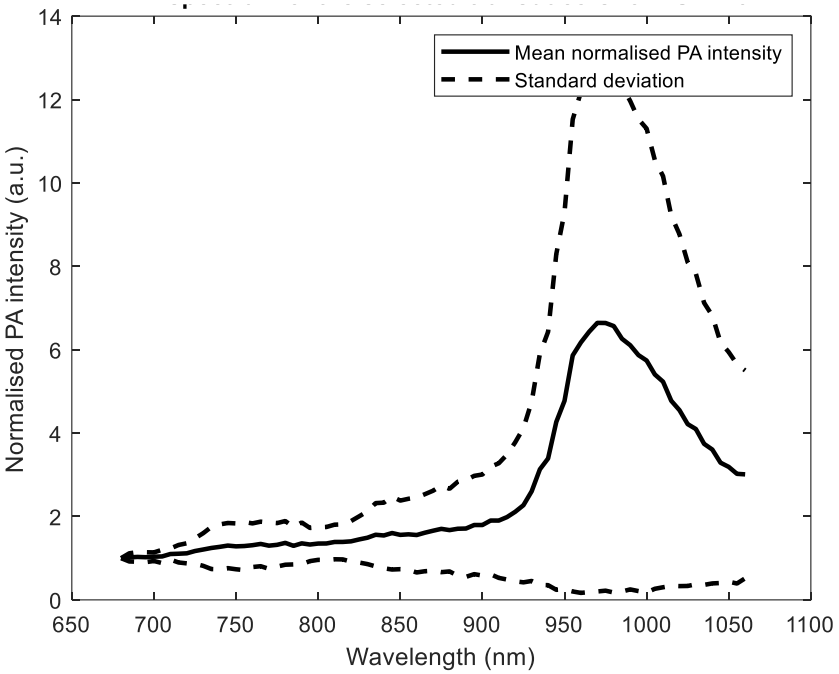

Figure 72: Peak PA intensity of a peak in the signal corresponding to a region in water in the imaging bowl for FSP VI.

Appendix K: Protocol volunteer experiment

Inclusion criteria

- Female
- Older than 18 years old
- Breast size of at least cup A
    - Due to the limited time, there is no preference for a specific breast size.
    - Should the population be large enough, the data can be grouped per breast size during the data analysis.

Exclusion criteria

- Skin lesions or inflamed skin (e.g. mastitis) on both breasts
- Large birthmarks on the breast on both breasts
- Nipple piercings in both nipples
- Tattoos on both breasts
- History of bilateral breast surgery
- Not able to lie down in a prone position for an extended period

Methods

1. Inform the volunteer of the full procedure.
2. Note down any birthmarks, scars, etc.
3. Determine the Fitzpatrick skin phototype of the volunteer using the questionnaire (See Figure 74).
4. Characterise the skin tone objectively using the SkinColorCatch.
    a. Place the SkinColorCatch (Delfin Technologies) lightly on the skin.
        i. The five measurement locations are in each quadrant and at the nipple (See Figure 73).
    b. Perform a measurement and write down the values shown on the screen: M-value (melanin), ITA°, E-value (erythema) and L*a*b* values.
    c. Repeat the measurements 3 times per location.
    d. Average the values for each location.
5. A stabilising cup with an appropriate size is chosen.
    a. Note down any remarks such as if the best-fitting cup is slightly too small or too big.
6. The volunteer is positioned on the examination table with the left positioned in the cup.
    a. Make sure the volunteer is comfortable.
    b. Inform the volunteer again that it is best to lie as still as possible, but that there will be some breaks.
    c. If there are any concerns about how still the volunteer can be, note it down.
7. Instruct the volunteer to lie still. Perform the wavelength sweep (about 229 seconds). Note down any particularities that occur during the measurements (vibrations in the building, movement of the volunteer, etc). Afterwards, inform the volunteer that she can reposition slightly if necessary.
    a. Use a wavelength range of 680-1060 nm with steps of 1 nm
    b. Bowl positions: 1
    c. US per position: 180
    d. Averages: 4
    e. Burst length: 2
8. Reposition the volunteer if necessary. Ask her to lie still. Perform the full scans (about 606 seconds). Tell the volunteer to relax after the scans are made. Note down any particularities that occur during the measurements (vibrations in the building, movement of the volunteer, etc).

a. Use the wavelengths: 680, 720, 755, 797, 833, 890, 930, 970, 1010, 1060
b. Bowl positions: 101
c. US per position: 180
d. Averages: 4
e. Burst length: 2

9. After a short break to give the volunteer some time to loosen the muscles, the right breast is positioned in the scanner.
10. Repeat step 7.
11. Repeat step 8.

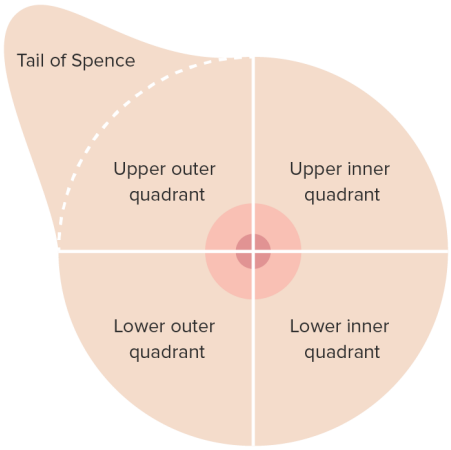

Figure 73: Schematic overview of the different areas of the breast surface [102].

Table A4. Questionnaire used for skin type scaling on the Fitzpatrick scale. Summing the points corresponding to the answers gives the six skin types described in Table A1. I: 0-6 points, II: 6-14 points III: 15-22 points, IV: 22-27 points, V and VI: >27 points

	0	1	2	3	4
What is your eye color?	light blue/ grey/ green	blue/ grey/ green	blue	dark brown	black brown
What is your hair color?	red	blond	chestnut/dark blond	dark brown	black
How dows your skin react to sunlight?	burns quickly, blisters directly form	burns quickly, blisters after a while	burns sometimes	incidental burns	never burns
Does your skin directly tan after exposure to sunlight?	never	rarely	sometimes	often	always
How much do you tan?	barely	light colouring	colouring	quickly colouring	quickly turn dark brown
What is the tone of your skin that has not been exposed to sunlight?	red	pale	pale with beige tones	brown	dark brown
How many birthmarks do you have?	many	some	few	rarely	none
How often is your breast directly exposed to sunlight or light from a tanning bed?	never	rarely	sometimes	often	always
When was the last time your breasts were exposed to sunlight?	>3 months ago	2-3 months ago	1-2 months ago	<1 month ago	<2 weeks ago

Figure 74: Questionnaire for the Fitzpatrick skin phototypes [76].